On the influence of cobamides on organohalide respiration and mercury methylation

A Dissertation Presented for the
Doctor of Philosophy
Degree
The University of Tennessee, Knoxville

Nannan Jiang
May 2019

Copyright © 2019 by Nannan Jiang
All rights reserved.

DEDICATION

To the taxpayers who funded this work, and to my students –
past, present, and future; you determine the sustainability of science over time.

ACKNOWLEDGEMENTS

The sustainability of science rests upon the ability and dedication to mentor the next generation. As such, I am indebted to my mentors who have given me the opportunity to enjoy science. Dr. Clifford F. Weil first taught me to look beyond my coursework by introducing me to the population theory of Thomas Malthus. It was Dr. Louis A. Sherman and Dr. Vilas B. Shukla who gave me my first research opportunity at Purdue University. Vilas helped me develop my day-to-day time management skills as I learned to balance classes and research, while Lou taught me the importance and feasibility of remaining positive under any circumstance.

My master's advisor Dr. William W. Metcalf taught me microbial genetics with a dose of healthy skepticism. Bill often cited a used car analogy that I still reference to this day. During my time at the University of Illinois at Urbana-Champaign, I have developed lifelong friendships with Dr. Madeline Mayrim López Muñoz, Dr. Nicolai Müller, and Rimpa Ghosh. Together we have shared successes and struggles, and continue to share these to this day.

Dr. James G. Elkins mentored me during my post-master's appointment at the Oak Ridge National Laboratory (ORNL). I was excited to learn of the many industries that were interested in our work on biofuels.

I met Dr. Juliane Hopf on my first day during orientation at ORNL. She was as productive in research as she was in organizing social events. Nicknamed "*GG*,"

she had the ability to unite everyone from undergraduate interns to postdoctoral research associates. GG was also responsible for my nomination and eventual election to the Oak Ridge Postdoctoral Association (ORPA) Executive Committee (ORPEX), where I served as an officer for over five years and as chair of the Professional Development Committee for over three years. During this time, I also made several other friends including Dr. Taniya R. Chowdhury, the "*Oprah of ORPA*," Dr. Prakash D. Nallathamby, Dr. James H. Campbell, Dr. Alisha G. Campbell, and Donna M. Kridelbaugh. I also thank Allison O. Doty, a consultant in the ORNL Employee and Organizational Development group who worked with me to host over 27 professional development seminars and postdocs for the postgraduate community at ORNL.

These apparent social activities developed into opportunities to receive professional and career advice. Former ORPA president Dr. Jibonananda Sanyal explained to me that if I expect to do my best work during graduate school, then I would set myself up for a failed career. Former ORPA vice president Dr. Larry J. Millet taught me how to properly document all my activities in our annual reports.

Another ORPA vice president Dr. Swapneeta S. Date served as a moderator for one of my presentations. Immediately afterwards, we realized there was ample room for us to collaborate. She has contributed heavily to the later parts of my dissertation work.

I would like to thank my committee for their time and support throughout the years. Dr. James G. Elkins always provided me with essential bacterial strains, many of which are used in this work. I took BCMB 515 with Dr. Gladys M. Alexandre my first semester at the University of Tennessee. I saw firsthand her care for students as she discussed options with a prospective rotation student. I would later attend many of her development seminars hosted through the Program for Excellence and Equity in Research (PEER). My initial project did not work for the first two years. Dr. Jun Yan and Dr. Frank E. Löffler gave me an entirely new project, which has now become the basis of my dissertation. Dr. Jerry M. Parks and Dr. Alexander Johs helped me expand the project by introducing me to the world of mercury. Alex of course was known for providing donuts in desperate times. I met Dr. Russell L. Zaretzki while taking STAT 578. He noticed I was a Bredesen Center student, and discussed with me the potential for another interdisciplinary program on data science. Little did I know at the time, the program he envisioned would eventually become the second Ph.D. program within the Bredesen Center focusing on Data Science and Engineering.

My entrance into the Bredesen Center was not a smooth one. The lab that initially agreed to take me fell through. I then found co-advisors, which lasted exactly one week, and again fell through. At the time, I was taking a MICR 650 journal club with Dr. Frank E. Löffler. Though I did not know anything about dechlorination at the time, what caught my attention was when he mentioned science is all about the student. Frank then explained that he had taken this

statement from his postdoctoral mentor Dr. James M. Tiedje, who confirmed this during his visit to the University of Tennessee. Though students should be free to choose their own careers, I have seen firsthand those who have chosen science, but ended up leaving it. It is true that the sustainability of science is challenged when papers and projects are placed above the student.

I am convinced that the Bredesen Center has taught me more about science than any disciplinary program could have done. I thank Dr. Lee L. Riedinger and Dr. S. Suresh Babu, both of whom managed to serve as mentors to over 120 students at any given point in time. I also thank the Bredesen Center staff Tracey L. Bucher, Allie Burns, Rebecca Christ, Wanda L. Davis, Erin E. Favier, Jessica H. Garner, and Cathy Milligan.

Lastly, I thank the taxpayers who have made this work possible – I hope I will be able to repay you in knowledge what you have paid in grant funding.

ABSTRACT

Corrinoids are metallic cofactors that serve as prosthetic groups for numerous reactions catalyzed by various microorganisms, ranging from carbon and nitrogen cycling to toxic waste remediation. Importantly, the number of organisms that require corrinoids far outweigh that which can produce corrinoid *de novo*. This imbalance in supply and demand reveals interdependencies at the molecular scale amongst various organisms, where a corrinoid auxotroph may need to coexist with a corrinoid prototroph. A further determinant of corrinoid function lies in the lower base, and essential component of functional corrinoids. In the case of *Dehalococcoides mccartyi*, studies have shown that differences in lower base structure impact the activity of corrinoid-binding reductive dehalogenase enzymes. This body of work examines a gene from *Geobacter lovleyi* implicated in the synthesis of the 5-methoxybenzimidazole lower base, and how this lower base may play a role in regulating corrinoid-dependent reactions including reductive dechlorination in *Dehalococcoides mccartyi* and mercury methylation.

TABLE OF CONTENTS

CHAPTER I Introduction 1
Abstract 2
Impact and availability of corrinoids 2
Effects of corrinoid lower base structure 3
Genes and pathways determining corrinoid lower base structure remain elusive 3
Research objectives 4
References 5
CHAPTER II Customization of an exogenous cobamide biosynthetic pathway rescues corrinoid auxotrophy in organohalide-respiring Dehalococcoidia 7
Abstract 8
Importance 9
Introduction 9
Materials and Methods 14
Chemicals 14
Cultures and growth conditions 15
Guided cobamide biosynthesis in *Geobacter* 18
Genome analysis 18
Corrinoid extraction and analysis 21
Plasmid construction 21
Strain construction 25
Co-cultures 31
Conserved domain search 31
Analysis of horizontal gene transfer 31
qPCR of G. sulfurreducens and *Dhc* 16S rRNA genes 32
Analytical methods 33
Results 33
5-OMeBza-Cba is the native cobamide synthesized in *G. lovleyi* strain SZ 33
Non-native cobamides do not affect *Geobacter* metabolism 33
Genome analysis 37
Functional characterization via heterologous expression 38
Dechlorination in co-cultures 38
Horizontal transfer of Glov_3676 41
Discussion 43
Acknowledgements 52
References 53
CHAPTER III *G. sulfurreducens* methylates mercury independent of the type of corrinoid lower base 63
Abstract 64
Importance 65
Introduction 65
Materials and Methods 66

Chemicals 66
Cultures 67
Medium and growth conditions 67
Growth curves 67
Guided cobalamin biosynthesis 68
Mercury methylation quantification 68
Sulfide quantification 68
PCR screens 68
Results 71
Growth of *Geobacter* strains producing different lower bases 71
Methylmercury analysis 75
Sulfide analysis 75
Discussion 78
Acknowledgements 80
References 81
CHAPTER IV Unexpected effects of vanillate on mercury methylation in *Geobacter sulfurreducens* 85
Abstract 86
Importance 87
Introduction 87
Materials and Methods 88
Chemicals 88
Cultures 89
Plasmid construction 89
Strain construction 102
PCR verification of mutant strains 102
MeHg washed cell assays 105
Statistical analysis 105
Results 106
Growth curves 106
Maximum optical density 110
Time to reach maximum optical density 110
Mercury methylation following lag phase induction 110
Mercury methylation following exponential phase induction 115
Discussion 115
Acknowledgements 123
References 124
CHAPTER V Conclusion 129
Summary 130
VITA 131

LIST OF TABLES

Table 1: Strains used in Chapter 2. 16
Table 2: Plasmids used in Chapter 2. 23
Table 3: Primers used in Chapter 2. 24
Table 4: Comparison of key genes encoding lower base methyltransferases. 40
Table 5: Strains used in Chapter 3. 67
Table 6: Primers used in Chapter 3. 69
Table 7: Expected amplicon sizes of the *imcH* locus for PCR verification suicide vector integrations. 70
Table 8: Strains used in Chapter 4. 90
Table 9: Plasmids used in Chapter 4. 94
Table 10: Primers used in Chapter 4. 96
Table 11: Protein BLAST results. 121
Table 12: Locus tag annotations. 122

LIST OF FIGURES

Figure 1: Corrinoid cofactor structure.....11
Figure 2: Interspecies corrinoid transfer.....13
Figure 3: Comparison of lower base biosynthesis genes.....20
Figure 4: Homologous recombination of pNJ052 into *G. sulfurreducens.*.....27
Figure 5: Chromosome map of PCR screening. 29
Figure 6: Identification and quantification of corrinoids carrying different lower bases. 34
Figure 7: Lower base methyltransferase domain hits.....39
Figure 8: Dechlorination profile in co-cultures.....42
Figure 9: Phylogenetic analysis. 47
Figure 10: Chromosome map of the *imcH* locus.....70
Figure 11: Growth of *Geobacter* cultures producing different corrinoids. 72
Figure 12: pH of different *Geobacter* strains. 74
Figure 13: Methylmercury analysis. 76
Figure 14: Sulfide content in different *Geobacter* strains. 77
Figure 15: Homologous recombination. 103
Figure 16: PCR screen. 104
Figure 17: Growth curve of wild type on varying concentrations of vanillate.....107
Figure 18: Growth curve of strain FEL273 on varying concentrations of vanillate. 108
Figure 19: Growth curve of strain FEL274 on varying concentrations of vanillate. 109
Figure 20: Maximum optical density.....111
Figure 21: Time to reach maximum optical density.....112
Figure 22: Optical density at harvesting.....113
Figure 23: Endpoint methylmercury concentrations following lag-phase induction. 114
Figure 24: Endpoint methylmercury concentrations following exponential-phase induction. 116

LIST OF SYMBOLS AND ABBREVIATIONS

5-MeBza	5-methylbenzimidazole
5-MeBza-Cba	5-methylbenzimidazole-cobamide
5-OHBza	5-hydroxybenzimidazole
5-OHBza-Cba	5-hydroxybenzimidazole-cobamide
5-OMeBza	5-methoxybenzimidazole
5-OMeBza-Cba	5-methoxybenzimidazole-cobamide
5-OMe-6-MeBza	5-methoxy-6-methyl-benzimidazole
5-OMe-6-MeBza-Cba	5-methoxy-6-methyl-benzimidazole-cobamide
AA	Amino acid
AIR	5-aminoimidazole ribotide
BLAST	Basic Local Alignment Search Tool
bp	Base pair
Bza	Benzimidazole
CAI	Codon Adaptation Index
Cba	Cobamide
cDCE	*cis*-1,2-dichloroethene
CDD	Conserved Domains Database
CDI	*Clostridium difficile* infections
DAP	2,6-Diaminopimelic acid
Dhc	*Dehalococcoides*
DMB	5,6-dimethylbenzimidazole
DMB-Cba	5,6-dimethylbenzimidazole-cobamide
DNA	Deoxyribonucleic acid
DSM	Deutsche Sammlung von Mikroorganismen und Zellkulturen
HEPES	4-(2-hydroxyethyl) piperazine-1-ethanesulfonic acid
HGT	Horizontal Gene Transfer
HPLC	High performance liquid chromatography
IMG	Integrated Microbial Genomes
JGI	Joint Genome Institute
KCN	Potassium cyanide
KOH	Potassium hydroxide
LB	Lysogeny broth
LC-MS	Liquid chromatography – mass spectrometry
MeHg	Methylmercury
NCBI	National Center for Biotechnology Information
ND132	*Desulfovibrio desulfuricans* strain ND132
NIH	National Institutes of Health
PCA	*Geobacter sulfurreducens* strain PCA
PCR	Polymerase chain reaction
PSSM	Position-Specific Scoring Matrix
qPCR	Quantitative Polymerase Chain Reaction

RDase	Reductive dehalogenase
rRNA	Ribosomal ribonucleic acid
rSAP	Recombinant shrimp alkaline phosphatase
SZ	*Geobacter lovleyi* strain SZ

CHAPTER I
INTRODUCTION

Abstract

The recently popularized Black Queen Hypothesis (1) proposes most if not all organisms began as prototrophs for all key nutritional components. Over evolutionary time, species gained auxotrophies for essential organic compounds due to an abundance in their respective environments. Common auxotrophies include the inability to produce amino acids, sugar metabolizing enzymes, and vitamins, including corrinoid cofactors (2, 3). Nutritional auxotrophy thus plays a determining role in the presence and growth rate of all auxotrophic species.

Impact and availability of corrinoids

Of the many auxotrophies that exist, this body of work will focus on corrinoid cofactors. There are several classes of corrinoid-dependent enzymes including methyltransferases, methionine synthase, mutases that cleave C-C bonds, and reductive dehalogenases (4, 5). Though corrinoid prototrophs do exist, a recent study surveying over 11,000 species of bacteria concluded only 37% possessed genes for *de novo* cobamide biosynthesis; surprisingly, 86% of these 11,000 species were predicted to have at least one cobamide-dependent enzyme (6). These results suggest a large population of corrinoid-dependent organisms is auxotrophic for corrinoids, rendering them completely dependent on corrinoids released into the environment by nearby prototrophs. The ability to synthesize corrinoid is limited to prokaryotes.

Effects of corrinoid lower base structure

Though some enzymatic reactions may carry very specific corrinoid cofactor requirements, others have been shown to be more promiscuous. For example, the reductive dehalogenases of *Dehalococcoides mccartyi* (*Dhc*) require corrinoids carrying very specific lower bases (3). We now know of at least 16 different lower bases that are found in nature (3). How the corrinoid lower base impacts enzyme function remains largely unknown.

Genes and pathways determining corrinoid lower base structure remain elusive

A 2015 study discovered the complete anaerobic biosynthesis pathway for 5,6-dimethylbenzimidazole (7), the preferred lower base in cobamides of *Dhc* RDases (3). However, only a handful of genes predicted to participate in lower base biosynthesis have biochemically confirmed functions (7). The dearth of experimentally validated lower base genes is a current bottleneck in our efforts to understand how lower base structure affects enzyme activity. Likewise, the same bottleneck stresses the need for genetic engineering approaches that provide conclusive evidence beyond the hypotheses generated by bioinformatics. We now know that the structure of corrinoid cofactors, particularly at the level of the lower base, can generate significant changes in enzyme function and microbial diversity. However, we still do not know how or why. We are now limited by the undiscovered genes involved in producing these critical structures.

Research objectives

1.) Determine how *G. lovleyi* supports *Dhc* reductive dechlorination.

2.) Identify the genetic basis for *G. lovleyi* serving as corrinoid partner for *Dhc.*

3.) Demonstrate functionality of gene(s) allowing *G. lovleyi* to serve as corrinoid partner for corrinoid auxotroph *Dhc.*

4.) Test *in vivo* functionality in co-culture experiments.

5.) Determine effect(s) of different lower bases on other corrinoid-dependent processes, such as mercury methylation.

6.) Assess potential to overexpress corrinoid-dependent mercury methylation genes.

References

1. J. Jeffrey Morris, Richard E. Lenski, Erik R. Zinser. 2012. The Black Queen Hypothesis: Evolution of dependencies through adaptive gene loss. mBio 3:1–7.

2. Helliwell KE, Wheeler GL, Smith AG. 2013. Widespread decay of vitamin-related pathways: Coincidence or consequence? Trends Genet TIG 29:469–478.

3. Yan J, Şimşir B, Farmer AT, Bi M, Yang Y, Campagna SR, Löffler FE. 2015. The corrinoid cofactor of reductive dehalogenases affects dechlorination rates and extents in organohalide-respiring *Dehalococcoides mccartyi*. ISME J 10:1092–1101.

4. Yan J, Ritalahti KM, Wagner DD, Löffler FE. 2012. Unexpected specificity of interspecies cobamide transfer from *Geobacter* spp. to organohalide-respiring *Dehalococcoides mccartyi strains* . Appl Environ Microbiol 78:6630–6636.

5. Rowena G. Matthews. 2009. Cobalamin- and corrinoid-dependent enzymes. Met Ions Life Sci 6:53–114.

6. Shelton AN, Seth EC, Mok KC, Han AW, Jackson SN, Haft DR, Taga ME. 2018. Uneven distribution of cobamide biosynthesis and dependence in bacteria predicted by comparative genomics. ISME J.

7. Hazra AB, Han AW, Mehta AP, Mok KC, Osadchiy V, Begley TP, Taga ME. 2015. Anaerobic biosynthesis of the lower ligand of vitamin B12. Proc Natl Acad Sci U S A 112:10792–10797.

CHAPTER II
CUSTOMIZATION OF AN EXOGENOUS COBAMIDE BIOSYNTHETIC PATHWAY RESCUES CORRINOID AUXOTROPHY IN ORGANOHALIDE-RESPIRING DEHALOCOCCOIDIA

Reproduced in part with permission from Jiang N, Jin H, Bourdon AK, YY, Swift CM, Campagna SR, Yan J, and Löffler FE. Customization of an exogenous cobamide biosynthetic pathway rescues corrinoid auxotrophy in organohalide-respiring Dehalococcoidia. In preparation. All copyright interests will be exclusively transferred to the publisher upon submission.

Abstract

Carbon and energy metabolism for the majority of organisms requires corrinoid, and corrinoid auxotrophs rely on corrinoid salvage. *Dehalococcoides mccartyi* (*Dhc*) is an obligate organohalide-respiring bacterium whose energy metabolism hinges on reductive dehalogenases (RDases), which are corrinoid-dependent enzyme systems. Remarkably, the organism lacks the ability to synthesize corrinoid and completely relies on salvage pathways to capture cobamides and corrinoid precursors from the environment. Complicating this dependency is the observation that *Dhc* RDases have specific cobamide preferences for catalytic activity. *Geobacter* lovleyi produces a cobamide supporting *Dhc* growth, whereas *Geobacter sulfurreducens* does not. Here, we demonstrate that *G. lovleyi* synthesizes 5-methoxybenzimidazole-cobamide whereas *G. sulfurreducens* produces 5-hydroxybenzimidazole-cobamide. A gene predicted to encode an O-methyltransferase involved in the methylation of 5-hydroxybenzimidazole-cobamide to 5-methoxybenzimidazole-cobamide was identified on the *G. lovleyi* genome. The plasmid-encoded O-methyltransferase gene showed evidence of horizontal gene transfer. Using a homologous recombination approach, this putative O-methyltransferase gene was inserted onto the *G. sulfurreducens* chromosome, and the mutant strain now produced 5-methoxybenzimidazole-

cobamide. Co-cultivation studies demonstrated that the *Geobacter sulfurreducens* mutant strain supported *Dhc* growth and complete reductive dechlorination of *cis*-1,2-dichloroethene to ethene. These findings assign a specific function to Glov_3676, and indicate that genes implicated in lower base biosynthesis are relevant determinants of metabolic activity of the corrinoid-auxotrophic *Dhc*.

Importance

The presence and availability of corrinoid prosthetic groups determine viability and functionality of key microbes in various environmental systems. Genetic pathways leading to the production of functional corrinoids have remained elusive, thus limiting predictive understanding how the availability of these essential prosthetic groups control corrinoid-dependent processes. This study identified a novel O-methyltransferase involved in producing the 5-methoxybenzimidazole lower base, which is an essential step for producing a cobamide that supports auxotrophic *Dhc* dechlorinators.

Introduction

Nutritional auxotrophy is a key determinant of microbial activity and viability in various environmental systems. Microorganisms often depend on exogenously derived micronutrients, including amino acids, vitamins, and other prosthetic

groups. This dependence links physical proximity of nutritional donors (i.e., prototrophs) to the survival of recipients (i.e., auxotrophs).

Cobamides are of particular importance as they have roles in the carbon and energy metabolisms in all domains of life. Key enzymes require cobalamin as a prosthetic group, including ribonucleotide reductase involved in DNA biosynthesis [1] and methionine synthase used in amino acid biosynthesis [2]. Globally relevant carbon turnover processes, such as methanogenesis and H_2/CO_2-reductive acetogenesis, strictly require corrinoid [3]. Additionally, the energy metabolism of organohalide-respiring bacteria hinges on corrinoid-dependent reductive dehalogenases (RDases) [4].

Corrinoids differ at the level of the upper β-axial ligand and the lower α-axial base **(Figure 1)** [5–7]. Common β-axial ligands include adenosyl, cyano, and methyl groups [8]. Of note, the cyano group in commercial cyanocobalamin is an artificial ligand and does not occur in biological systems. To date, 17 lower base structures have been identified, and previous work has demonstrated that the type of lower base incorporated into the corrinoid molecule affects the activity of RDases [9]. Only four cobamides are known to support complete reductive dechlorination of *c*DCE to ethene by *Dhc*, including cobamides carrying 5,6-dimethylbenzimidazole (DMB), 5-methylbenzimidazole (5-MeBza), 5-methoxybenzimidazole (5-OMeBza), or benzimidazole (Bza) as lower base [9].

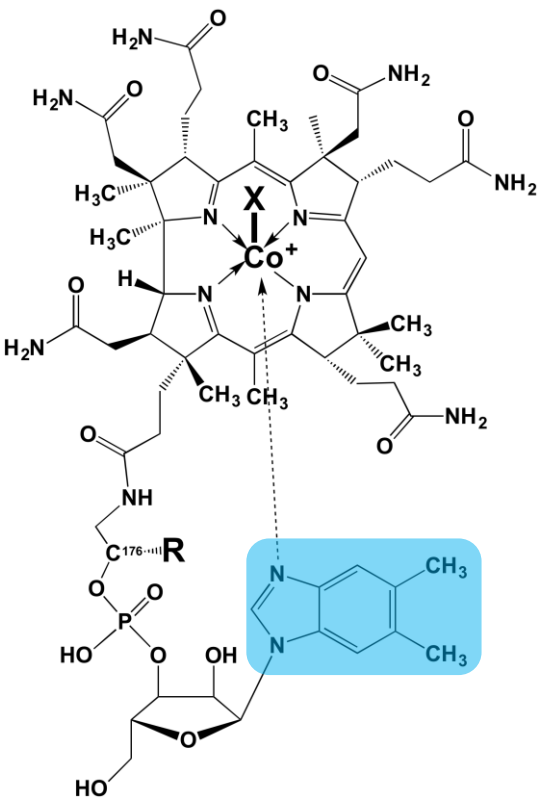


Figure 1: Corrinoid cofactor structure.

Corrinoid structure containing a corrin ring coordinating a central cobalt. The lower base (highlighted in blue) attaches to the corrin ring via a nucleotide tail. In the case of vitamin B_{12}, X is a cyano group and R is a methyl group.

Corrinoid auxotrophs rely on salvaging exogenous complete cobamides or incomplete precursor molecules or breakdown products [7, 10]. Auxotrophs that lack the machinery for *de novo* synthesis of the corrin ring system possess B_{12} uptake systems such as BtuB, TonB, and ABC transporters [11–13] and have remodeling capabilities by replacing the upper β-axial ligand and the lower α-axial base [7]. Considering that the majority of bacteria cannot synthesize the corrin ring system *de novo*, corrinoid prototrophs are likely to control key functions at the community level [14] **(Figure 2)**.

This study investigated the important interplay between corrinoid prototrophs and corrinoid auxotrophs by examining a novel O-methyltransferase gene in *G. lovleyi* strain SZ (SZ). Using *in vivo* heterologous expression, the following hypothesis was tested: Does Glov_3676 encode an O-methyltransferase that methylates 5-OHBza produced in *G. sulfurreducens* to 5-OMeBza produced in *G. lovleyi*? Because many organisms like *Dhc* salvage exogenous corrinoids and remodel their lower bases, the functional identity of Glov_3676 may provide predictive power in assessing functionality of corrinoid auxotrophs. For example, the presence and expression of this gene may correlate with *Dhc* activity and the complete detoxification of chlorinated ethenes to non-toxic ethene. The current study identifies an O-methyltransferase that modifies the corrinoid lower base structure with direct effects (i.e., control) over the growth and activity of microorganisms requiring specific cobamides in their energy metabolism.

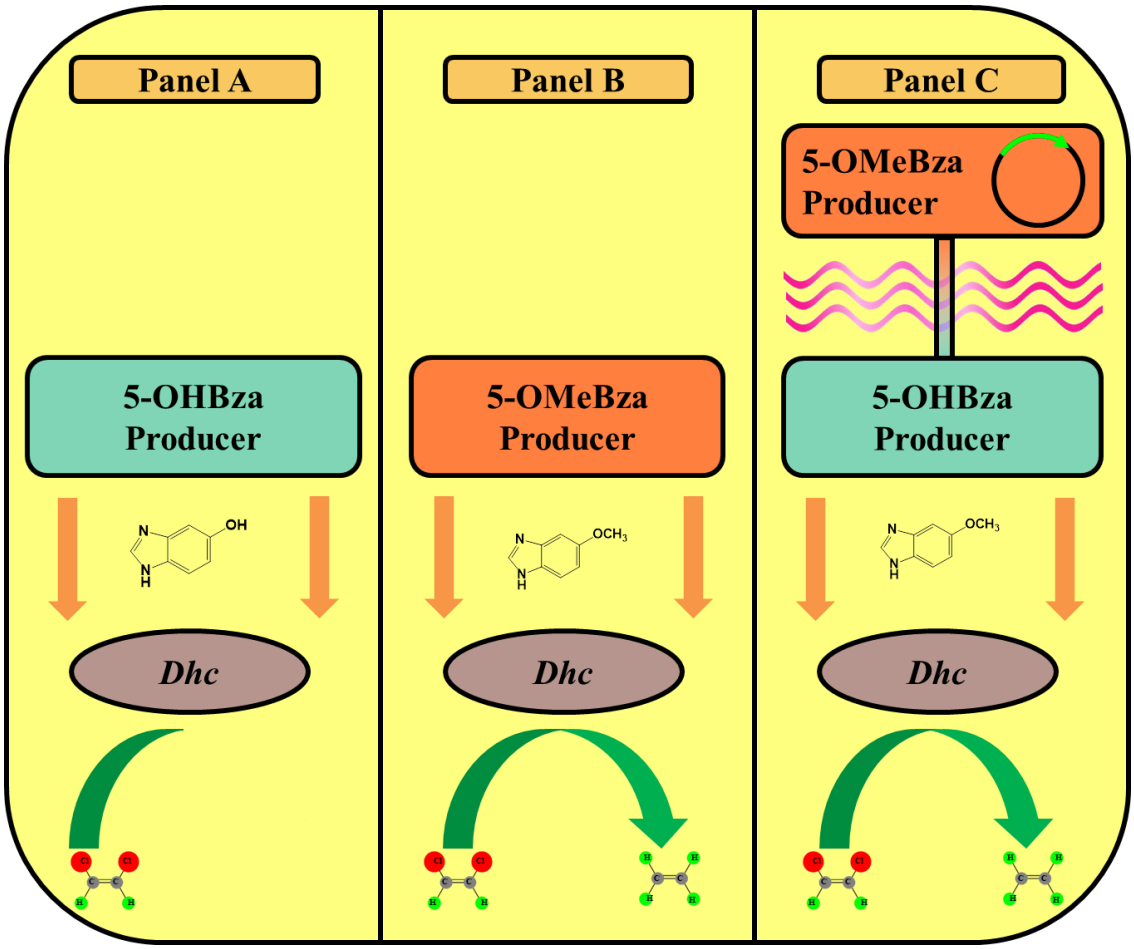


Figure 2: Interspecies corrinoid transfer.

(Panel A) 5-OHBza producer supplies *Dhc* with 5-OHBza, which fails to support dechlorination of *c*DCE. (Panel B) 5-OMeBza producer supplies *Dhc* with 5-OMeBza, which supports dechlorination of *c*DCE to ethene. (Panel C) 5-OMeBza producer exists in a nearby environment, and passes a Glov_3676 ortholog (green arrow) on an extrachromosomal element via conjugal mating to an otherwise native 5-OHBza producer. The recombinant 5-OMeBza producer then creates 5-OMeBza, which supports dechlorination of *c*DCE to ethene via *Dhc*. 5-OHBza, 5-hydroxybenzimidazole; 5-OMeBza, 5-methoxybenzimidazole.

Materials and Methods

Chemicals

Lower base compounds 5,6-dimethylbenzimidazole (DMB) (99%) and 5-methoxybenzimidazole (5-OMeBza) (97%) were purchased from Sigma-Aldrich (St. Louis, MO, USA). Vitamin B_{12} (96%) was purchased from Fisher Scientific (Hampton, NH, USA). Cobamide standards 5-OMeBza-Cba and 5-OHBza-Cba were prepared from *Sporomusa* sp. strain KB-1 via guided cobamide biosynthesis and *Methanosarcina barkeri* strain Fusaro (DSM 804), respectively [15]. Concentrations of purified cobamides were spectrophotometrically determined as described [16]. Ethene (99.9%) and chlorinated ethenes PCE (99%), TCE (99%), *c*DCE (99.5%) and vinyl chloride (99.5%) were purchased from Sigma-Aldrich (St. Louis, MO, USA). 2,6-Diaminopimelic acid (DAP) was acquired from Sigma-Aldrich (St. Louis, MO). 4-(2-hydroxyethyl) piperazine-1-ethanesulfonic acid (HEPES) and L-cysteine hydrochloride monohydrate were purchased from Fisher Scientific (Hampton, NH). Shrimp alkaline phosphatase (rSAP) and all restriction endonucleases were purchased from New England Biolabs (NEB) (Ipswich, MA). Sodium acetate (anhydrous, ≥99%) was purchased from J.T. Baker Chemical Co. (Phillipsburg, NJ). Sodium fumarate (98%) was purchased from Acros Organics (Fair Lawn, NJ). All other chemicals used in this study were reagent grade or higher.

Cultures and growth conditions

G. lovleyi strain SZ (ATCC BAA-1151), *G. sulfurreducens* strain PCA (ATCC 51573), and *Dehalococcoides mccartyi* strain BAV1 (ATCC BAA-2100) were obtained from laboratory stocks. *Geobacter* strains FEL048 and FEL050 were constructed as described in the *Strain Construction* section below. All *E. coli* liquid cultures were maintained in lysogeny broth (LB) medium [17] without glucose, amended with appropriate antibiotics, and incubated at 35°C on a rotary shaker at 250 rpm. Strains derived from strain FEL003 **(Table 1)** were supplemented with 100 µg/mL DAP to compensate for DAP auxotrophy. All *Geobacter* cultures were maintained in basal salts medium [18] with 15 mM acetate as the electron donor and 30 mM fumarate or 78 µmoles/bottle PCE as the electron acceptor. Medium preparation followed established procedures [18] except that sulfide was omitted, the L-cysteine concentration was increased to 1 mM, the bicarbonate buffer was replaced with 25 mM HEPES, and the pH was adjusted with 45% (w/v) KOH to 7.2. All components were autoclaved collectively except for fumarate, which was autoclaved separately and amended to sterilized medium. Plates with solid medium were prepared with 1.2% (w/v) agar purchased from Fisher Scientific (Hampton, NH) [19]. Cultures for isolating *Geobacter* native cobamides were scaled up to 1.8-L in 2.2-L vessels under the growth conditions described. *Dhc* cultures were grown anaerobically in 160-mL serum bottles containing 100 mL bicarbonate buffered synthetic mineral salt medium, a CO_2/N_2 (20/80, v/v) headspace and Wolin vitamin mixture with or w/o

Table 1: Strains used in Chapter 2.

Lab stock #	Strain	Species	Genotype	Reference
FEL002	BW25113	*E. coli*	*lacI*$^{+}$*rrnB*$_{T14}$ Δ*lacZ*$_{WJ16}$ *hsdR*514 Δ*araBAD*$_{AH33}$ Δ*rhaBAD*$_{LD78}$ *rph-1* Δ*(araB–D)567* Δ*(rhaD–B)568* Δ*lacZ4787*(::*rrnB-3*) *hsdR514 rph-1*	[38]
FEL003	BW29427	*E. coli*	*thrB1004 pro thi rpsL hsdS lacZ*Δ*M15 RP4-1360* Δ*(araBAD)567* Δ*dapA1341*::[*erm pir*]	K. Datsenko and B.L. Wanner
FEL004	—	*G. lovleyi* strain SZ	Wildtype	[39]
FEL005	—	*G. sulfurreducens* strain PCA	Wildtype	[40]
FEL031	—	*E. coli*	F-Δ(*argF lac)169*Φ*80dlacZ58*(ΔM15) *glnV44*(AS) *rfbD1 gyrA96*(Nal^{R}) *recA1 endA1spoT1 thi-1 hsdR17 deoR*λ*pir*+ / pDImcH2	[15]
FEL036	—	*E. coli*	*thrB1004 pro thi rpsL hsdS lacZ*Δ*M15 RP4-1360* Δ*(araBAD)567* Δ*dapA1341*::[*erm pir*] / pDImcH2	This study
FEL045	—	*E. coli*	*lacI*$^{+}$*rrnB*$_{T14}$ Δ*lacZ*$_{WJ16}$ *hsdR*514 Δ*araBAD*$_{AH33}$ Δ*rhaBAD*$_{LD78}$ *rph-1* Δ*(araB–D)567* Δ*(rhaD–B)568* Δ*lacZ4787*(::*rrnB-3*) *hsdR514 rph-1* / pNJ051	This study

Table 1: Strains used in Chapter 2 (continued).

Lab stock #	Strain	Species	Genotype	Reference
FEL046	—	*E. coli*	*lacI*$^{+}$*rrnB*$_{T14}$ Δ*lacZ*$_{WJ16}$ *hsdR*514 Δ*araBAD*$_{AH33}$ Δ*rhaBAD*$_{LD78}$ *rph-1* Δ*(araB–D)567* Δ*(rhaD–B)568* Δ*lacZ4787*(::*rrnB-3*) *hsdR514 rph-1* / pNJ052	This study
FEL047	—	*E. coli*	*thrB1004 pro thi rpsL hsdS lacZ*Δ*M15 RP4-1360* Δ*(araBAD)567* Δ*dapA1341*::[*erm pir*] / pNJ052	This study
FEL048	—	*G. sulfurreducens* strain PCA	Δ*imcH*::pDImcH2	This study
FEL050	—	*G. sulfurreducens* strain PCA	Δ*imcH*::pNJ052	This study

vitamin B_{12} as described [16]. *Dhc* strain BAV1 vessels received acetate (5 mM) as carbon source, hydrogen (10 mL/bottle) as electron donor, *c*DCE (66 µmoles/bottle) as electron acceptor and an addition of 50 µg/L vitamin B_{12} [18].

Guided cobamide biosynthesis in Geobacter

The impact of non-native cobamide biosynthesis on *Geobacter* growth and metabolisms was tested in 160-mL vessels containing 100 mL of the same synthetic mineral medium. Lower base stock solutions (5 mM) were prepared by dissolving 5-OMeBza or DMB powder in 10 mM hydrochloric acid and were then sterilized by passing through a 0.22 µm membrane filter (Fisher Scientific, Hampton, NH, USA). Triplicate strain PCA cultures received 20 µM of 5-OMeBza or DMB were grown under fumarate (10 mM) reducing conditions. Triplicate strain SZ cultures received 20 µM DMB and were grown under fumarate (10 mM) or PCE (0.5 mM in aqueous phase) reducing conditions. *Geobacter* growth was measured by a quantitative real time PCR assay or cell optical density reading at 600 nm (OD_{600}) using a spectrophotometer a Lambda 35 UV/VIS spectrometer (PerkinElmer, Waltham, MA, USA).

Genome analysis

Analysis of *G. lovleyi* and *G. sulfurreducens* genomes revealed genes implicated in the pathway for anaerobic DMB biosynthesis **(Figure 3)**, and suggested Glov_3676 as a gene involved in lower base biosynthesis. A Neighbor-Joining [20] tree was calculated based on nucleotide sequences of Glov_3676 and

displayed using MEGA7 [21]. Sequences were identified using neighborhood regions with best bidirectional blast hits (E-value 1e-20) on the Integrated Microbial Genomes (IMG) platform of the Joint Genome Institute (JGI). Gaps and missing data were removed by default. The nucleotide tree contains a sum branch length of 2.98588681, with evolutionary distances calculated by the p-distance method [22]. Reference genomes included (NCBI Biosample Accession Number given in parentheses): Composite genome from Trout Bog Hypolimnion pan-assembly TBhypo.metabat.2922.v2 (SAMN05518444), *Desulfobacterium vacuolatum* DSM 3385 (SAMN02746065), *Desulfobulbus mediterraneus* DSM 13871 (SAMN02441536), *Desulfoluna spongiiphila* AA1 (SAMN05216233), *Desulfospira joergensenii* DSM 10085 (SAMN02440566), *Desulfosporosinus orientis* Singapore I, DSM 765 (SAMN02261424), *Desulfuromonadales bacterium* GWD2_54_10 (SAMN03203001), *Eubacterium limosum* KIST612 (SAMN02603161), *Geobacter lovleyi* SZ (SAMN00623044), *Geobacter* sp. OR-1 (SAMD00017486), Geobacteraceae bacterium GWB2_52_12 (SAMN03202997), Geobacteraceae bacterium GWC2_53_11 (SAMN03202999), Geobacteraceae bacterium GWC2_55_20 (SAMN03202999), Geobacteraceae bacterium GWF2_54_21 (SAMN03203005), and KB-1 consortium (AY146780).

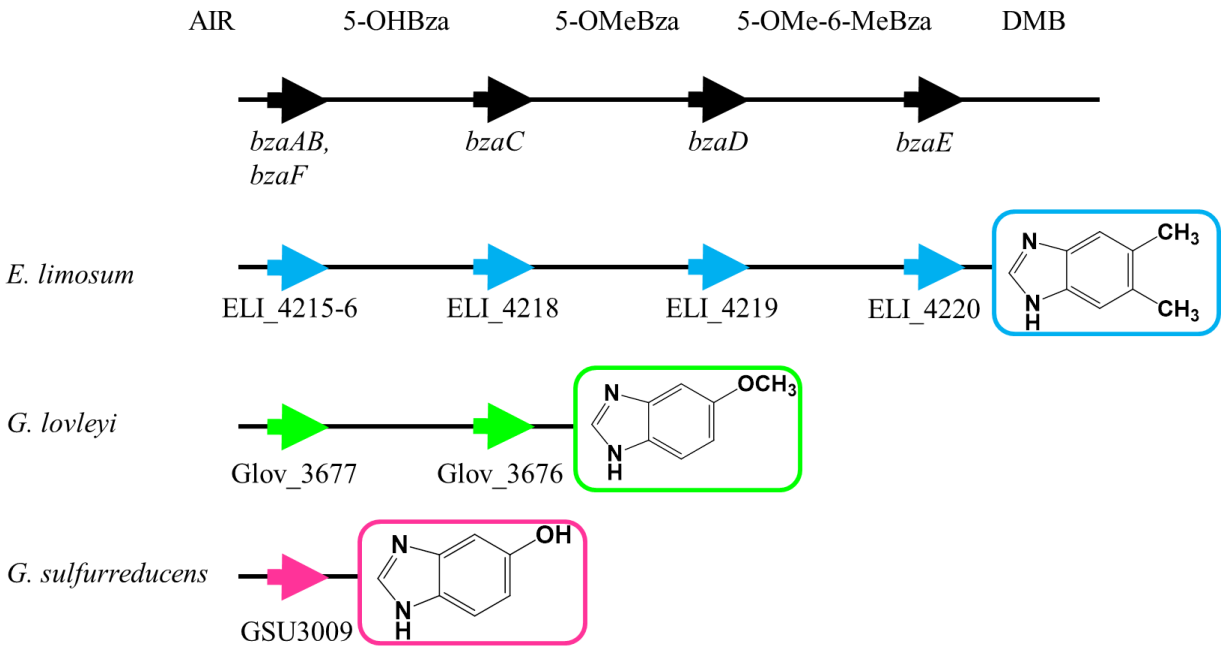


Figure 3: Comparison of lower base biosynthesis genes.

Genome analysis results comparing the previously published DMB pathway in *E. limosum* [29] to lower base biosynthesis genes in *G. lovleyi* and *G. sulfurreducens*. Colored arrows represent open reading frames (ORFs). Annotations are gene names or locus tags. Highlighted chemical structures indicate native lower base produced in each species. AIR, 5-aminoimidazole ribotide; 5-OHBza, 5-hydroxybenzimidazole; 5-OMeBza, 5-methoxybenzimidazole; 5-OMe-6-MeBza, 5-methoxy-6-methylbenzimidazole; DMB, 5,6-dimethylbenzimidazole.

Corrinoid extraction and analysis

Biomass was harvested by centrifugation at 10,000 x g for 30 min at 4°C from 0.3-1.8 L SZ and PCA cultures. Total intracellular corrinoids were extracted using the KCN extraction protocol and were purified using a C18 Sep-Pak cartridge (Waters Corp, Milford, MA) as described [4]. Corrinoid samples were analyzed using an Agilent 1200 high-performance liquid chromatography (HPLC) system equipped with an Eclipse XDB-C18 column (Agilent Technologies, 5 µm, 4.6 x 250 mm) and a diode array detector set at 361 nm. Samples (20-100 µL) were injected and separated at a flowrate of 1 mL/min at 30°C using 0.1% (v/v) formic acid in water (eluent A) and 0.1% (v/v) formic acid in methanol (eluent B) as mobile phases. The initial eluent composition was 82% eluent A and 18% eluent B, and eluent B increased linearly to 20% B over 34-min. and further to 90% over an additional 2-min. time period. Eluent B was held at 90% for 3 min. before the column was equilibrated to initial conditions. Mass spectrometry analysis was performed using a Dionex Ultimate 3000 system (Thermo Fisher Scientific, Waltham, MA) under described conditions [16].

Plasmid construction

Two plasmids were constructed to fuse the P_{acp}(vanO) synthetic promoter to Glov_3676, and move the expression cassette into the pDImcH2 [19] suicide vector backbone. To construct pNJ051, Glov_3676 was PCR-amplified with primers NJ475 (5'-GGCGCGCCCATATGATCCCGATTGTGGATGACTC-3') and NJ476 (5'-GGCGCGCCCATATGTCATAGTTCGTCCCTGTGCAGG-3') using the

G. lovleyi pSZ77 plasmid as template [23]. The resulting amplicon carried NdeI restriction sites flanked by AscI restriction sites. This amplicon was digested with NdeI and ligated into the pRK2-Geo2i-lacZa vector [19]. The pRK2-Geo2i-lacZa vector was digested with NdeI and treated with rSAP as per the manufacturer's instructions. The rSAP was heat-killed at 65°C for at least 15 min. Ligation was performed overnight at 4°C. All PCR amplicons used to construct pNJ051 were sequence-verified with primers NJ483 (5'-CGCTCCGCAGAGTTGTGGCAC-3') and NJ484 (5'-GAAAAGCGCGGAGATAAGCCCC-3') using Sanger sequencing performed at the University of Tennessee Genomics Core. **Table 2** and **Table 3** contain all plasmids and primers used in this study, respectively.

To construct pNJ052, The synthetic acyl carrier protein P_{acp}(vanO) promoter driving Glov_3676 was PCR-amplified with primers NJ481 (5'-GGCGCGCCCCCGGGATTGGATCCAATCTTGAAATTTAGGCG-3') and NJ482 (5'-GGCGCGCCCCCGGGTCATAGTTCGTCCCTGTGCAGGG-3') from pNJ051 to produce an amplicon carrying XmaI restriction sites flanked by AscI restriction sites. This amplicon was digested with XmaI and ligated into the pDImcH2 vector [19]. The pDImcH2 vector was digested with XmaI and treated with rSAP. The rSAP was heat-killed at 65°C for at least 15 min. Ligation was performed overnight at 4°C. All PCR amplicons used to construct pNJ052 were sequence-verified with NJ468 (5'-GGAATTGTGAGCGGATAACAATTTC-3'), NJ483 (5'-

Table 2: Plasmids used in Chapter 2.

	Plasmids	
Plasmid	**Description**	**Reference**
pDImcH2	Suicide vector designed to delete *imcH* (GSU3259) in *G. sulfurreducens* strain PCA	[15]
pNJ051	pRK2-Geo2i-lacZa with vanillate-inducible expression of Glov_3676 driven by P_{acp}(vanO) promoter	This study
pNJ052	pDImcH2 with Glov_3676 driven by P_{acp}(vanO) promoter	This study
pRK2-Geo2i-lacZa	Autonomously replicating vector in *G. sulfurreducens* strain PCA containing vanillate-inducible promoter P_{acp}(vanO)	[15]

Table 3: Primers used in Chapter 2.

Primers		
#	Sequence (5'-3')	5' Terminus
NJ013	GCCCCTGATGCTCTTCGTCC	N/A
NJ468	GGAATTGTGAGCGGATAACAATTTC	N/A
NJ475	GGCGCGCCCATATGATCCCGATTGTGGATGACTC	AscI, NdeI (partial)
NJ476	GGCGCGCCCATATGTCATAGTTCGTCCCTGTGCAGG	AscI, NdeI
NJ481	GGCGCGCCCCCGGGATTGGATCCAATCTTGAAATTTAGGCG	AscI, XmaI
NJ482	GGCGCGCCCCCGGGTCATAGTTCGTCCCTGTGCAGGG	AscI, XmaI
NJ483	CGCTCCGCAGAGTTGTGGCAC	N/A
NJ484	GAAAAGCGCGGAGATAAGCCCC	N/A
NJ489	CGGGATAGTTCCGCAGGACCCGG	N/A
NJ490	AGCGCCATCGGTGCCGCTCATC	N/A
NJ491	CCGCCGGCCTCAAGCGGGTACTG	N/A
NJ492	GAGCGCCCAATACGCAAACCGCC	N/A

Primers used in this study are presented in the 5'-3' orientation. Restriction endonuclease sites at the 5'-end of the primer are highlighted in green while those internal to the primer are highlighted in red.

CGCTCCGCAGAGTTGTGGCAC-3'), NJ484 (5'-GAAAAGCGCGGAGATAAGCCCC-3'), NJ491 (5'-CCGCCGGCCTCAAGCGGGTACTG-3'), and NJ492 (5'-GAGCGCCCAATACGCAAACCGCC-3').

Strain construction

E. coli strains were constructed via transformation of plasmid DNA using a Gene Pulser Xcell™ electroporation system (Bio-Rad, Hercules, CA) set at 1800 V, capacitance of 25 μF and resistance of 200 Ω in cuvettes with a 1-mm gap size. *E. coli* competent cells were prepared as recommended by the manufacturer. Donor strains of FEL036 and FEL047 and recipient strain FEL005 **(Table 1)** were diluted with LB to an OD_{600} of 0.35. Mating was initiated by plating the strains in donor:recipient ratios of 1:1, 1:3, 1:10 and 1:20. Conjugation mixtures were plated with the addition of 100 μg/mL of DAP to allow for growth of strains FEL036 and FEL047. Initial selection plates were incubated at 35°C overnight in an incubator placed inside an anoxic chamber containing N_2, CO_2 (10%), and H_2 (3%). Colonies on overnight selection plates for each donor:recipient ratio were suspended in 1 mL of basal salts medium [18]. The suspended conjugation mixtures were plated in 100 μL and 900 μL aliquots on solidified basal salts medium amended with 200 μg/mL kanamycin [24] to select for *G. sulfurreducens* conjugants. Conjugants were selected after 7 days into appropriate basal salts medium for strain verification. pDImcH2 and pNJ052 suicide vectors recombined

onto the *G. sulfurreducens* chromosome at the GSU3259 locus as described [19]. A detailed recombination graphic is presented in **Figure 4**.

Verification of pNJ052 integration on the G. sulfurreducens chromosome

Four different PCR screens were performed to verify the integration, localization, and orientation of the pNJ052 vector. A graphical chromosome map is presented in **Figure 5** with primers listed in **Table 3**.

To verify the presence of Glov_3676, PCR amplification with primer NJ491 (5'-CCGCCGGCCTCAAGCGGGTACTG-3') and primer NJ492 (5'-GAGCGCCCAATACGCAAACCGCC-3') produced a 1,633-bp band flanking the Glov_3676 locus in *G. lovleyi*. Conjugants producing this 1,633-bp band were presumed to harbor Glov_3676. When applied to the empty pDImcH2 vector, these primers produced a 500-bp band, indicating the absence of the 1,133-bp P_{acp}(vanO)+Glov_3676 cassette.

To determine the location of integration, isolates were screened by colony PCR with primers NJ489 (5'-CGGGATAGTTCCGCAGGACCCGG-3') and NJ490 (5'-AGCGCCATCGGTGCCGCTCATC-3') that flank the GSU3259 region of homology in *G. sulfurreducens*. This screen produced a 3,157-bp product from the wild type strain and an 11,438-bp product from the mutant strain, which encompasses the pNJ052 vector sequence following chromosomal integration. The results of this screen are indicative of site-specific integration.

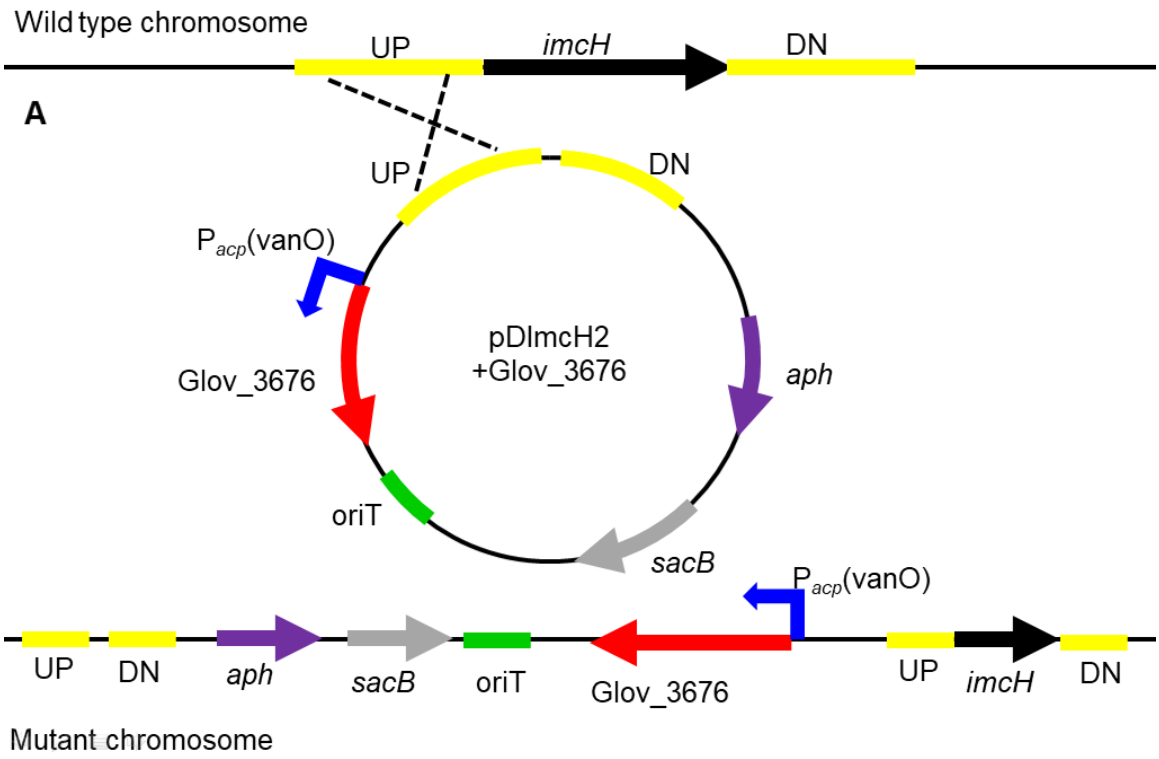


Figure 4: Homologous recombination of pNJ052 into *G. sulfurreducens.*

Chromosome maps of *G. sulfurreducens* GSU3259 locus before and after integration of pNJ052. **(a)** Upstream integration of pNJ052 onto the *G. sulfurreducens* chromosome via homologous recombination (upper fragment). Lower fragment represents mutant chromosome following pNJ052 recombination event. **(b)** Comparison of mutant chromosomes following homologous recombination of pDImcH2 (top fragment) and pNJ052 (bottom fragment). UP, 1 kB upstream of GSU3259; DN, 1 kB downstream of GSU3259; *aph*, aminoglycoside phosphotransferase gene conferring resistance to kanamycin; P_{acp}(vanO), synthetic *acp* promoter with integrated vanillate operator site; *sacB*, levansucrase gene conferring sensitivity to sucrose; Glov_3676, O-methyltransferase locus tag; *imcH*, inner membrane cytochrome H gene; oriT, origin of transfer.

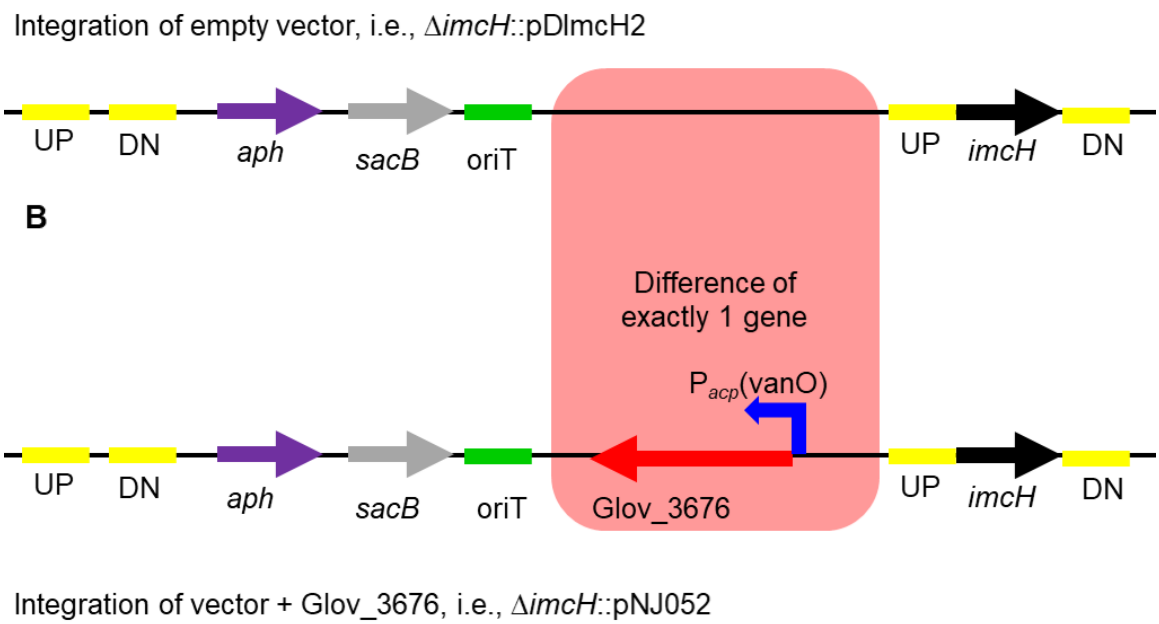


Figure 4: Homologous recombination of pNJ052 into *G. sulfurreducens* (continued).

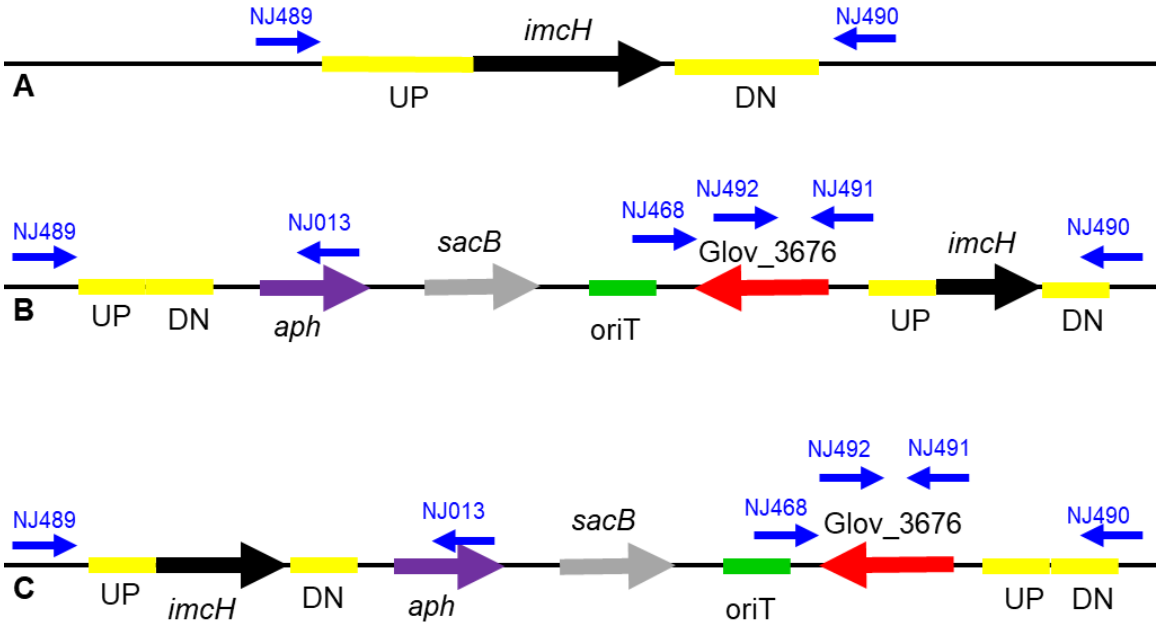


Figure 5: Chromosome map of PCR screening.

(a) Chromosome map of *imcH* (GSU3259) in wild type *G. sulfurreducens*. **(b)** Chromosome map of *imcH* (GSU3259) in *G. sulfurreducens* following chromosomal integration of pNJ052 upstream of GSU3259. **(c)** Chromosome map of *imcH* (GSU3259) in *G. sulfurreducens* following chromosomal integration of pNJ052 downstream of GSU3259. UP, 1 kB upstream of GSU3259; DN, 1 kB downstream of GSU3259; *aph*, aminoglycoside phosphotransferase gene conferring resistance to kanamycin; *sacB*, levansucrase gene conferring sensitivity to sucrose; Glov_3676, O-methyltransferase locus tag; *imcH*, inner membrane cytochrome H gene; oriT, origin of transfer; all NJ primers are described in **Table 3**.

To assess the integration orientation at the 5'-end of GSU3259, isolates were screened by colony PCR using primers NJ489 (5'-CGGGATAGTTCCGCAGGACCCGG-3') and NJ013 (5'-GCCCCTGATGCTCTTCGTCC-3') that flank the 5'-end of the integration site following the integration of pNJ052 into the GSU3259 locus. A 2,576-bp band is diagnostic of a recombination event via the upstream region of homology while a 4,079-bp band is indicative of a recombination event via the downstream region of homology.

To assess the integration orientation at the 3'-end of GSU3259, isolates were screened using colony PCR with primers NJ490 (5'-AGCGCCATCGGTGCCGCTCATC-3') and NJ468 (5'-GGAATTGTGAGCGGATAACAATTTC-3') that flank the 3'-end of the integration site following the integration of pNJ052 into the GSU3259 locus. A 4,271-bp band is diagnostic of a recombination via the upstream region of homology while a 2,768-bp band is indicative of a recombination event via the downstream region of homology. Similarly, to characterize the integration of the empty pDImcH2 vector, a 3,138-bp band is diagnostic of a recombination event via the upstream region of homology while a 1,635-bp band is indicative of a recombination event via the downstream region of homology.

Co-cultures

Defined co-cultures of a strain PCA mutant and *Dhc* were established in 160-mL serum bottles containing 100-mL vitamin B_{12}-free medium amended with acetate (10 mM), fumarate (20 mM) and *c*DCE (66 µmoles/bottle). Hydrogen (10 mL/bottle) was provided in the headspace as electron donor for *Dhc*. Each vessel received inocula from fumarate-grown strain PCA mutant culture (1%,v/v) and *c*DCE-grown *Dhc* culture (1%, v/v), the latter was centrifuged to remove supernatant and was re-suspended in vitamin B_{12}-free medium to minimize corrinoid carryover as described [16].

Conserved domain search

Conserved domain search was performed on lower base methyltransferases ELI_4218 (*E. limosum*) and Glov_3676 (*G. lovleyi*) against the CDD v3.16 – 50369 PSSMs database. Search conditions were set to an expect value threshold of 0.010000 and a maximum number of hits of 500. Results were adjusted for composition based statistics, which replaced the need for a low complexity filter, which would otherwise mask regions of low complexity [25–28].

Analysis of horizontal gene transfer

The IMG Putative Horizontally Transferred Genes tool [29] was applied to the *G. lovleyi* genome to identify possible horizontally transferred genes. Candidates for horizontal gene transfer (HGT) were identified within 95% of best hits (based on bitscore) belonging to a phylum outside that of the queried organism.

qPCR of G. sulfurreducens and Dhc 16S rRNA genes

Genomic DNA was extracted from cells harvested on 0.22 µm pore size membrane filters (Merck Millipore Ltd, Darmstadt, Germany) as described [16]. TaqMan qPCR assays consisted of two-fold Premix Ex Taq™ master mix (Takara Biomedical Technology Co. Ltd., Beijing, China), nuclease-free water, 250 nM probe, 250 nM of each primer and a DNA template, and were performed on a QuantStudio 3 Real-Time PCR system (Thermo Fisher Scientific, Waltham, MA). *Dhc* 16S rRNA gene copies were enumerated using primer set *Dhc*1200F/*Dhc*1271R and probe *Dhc*1240probe following established protocols [16]. To quantify the growth of the strain PCA mutant in co-cultures, a TaqMan qPCR assay targeting a number of *Geobacter* 16S rRNA genes, including those of strain PCA and strain SZ, was developed in this study. The forward primer GeoPCASZ16S_762qF (5'-GACGCTGAGACGCGAAAGC-3'), reverse primer GeoPCASZ16S_899qR (5'-TCCCAGGCGGAGTACTTAA-3') and probe GeoPCASZ_865P (5'-6FAM-CTGCAGTGCCGYAGCTAACGC-MGB-3') **(Table 3)** were designed using the Primer3 plug-in in Geneious 11.0. The thermal cycle conditions were as follows: 95°C for 30 sec., followed by 40 cycles of 5 sec at 95°C and 30 sec. at 60°C. Plasmid carrying the nearly complete sequence of the strain PCA 16S rRNA gene was used as DNA template to generate *Geobacter* assay standard curve as described [16].

Analytical methods

Ethene and chlorinated ethenes were quantified using an Agilent 7890 gas chromatograph and published methods [16]. Fumarate and succinate were analyzed using an Agilent 1200 HPLC system as described [16].

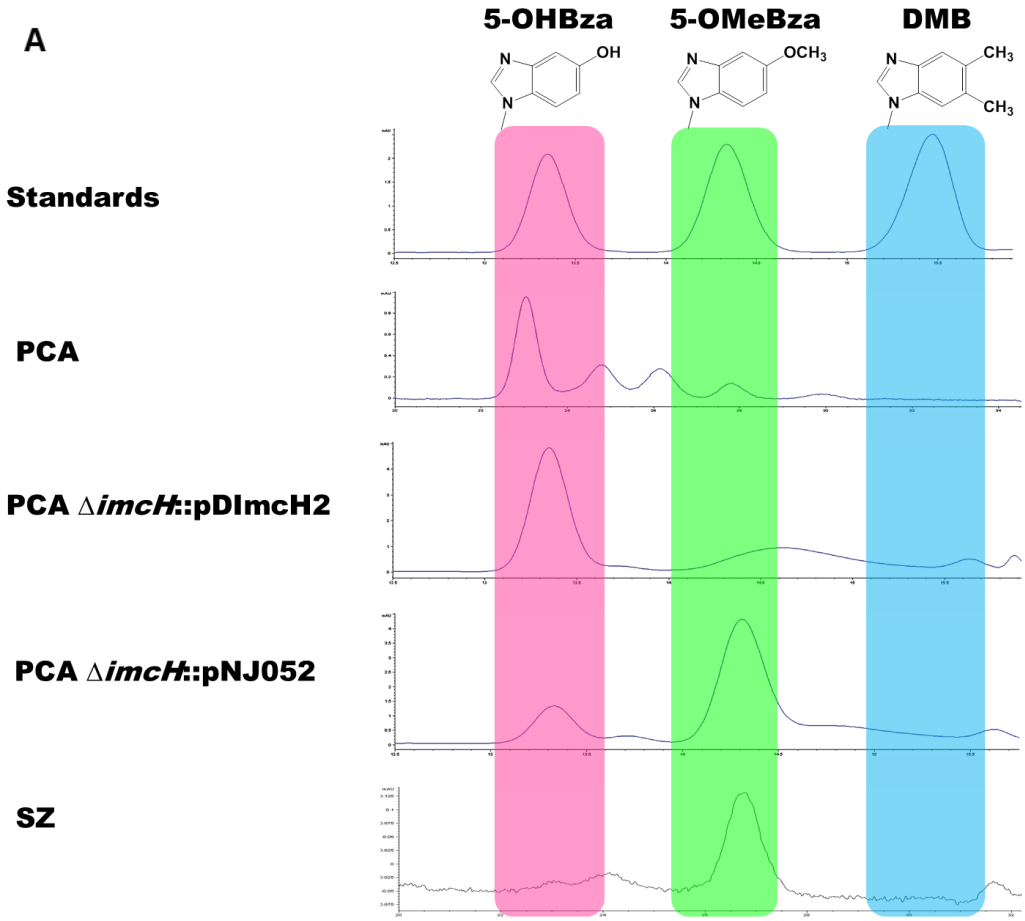
Results

5-OMeBza-Cba is the native cobamide synthesized in G. lovleyi strain SZ

Cobamide standards 5-OHBza-Cba, 5-OMeBza-Cba, and vitamin B_{12} were well separated into distinct peaks **(Figure 6)**. Corrinoid extracted from fumarate-grown PCA culture displayed an identical retention time with 5-OHBza-Cba **(Figure 6A)**, which is expected as 5-OHBza-Cba production in PCA had been reported. For SZ, a corrinoid with matching retention time to 5-OMeBza-Cba but not 5-OHBza-Cba or vitamin B_{12} was identified under both the fumarate reduction and PCE dechlorinating conditions **(Figure 6A)**. The mass spectrum of the SZ corrinoid **(Figure 6B)** corresponded to $[M+H^+]$ and $[M+Na^+]$ ions, confirming that the native corrinoid synthesized in SZ is indeed 5-OMeBza-Cba.

Non-native cobamides do not affect Geobacter metabolism

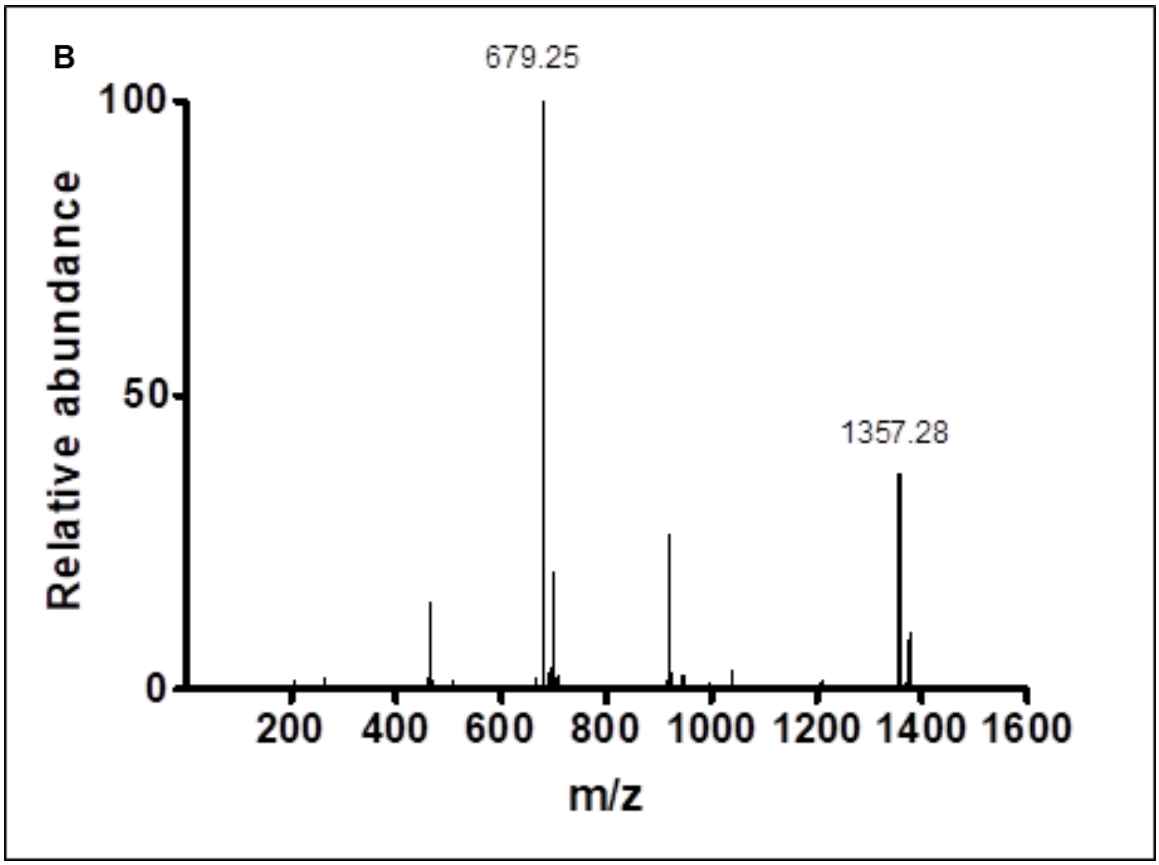
The amendment of DMB or a DMB precursor (i.e., 5-OMeBza-Cba) to strain PCA and strain SZ cultures resulted in the formation of respective cobamide (i.e., cobalamin, 5-OMeBza-Cba). The fumarate-grown strain PCA cultures producing 5-OHBza-Cba, 5-OMeBza-Cba, or cobalamin reached identical final cell densities with statistically indifferent growth rates **(Figure 6C)**. Similarly, strain



A. HPLC chromatograms of whole corrinoid extractions.

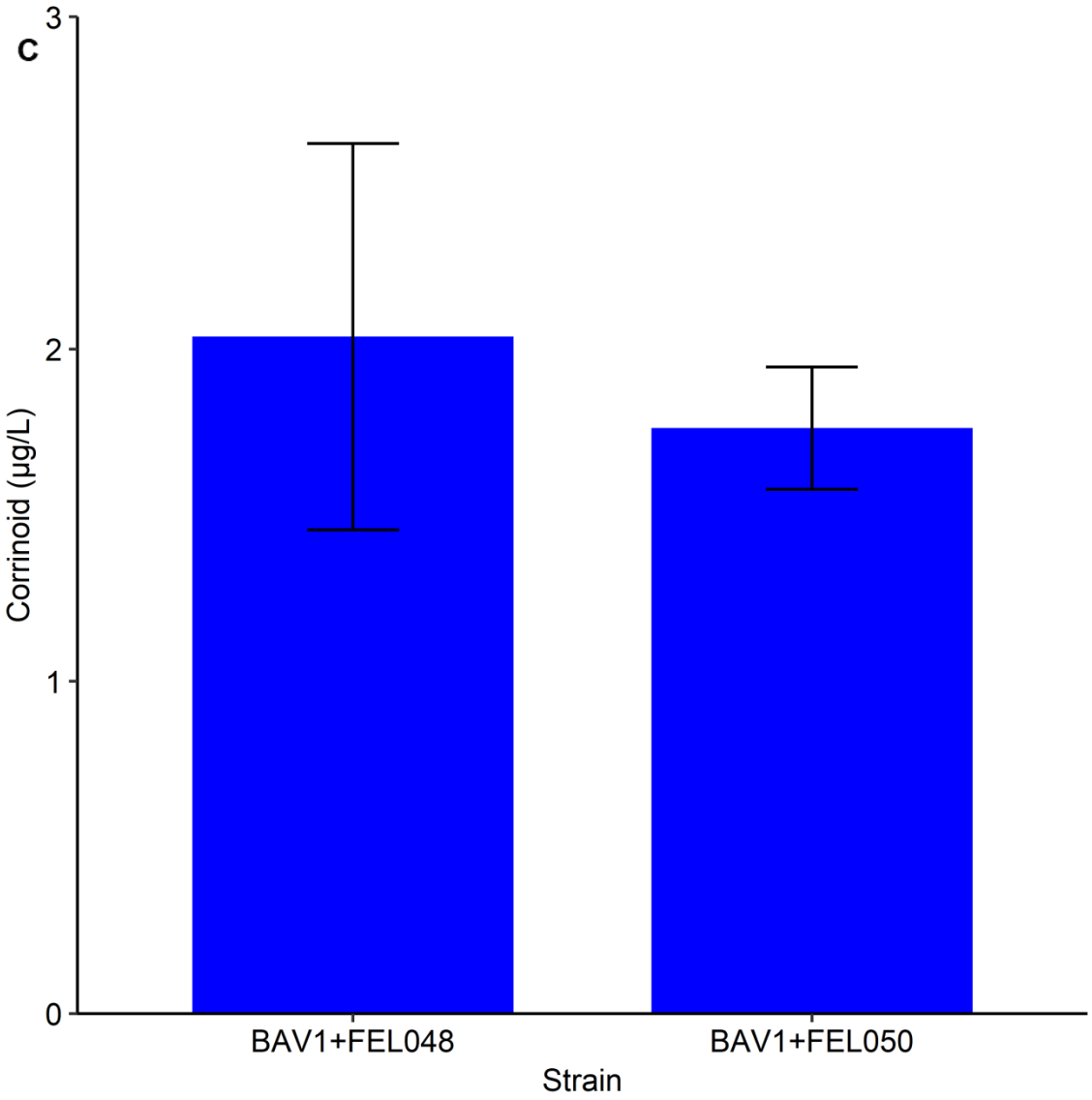
Figure 6: Identification and quantification of corrinoids carrying different lower bases.

(a) HPLC chromatograms of corrinoids compared to standards carrying 5-OHBza, 5-OMeBza, and DMB lower bases. PCA, wild type *G. sulfurreducens*; PCA Δ*imcH*::pDImcH2, *G. sulfurreducens* with the empty pDImcH2 vector integrated at the *imcH* gene (GSU3259 locus); PCA Δ*imcH*::pNJ052, *G. sulfurreducens* with pNJ052 carrying Glov_3676 integrated at the *imcH* gene (GSU3259 locus); SZ, wild type *G. lovleyi*. **(b)** LC-MS chromatograms of strains FEL005, FEL004, FEL048, and FEL050. **(c)** Concentration of 5-OHBza-Cba extracted from BAV1+FEL048 co-culture and 5-OMeBza-Cba extracted from BAV1+FEL050 co-culture.



B. LC-MS. Liquid chromatography (LC) separation and mass spectrometry (MS) analysis of 5-OMeBza-Cba isolated from strain FEL050.

Figure 6: Identification and quantification of corrinoids carrying different lower bases (continued).



C. Concentrations of corrinoids extracted from wild type and mutant strains

Figure 6: Identification and quantification of corrinoids carrying different lower bases (continued).

SZ cultures exhibited no difference in growth rates, growth yields and fumarate reduction / dechlorination rates under fumarate-reducing or PCE-dechlorinating conditions, respectively **(Figure 6C)**.

Genome analysis

A comprehensive comparison of putative lower base biosynthesis genes was performed between *G. lovleyi* and *G. sulfurreducens.* A single copy of *bzaF* was found in both genomes **(Figure 3)**, consistent with the production of 5-OHBza in *G. sulfurreducens* cultures. Compared to all other closed *Geobacter* genomes, only *G. lovleyi* was found to possess a gene immediately downstream of *bzaF*, in this case annotated as an O-methyltransferase (Glov_3676). The only other *Geobacter* species containing a similar gene directly downstream of *bzaF* is *Geobacter* sp. strain OR-1 (draft genome) [30].

The proximity and positioning of Glov_3676 with respect to *bzaF* in *G. sulfurreducens* suggested similar function with respect to *bzaC* of *E. limosum* (ELI_4218), a gene also located directly downstream of *bzaAB* [31]. However, an alignment comparing the amino acid sequences encoded by ELI_4218 and Glov_3676 yielded only 27.7% identity, well within the twilight zone of sequence alignments (i.e., 20-35% sequence identity) [32]. An in-depth comparison between these putative methyltransferases, along with two other closely related methyltransferases DCKB1_49050 from the KB-1 consortium [33] and

Ga0098289_103293 from *Geobacter* sp. OR-1, is presented in **Figure 7** and **Table 4**.

Functional characterization via heterologous expression

To identify the function of Glov_3676, the gene was cloned from *G. lovleyi* and heterologously expressed in *G. sulfurreducens* using the pNJ052 vector to create strain FEL050 **(Table 1)**. Approximately 2,000 conjugants/mL were typically observed on counter-selection plates from 1:1 donor:recipient ratios. Higher ratios of 1:10 and 1:20 produced too many colonies to count (data not shown). HPLC and LC-MS analyses revealed that each strain produced different corrinoids **(Figure 6)**. As expected, strain FEL048 produced 5-OHBza-Cba, indicating that the integration of pDImcH2 at the *imcH* locus carried no impact on corrinoid biosynthesis. Strain FEL050, in contrast, produced 5-OMeBza-Cba, which supported the hypothesis that Glov_3676 encodes an O-methyltransferase that is responsible for methylating 5-OHBza to 5-OMeBza.

Dechlorination in co-cultures

Previous studies have demonstrated the importance of the lower base in reductive dechlorination by corrinoid auxotrophic *Dhc* [9]. To test whether the FEL050 mutant strain of *G. sulfurreducens* can support the reductive dechlorination and thus growth of *Dhc* strain BAV1, co-cultures were established using these two species in the presence of *c*DCE. Unlike *G. lovleyi*, *G.*

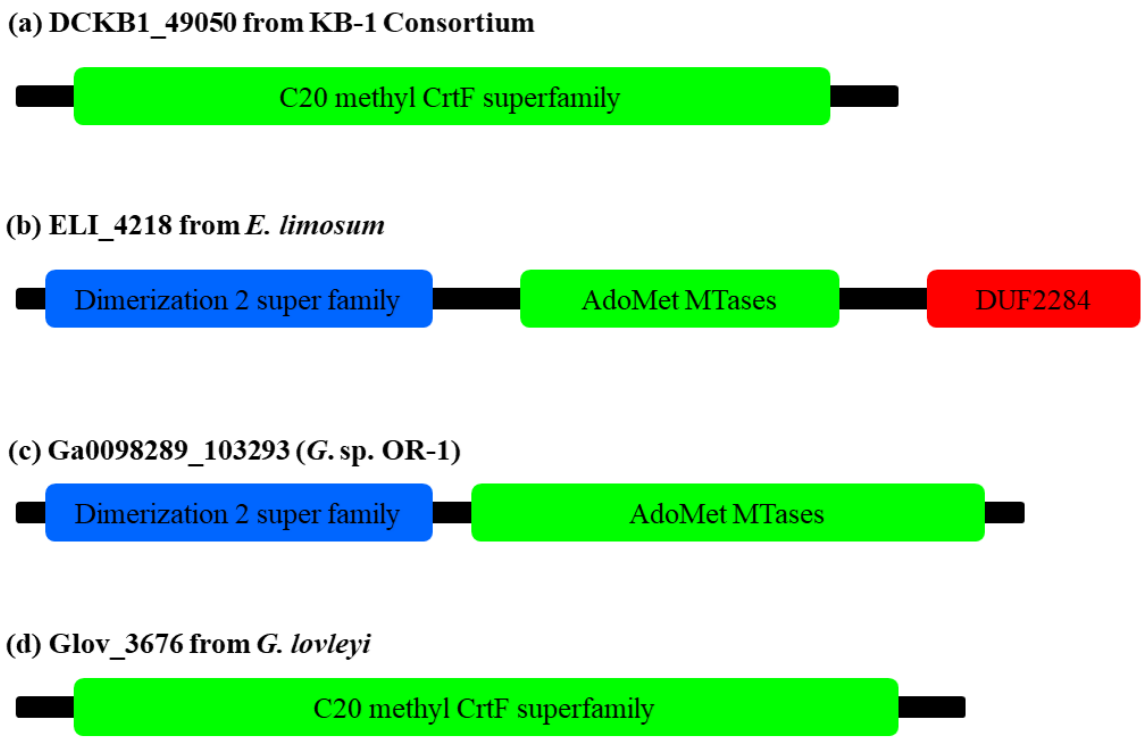


Figure 7: Lower base methyltransferase domain hits.

Graphical summary of domain hits of key lower base methyltransferases **(a)** DCKB1_49050 from KB-1 consortium, **(b)** ELI_4218 from *E. limosum*, **(c)** Ga0098289_103293 from *Geobacter* sp. OR-1, and **(d)** Glov_3676 from *G. lovleyi*. Details presented in **Table 4**. Figure is not drawn to scale.

Table 4: Comparison of key genes encoding lower base methyltransferases.

Locus tag	Annotation	Length		Domains	
		bp	AA	Name	Description
DCKB1_49050 (KB-1 Consortium)	Methyltransferase domain	1017	338	C20 methyl CrtF superfamily	C-20 methyltransferase BchU
ELI_4218 (*E. limosum*)	Protein of unknown function	1554	518	Dimerization 2 super family	Dimerization domain
				AdoMet MTases	S-adenosyl methionine-dependent methyltransferases
				DUF2284	Predicted metal-binding domain
Ga0098289_103293 (*G*. sp. OR-1)	O-methyltransferase	1065	533	Dimerization 2 super family	Dimerization domain
				AdoMet MTases	S-adenosyl methionine-dependent methyltransferases
Glov_3676 (*G. lovleyi*)	O-methyl-transferase family 2	1032	344	C20 methyl CrtF superfamily	C-20 methyltransferase BchU

DUF2284 domain belongs to Pfam10050. AdoMet_MTases domain belongs to cd02440 sequence cluster (superfamily cl17173). Dimerization 2 superfamily domain belongs to Pfam16864. C20 methyl CrtF superfamily belongs to the cl25581 superfamily. The C-20 methyltransferase BchU is responsible for bacteriochlorophyll c production in photosynthetic green sulfur bacteria [20–23]. bp, base pair; AA, amino acid.

sulfurreducens was unable to support reductive dechlorination of *Dhc* in co-cultures [16]. However, *Dhc* strain BAV1 dechlorination activity and ethene formation were observed in the co-culture with strain FEL050 **(Figure 8)**. This observation confirmed the hypothesis that strain FEL050 supports *Dhc* reductive dechlorination due to its newly acquired ability to synthesize the same lower base as *G. lovleyi*.

Horizontal transfer of Glov_3676

The IMG Putative Horizontally Transferred Genes tool [29] was applied to the *G. lovleyi* genome and revealed 253 genes classified as originating from outside the proteobacterium phylum, 56 of which, including Glov_3676, trace back to the phylum Firmicutes. Closer analysis using the same tool revealed Glov_3676 may trace back to Desor_2488, an annotated predicted metal-binding protein, in the Firmicute *Desulfosporosinus orientis* strain Singapore I (DSM 765) **(Figure** 9**)**. The converse search applying the Putative Horizontally Transferred Genes tool to *D. orientis* did not classify Desor_2488 as a product of horizontal gene transfer, suggesting it originated from within the Firmicute phylum. Though the type(s) of corrinoid produced by *D. orientis* has not been experimentally determined, the strain is likely a corrinoid prototroph, suggested by the 19 cobalamin riboswitches in *D. orientis* and 22 in its close relative *D. meridei* (DSM 13257) [34].

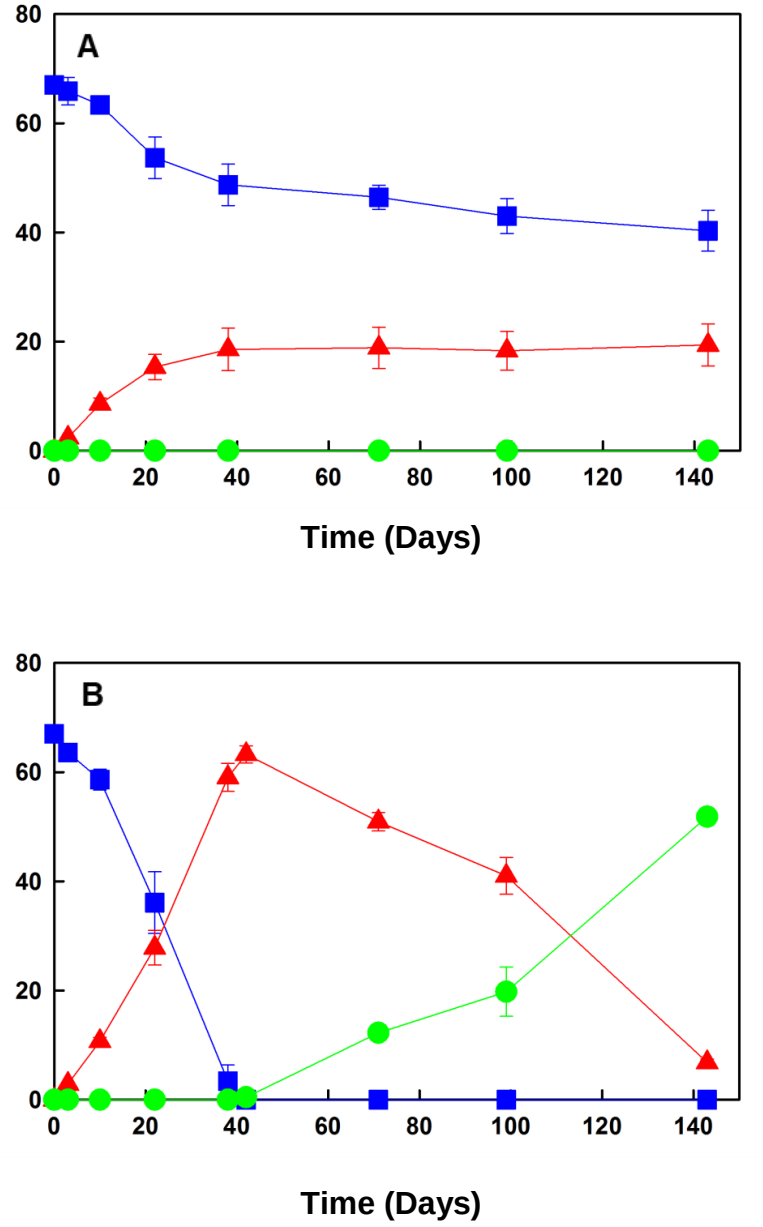


Figure 8: Dechlorination profile in co-cultures.

Dechlorination in co-cultures of (a) strain FEL048 with *Dhc* and (b) strain FEL050 with *Dhc*. Blue squares, *cis*-1,2-dichloroethene; red triangles, vinyl chloride; green circles, ethene.

Geobacter sp. strain OR-1 is the only other strain of *Geobacter* computationally predicted to carry a Glov_3676 ortholog (Ga0098289_103293), but its corrinoid profile is unknown. Protein BLAST against both copies of *G. lovleyi* PceAB did not reveal any orthologs in strain OR-1 (E-value 1e-5), suggesting the strain cannot perform reductive dechlorination. Ga0098289_103293 in *Geobacter* sp. strain OR-1 was identified as the only Glov_3676 ortholog (E-value 1e-125). Closer analysis of Ga0098289_103293 revealed that it is one of 81 putative horizontally transferred genes [29] from the order Desulfobacterales, specifically hitting a dimerization domain-containing protein (G494DRAFT_00354) in *Desulfobulbus mediterraneus* DSM 13871. Searching all the putative horizontally transferred genes in *D. mediterraneus* revealed that G494DRAFT_00354 is one of 39 predicted to be acquired from the order Desulfuromonadales, specifically Glov_3676 in *G. lovleyi*. This lineage tracing back to *G. lovleyi* suggests this O-methyltransferase ortholog was initially present in the Firmicute *D. orientis*, which was then transferred to the proteobacterium *G. lovleyi*, then transferred to the proteobacterium *D. mediterraneus*, and finally to the proteobacterium *Geobacter* sp. strain OR-1.

Discussion

The vast majority of organisms on our planet contain auxotrophies that must be complemented to permit metabolic activity. Nutritional auxotrophies and efforts to alleviate them can contribute to sculpting microbial communities across space and time [35, 36]. The *Dhc* group constitutes one such case as demonstrated by

its inability to produce its indispensable corrinoid cofactor. Importantly, *Dhc* uses this cofactor in an anaerobic respiratory process that is obligatorily coupled to the transformation of organohalogens as electron acceptors. Additionally, *Dhc* strains have been shown to scavenge or remodel corrinoids to suite their distinctive needs [7].

The *G. lovleyi* gene Glov_3676 was hypothesized to encode an O-methyltransferase that converts the 5-OHBza corrinoid lower base to 5-OMeBza. Two clues led to testing this hypothesis, namely genome analysis based on gene positioning and a relatively weak similarity of 27.7% based on a previous biochemically characterized methyltransferase (ELI_4218) from *E. limosum* [31]. The same study proposed that only a handful of anaerobic microorganisms is capable of synthesizing cobalamin, which is in fact required by a significant proportion of microorganisms [31]. A more recent study surveying over 11,000 species of bacteria found that 86% possess at least one cobamide-dependent enzyme, yet only 37% have the ability for *de novo* cobamide biosynthesis [37]. Based on gene content, the same survey [37] predicted only 9 species producing 5-OMeBza-Cba and 15 species producing DMB-Cba. Interestingly, all 15 DMB-producing species are predicted to produce DMB via *bzaAB*, and none through *bzaF* [37].

As shown in the current study, genes with less than 28% sequence similarity can encode enzymes with similar functions. The lower base can affect the activity of corrinoid-dependent enzymes [9], but only approximately half of these lower base structures can be predicted by sequence information alone [37]. Due to the lack of information about genes and pathways, bioinformatics cannot identity additional genes involved in elusive biosynthesis pathways of lower bases. Due to the prevalence of corrinoid auxotrophs compared to prototrophs, a reasonable postulate is that additional alternative pathways for lower base biosynthesis may exist. In anoxic environments, 62 species are predicted to produce 5-OHBza, 9 produce 5-OMeBza, 0 produce 5-methoxy-6-methyl-benzimidazole, and 15 produce DMB [37]. Organisms producing 5-OMeBza (including those harboring Glov_3676 orthologs) may therefore lead the community one step closer to DMB. Conversely, organisms producing 5-OMeBza may shift the community corrinoid pool away from 5-OHBza, which carries implications in cofactor competition. Shifting the corrinoid pool away from 5-OHBza-Cba and towards 5-OMeBza-Cba may provide a competitive advantage for organisms requiring 5-OMeBza-Cba over those that require 5-OHBza-Cba.

Glov_3676 not only allows *G. lovleyi* to produce 5-OMeBza-Cba, the gene also allows the corrinoid-auxotrophic community members access to the 5-OMeBza lower base. Cobamide release in the supernatant has been reported in pure cultures of *G. sulfurreducens* and *G. lovleyi*, in co-cultures with *Dhc* [16], and in

groundwater enrichments [38]. Corrinoid release and subsequent utilization by corrinoid-auxotrophs can impact community members, such as *Dhc* [39, 40]. As shown in **Figure 8**, negligible amounts of vinyl chloride were observed in cultures inoculated with *G. sulfurreducens* strain FEL048 and *Dhc,* but no ethene was produced. The engineered *G. sulfurreducens* mutant not only produced 5-OMeBza-Cba intracellularly, but also released this corrinoid extracellularly (even during exponential growth phase when cell lysis is not expected). The release of engineered corrinoids from *G. sulfurreducens* underscores and expands the importance of Glov_3676 as it not only alters lower base biosynthesis in the host carrying Glov_3676, but also makes 5-OMeBza available to the community.

Adding to the ecological significance of corrinoids is the potential for horizontal transfer of Glov_3676 amongst community members. A previous study has indicated the foreign acquisition of pSZ77 through the Codon Adaptation Index (CAI) of the replication initiation protein RepA (Glov_3681) and plasmid partitioning ATPase ParA (Glov_3684). Phylogenetic analysis further suggested that RepA was acquired from betaproteobacteria and gammaproteobacteria [23]. During plasmid maintenance, RepA binds and replicates the plasmid origin of replication while ParA partitions the plasmid copies to daughter cells. The lateral acquisition of pSZ77 carrying Glov_3676 indicates the potential for the plasmid-encoded O-methyltransferase gene to move across different hosts and impact corrinoid type and availability in different environments, in this case possibly into

the deltaproteobacteria (including *Geobacter* species) from the betaproteobacteria and gammaproteobacteria. Moreover, the 16 orthologs used to generate **Figure 9** span 2 phyla, highlighting the phylogenetic diversity of Glov_3676. Therefore, community members may not only be impacted by the released 5-OMeBza-Cba, but also by acquiring the genetic information leading to its synthesis. Glov_3676 can alter corrinoid pools not only through extracellular release of the corrinoid, but also through mobilization of genetic elements. Functional heterologous expression of Glov_3676 did not indicate other genes required to maintain functionality of the O-methyltransferase, suggesting consistent function of the Glov_3676 gene product being maintained following interspecies transfer. As demonstrated in strain FEL050, the introduction of a single Glov_3676 gene is sufficient to modify lower base structure.

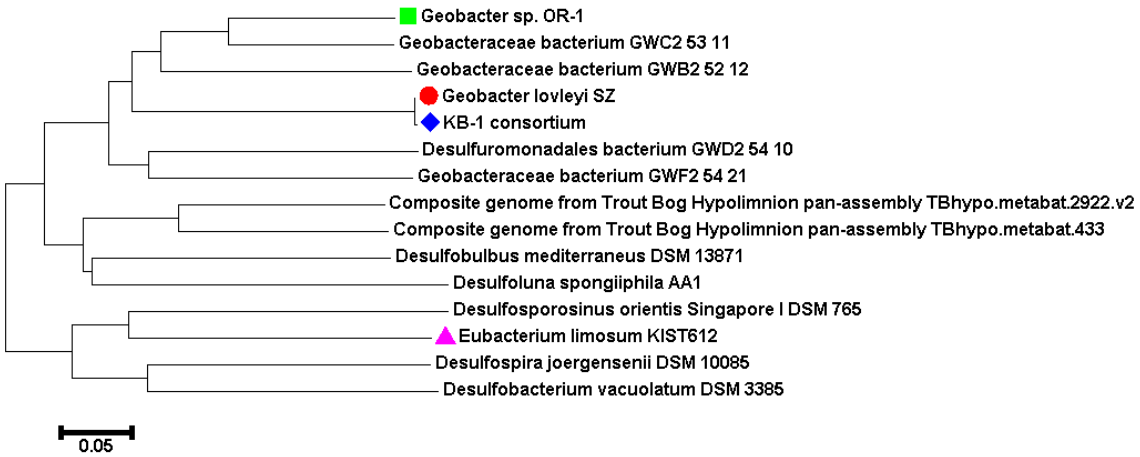


Figure 9: Phylogenetic analysis.

Neighbor-joining phylogenetic tree of Glov_3676 nucleotide sequence. Scale bar represents number of base differences per site. Key Glov_3676 orthologous sequences are denoted as ● *G. lovleyi* strain SZ, ♦ KB-1 consortium, ■ *Geobacter* sp. strain OR-1, and ▲ *E. limosum*.

To date, *G. lovleyi* is the only species of *Geobacter* known for organohalide respiration [23, 41]. Likewise, *G. lovleyi* is also the only *Geobacter* species confirmed to produce the 5-OMeBza corrinoid lower base. Previous studies have established that 5-OHBza is insufficient to sustain dechlorination activity in *Dhc* [9]. By extension, it may be possible that the *G. lovleyi* PCE RDase requires 5-OMeBza for activity. There is currently no genetic system in *G. lovleyi* that would test this possibility conclusively.

Assigning a biological function to Glov_3676 carries application potential for monitoring the activity of corrinoid-auxotrophic *Dhc*. Numerous studies have used the *Dhc* 16S rRNA gene as a biomarker to imply active dechlorination of sites contaminated with chlorinated solvents [42–44]. The detection of *Dhc* DNA in itself may be insufficient to confirm active dechlorination. Because *Dhc* strains require specific exogenous corrinoid cofactors to dechlorinate and thus respire, the co-occurrence of *Dhc* 16S rRNA genes with those involved in lower base biosynthesis may together provide more accurate evidence of dechlorination potential. The presence of Glov_3676 provides an additional line of evidence for *Dhc* activity. Therefore, Glov_3676 may serve as a biomarker to suggest that the community provides a cobamide that supports *Dhc* reductive dechlorination activity. For example, the KB-1 consortium [33] contains *G. lovleyi*, whose presence would suggest the availability of 5-OMeBza.

Data establishing the presence and quantification of lower base biosynthesis genes such as Glov_3676 (e.g., using qPCR) can serve as a strong complement to current remediation monitoring plans. The presence of DNA encoding essential cofactors carries actionable information for bioremediation practices in the field. The use of corrinoid lower base biomarkers, such as Glov_3676, offers increased predictive power when monitoring contaminated sites. Identifying the corrinoid pool of local microbial communities can thus translate into improved site management decision making. This application would be particularly useful in anoxic groundwater aquifers where cobalamin may be limiting, especially given that only 15 out of over 11,000 species are predicted to synthesize cobalamin *de novo* [37]. Identifying additional genes involved in lower base biosynthesis may improve understanding of dependencies and specific functionalities in complex microbial communities.

Corrinoid auxotrophy determines the growth of the majority of bacteria, as is the case with *Dhc*. A recent study predicts only 24% of bacteria can produce cobalamin [37]. By extension, obligatory dependence on exogenous sources of corrinoid may affect over half of all bacterial diversity. Through functional heterologous expression, the current study demonstrates that Glov_3676 plays a key role in 5-OMeBza-Cba biosynthesis. This study thus introduces the possibility of engineering corrinoids or corrinoid producers, which could be

exploited in synthetic ecology experiments to explore corrinoid specificity requirements of corrinoid auxotrophs.

Corrinoids impact microbiomes and biogeochemical cycles on a global scale. For example, corrinoid auxotrophs may impact the global carbon and nitrogen cycles. Algae have major contribution to carbon fixation [45–47], but a survey of over 300 species of microalgae revealed that over 50% require exogenous cobalamin [45]. The denitrifying *Paracoccus denitrificans* requires exogenous cobalamin for growth on nitrate, nitrite, or nitrous oxide [48]. The plant root nodule bacterium *Sinorhizobium meliloti* has also been shown to require vitamin B_{12} to fix nitrogen [49].

Introducing corrinoid availability as one of the many determinants of microbial activity demonstrates how microscopic organisms can have macroscopic effects, ranging from carbon and nitrogen cycling to medical complications including atrophic gastritis and pernicious anemia [45, 48–51]. At the same time, corrinoid auxotrophy also serves to interconnect microorganisms, where the initial existence of one establishes the necessarily subsequent existence of the other. This interdependence spans beyond the microscopic scale, as humans are also corrinoid auxotrophs.

Adverse changes to the gut microbiome can lead to disease states, and reversing these changes can restore healthy conditions [52]. In fact, the NIH

stresses several disease states related to the human microbiome, the majority of which lies in the gut [53]. One effective method of manipulating the gut microbiome involves introducing prebiotic substrates to select for a healthy microbiome [52, 54], including use of cobalamin [55]. Alternatively, live strains of probiotics can be used to regulate intestinal pH [56]. Synbiotics combines both methods by coupling the use of prebiotics to selectively aid growth of probiotics [52, 57]. Engineered probiotics with synthetic strains have been used to combat diseases [58, 59], suggesting corrinoid engineering could extend to manipulating the human microbiome [60].

Gut microbiota have been implicated in producing corrinoids with no bioavailability to humans, which could conceal deficiencies of vitamin B_{12} [61]. Furthermore, the same microbial corrinoid prototrophs supplying corrinoids to prokaryotic auxotrophs may also be doing so for their eukaryotic hosts. On the contrary, *Bacteroides* in the human gut can compete for vitamin B_{12} against their human hosts [62].

The specificity of the lower base of corrinoid molecules has been shown to confer different enzymatic effects on corrinoid-dependent enzymatic reactions [9, 63]. The corrinoid molecule can be transferred across species to maintain diverse community populations [38]. In the case of the horizontally acquired Glov_3676, its lateral acquisition may impose large effects at the community level by

supporting growth of corrinoid auxotrophs requiring 5-OMeBza as the lower base. Therefore, lateral acquisition of corrinoid biosynthesis genes has the potential to alter community diversity and function. For example, in environments with limited or no cobamide for *Dhc*, the introduction of genes such as Glov_3676 can alter the corrinoid pool. These findings emphasize the critical role of the community for sustaining the activity of corrinoid-auxotrophic organohalide-respiring Chloroflexi, including *Dhc*. The study further carries evolutionary implications on how new niches may be colonized by corrinoid prototrophs.

Acknowledgements

We thank D. R. Bond at the University of Minnesota for graciously providing vectors pDImcH2 and pRK2-Geo2i-lacZa, and N. Ivanova at the Joint Genome Institute (JGI) for clarifying bidirectional best hits on the Integrated Microbial Genomes (IMG) platform.

References

1. Marsh EN. Coenzyme B_{12} (cobalamin)-dependent enzymes. *Essays Biochem* 1999; **34**: 139–154.

2. González JC, Banerjee RV, Huang S, Sumner JS, Matthews RG. Comparison of cobalamin-independent and cobalamin-dependent methionine synthases from *Escherichia coli*: Two solutions to the same chemical problem. *Biochemistry (Mosc)* 1992; **31**: 6045–6056.

3. Ferguson T, Soares JA, Lienard T, Gottschalk G, Krzycki JA. RamA, a protein required for reductive activation of corrinoid-dependent methylamine methyltransferase reactions in methanogenic archaea. *J Biol Chem* 2009; **284**: 2285–2295.

4. Yan J, Bi M, Bourdon AK, Farmer AT, Wang P-H, Molenda O, et al. Purinyl-cobamide is a native prosthetic group of reductive dehalogenases. *Nat Chem Biol* 2017.

5. Froese DS, Gravel RA. Genetic disorders of vitamin B_{12} metabolism: eight complementation groups – eight genes. *Expert Rev Mol Med* 2010; **12**.

6. Crofts TS, Seth EC, Hazra AB, Taga ME. Cobamide structure depends on both lower ligand availability and CobT substrate specificity. *Chem Biol* 2013; **20**: 1265–1274.

7. Yi S, Seth EC, Men Y-J, Stabler SP, Allen RH, Alvarez-Cohen L, et al. Versatility in corrinoid salvaging and remodeling pathways supports corrinoid-dependent metabolism in *Dehalococcoides mccartyi*. *Appl Environ Microbiol* 2012; **78**: 7745–7752.

8. Rowena G. Matthews. Cobalamin- and corrinoid-dependent enzymes. *Met Ions Life Sci* 2009; **6**: 53–114.

9. Yan J, Şimşir B, Farmer AT, Bi M, Yang Y, Campagna SR, et al. The corrinoid cofactor of reductive dehalogenases affects dechlorination rates and extents in organohalide-respiring *Dehalococcoides mccartyi*. *ISME J* 2015; **10**: 1092–1101.

10. Men Y, Seth EC, Yi S, Allen RH, Taga ME, Alvarez-Cohen L. Sustainable growth of *Dehalococcoides mccartyi* 195 by corrinoid salvaging and remodeling in defined lactate-fermenting consortia. *Appl Environ Microbiol* 2014; **80**: 2133–2141.

11. Cadieux N, Bradbeer C, Reeger-Schneider E, Köster W, Mohanty AK, Wiener MC, et al. Identification of the periplasmic cobalamin-binding protein BtuF of *Escherichia coli*. *J Bacteriol* 2002; **184**: 706–717.

12. Gudmundsdottir A, Bell PE, Lundrigan MD, Bradbeer C, Kadner RJ. Point mutations in a conserved region (TonB box) of *Escherichia coli* outer membrane protein BtuB affect vitamin B_{12} transport. *J Bacteriol* 1989; **171**: 6526–6533.

13. Postle K, Kadner RJ. Touch and go: Tying TonB to transport. *Mol Microbiol* 2003; **49**: 869–882.

14. Romine MF, Rodionov DA, Maezato Y, Anderson LN, Nandhikonda P, Rodionova IA, et al. Elucidation of roles for vitamin $_{B12}$ in regulation of folate, ubiquinone, and methionine metabolism. *Proc Natl Acad Sci* 2017; **114**: E1205–E1214.

15. Yan J, Im J, Yang Y, Löffler FE. Guided cobalamin biosynthesis supports *Dehalococcoides mccartyi* reductive dechlorination activity. *Philos Trans R Soc B Biol Sci* 2013; **368**: 20120320.

16. Yan J, Ritalahti KM, Wagner DD, Löffler FE. Unexpected specificity of interspecies cobamide transfer from *Geobacter* spp. to organohalide-respiring *Dehalococcoides mccartyi strains* . *Appl Environ Microbiol* 2012; **78**: 6630–6636.

17. Bertani G. Studies on lysogenesis. I. The mode of phage liberation by lysogenic *Escherichia coli*. *J Bacteriol* 1951; **62**: 293–300.

18. Löffler FE, Sanford RA, Tiedje JM. Initial characterization of a reductive dehalogenase from *Desulfitobacterium chlororespirans* Co23. *Appl Environ Microbiol* 1996; **62**: 3809–3813.

19. Chan CH, Levar CE, Zacharoff L, Badalamenti JP, Bond DR. Scarless genome editing and stable inducible expression vectors for *Geobacter sulfurreducens*. *Appl Environ Microbiol* 2015; **81**: 7178–7186.

20. Saitou N, Nei M. The neighbor-joining method: a new method for reconstructing phylogenetic trees. *Mol Biol Evol* 1987; **4**: 406–425.

21. Kumar S, Stecher G, Tamura K. MEGA7: Molecular evolutionary genetics analysis version 7.0 for bigger datasets. *Mol Biol Evol* 2016; **33**: 1870–1874.

22. Masatoshi Nei, Sudhir Kumar. Molecular evolution and phylogenetics. 2000. Oxford University Press, Oxford, New York.

23. Wagner DD, Hug LA, Hatt JK, Spitzmiller MR, Padilla-Crespo E, Ritalahti KM, et al. Genomic determinants of organohalide-respiration in *Geobacter lovleyi*, an unusual member of the Geobacteraceae. *BMC Genomics* 2012; **13**: 200.

24. Coppi MV, Leang C, Sandler SJ, Lovley DR. Development of a genetic system for *Geobacter sulfurreducens*. *Appl Environ Microbiol* 2001; **67**: 3180–3187.

25. Marchler-Bauer A, Bryant SH. CD-Search: Protein domain annotations on the fly. *Nucleic Acids Res* 2004; **32**: W327-331.

26. Marchler-Bauer A, Lu S, Anderson JB, Chitsaz F, Derbyshire MK, DeWeese-Scott C, et al. CDD: A Conserved Domain Database for the functional annotation of proteins. *Nucleic Acids Res* 2011; **39**: D225-229.

27. Marchler-Bauer A, Derbyshire MK, Gonzales NR, Lu S, Chitsaz F, Geer LY, et al. CDD: NCBI's conserved domain database. *Nucleic Acids Res* 2015; **43**: D222-226.

28. Marchler-Bauer A, Bo Y, Han L, He J, Lanczycki CJ, Lu S, et al. CDD/SPARCLE: Functional classification of proteins via subfamily domain architectures. *Nucleic Acids Res* 2017; **45**: D200–D203.

29. Markowitz VM, Chen I-MA, Palaniappan K, Chu K, Szeto E, Grechkin Y, et al. The integrated microbial genomes system: An expanding comparative analysis resource. *Nucleic Acids Res* 2010; **38**: D382–D390.

30. Ehara A, Suzuki H, Amachi S. Draft genome sequence of *Geobacter* sp. strain OR-1, an arsenate-respiring bacterium isolated from Japanese paddy soil. *Genome Announc* 2015; **3**.

31. Hazra AB, Han AW, Mehta AP, Mok KC, Osadchiy V, Begley TP, et al. Anaerobic biosynthesis of the lower ligand of vitamin B12. *Proc Natl Acad Sci U S A* 2015; **112**: 10792–10797.

32. Rost B. Twilight zone of protein sequence alignments. *Protein Eng* 1999; **12**: 85–94.

33. Duhamel M, Mo K, Edwards EA. Characterization of a highly enriched *Dehalococcoides*-containing culture that grows on vinyl chloride and trichloroethene. *Appl Environ Microbiol* 2004; **70**: 5538–5545.

34. Choudhary PK, Duret A, Rohrbach-Brandt E, Holliger C, Sigel RKO, Maillard J. Diversity of cobalamin riboswitches in the corrinoid-producing organohalide respirer *Desulfitobacterium hafniense*. *J Bacteriol* 2013; **195**: 5186–5195.

35. Zengler K, Zaramela LS. The social network of microorganisms - how auxotrophies shape complex communities. *Nat Rev Microbiol* 2018; **16**: 383–390.

36. Jiang X, Zerfaß C, Feng S, Eichmann R, Asally M, Schäfer P, et al. Impact of spatial organization on a novel auxotrophic interaction among soil microbes. *ISME J* 2018; **12**: 1443–1456.

37. Shelton AN, Seth EC, Mok KC, Han AW, Jackson SN, Haft DR, et al. Uneven distribution of cobamide biosynthesis and dependence in bacteria predicted by comparative genomics. *ISME J* 2018.

38. Men Y, Seth EC, Yi S, Crofts TS, Allen RH, Taga ME, et al. Identification of specific corrinoids reveals corrinoid modification in dechlorinating microbial communities. *Environ Microbiol* 2015; **17**: 4873–4884.

39. Seth EC, Taga ME. Nutrient cross-feeding in the microbial world. *Front Microbiol* 2014; **5**.

40. Abreu NA, Taga ME. Decoding molecular interactions in microbial communities. *FEMS Microbiol Rev* 2016; **40**: 648–663.

41. Sung Y, Fletcher KE, Ritalahti KM, Apkarian RP, Ramos-Hernández N, Sanford RA, et al. *Geobacter lovleyi* sp. nov. strain SZ, a novel metal-reducing and tetrachloroethene-dechlorinating bacterium. *Appl Environ Microbiol* 2006; **72**: 2775–2782.

42. Matturro B, Frascadore E, Rossetti S. High-throughput sequencing revealed novel Dehalococcoidia in dechlorinating microbial enrichments from PCB-contaminated marine sediments. *FEMS Microbiol Ecol* 2017; **93**.

43. Munro JE, Kimyon Ö, Rich DJ, Koenig J, Tang S, Low A, et al. Co-occurrence of genes for aerobic and anaerobic biodegradation of dichloroethane in organochlorine-contaminated groundwater. *FEMS Microbiol Ecol* 2017; **93**.

44. Lu Q, Yu L, Liang Z, Yan Q, He Z, Luan T, et al. *Dehalococcoides* as a potential biomarker evidence for uncharacterized organohalides in environmental samples. *Front Microbiol* 2017; **8**: 1677.

45. Croft MT, Warren MJ, Smith AG. Algae need their vitamins. *Eukaryot Cell* 2006; **5**: 1175–1183.

46. Sayre R. Microalgae: The potential for carbon capture. *BioScience* 2010; **60**: 722–727.

47. Field CB, Behrenfeld MJ, Randerson JT, Falkowski P. Primary production of the biosphere: Integrating terrestrial and oceanic components. *Science* 1998; **281**: 237–240.

48. Shearer N, Hinsley AP, Spanning RJMV, Spiro S. Anaerobic growth of *Paracoccus denitrificans* requires cobalamin: Characterization of *cobK* and *cobJ* genes. *J Bacteriol* 1999; **181**: 6907–6913.

49. Campbell GRO, Taga ME, Mistry K, Lloret J, Anderson PJ, Roth JR, et al. *Sinorhizobium meliloti bluB* is necessary for production of 5,6-dimethylbenzimidazole, the lower ligand of B_{12}. *Proc Natl Acad Sci U S A* 2006; **103**: 4634–4639.

50. Allen LH, Miller JW, de Groot L, Rosenberg IH, Smith AD, Refsum H, et al. Biomarkers of nutrition for development (BOND): Vitamin B_{12} review. *J Nutr* 2018; **148**: 1995S–2027S.

51. Rodriguez-Castro KI, Franceschi M, Noto A, Miraglia C, Nouvenne A, Leandro G, et al. Clinical manifestations of chronic atrophic gastritis. *Acta Bio-Medica Atenei Parm* 2018; **89**: 88–92.

52. Lee HL, Shen H, Hwang IY, Ling H, Yew WS, Lee YS, et al. Targeted approaches for *in situ* gut microbiome manipulation. *Genes* 2018; **9**.

53. NIH HMP Working Group, Peterson J, Garges S, Giovanni M, McInnes P, Wang L, et al. The NIH Human Microbiome Project. *Genome Res* 2009; **19**: 2317–2323.

54. Gibson GR, Hutkins R, Sanders ME, Prescott SL, Reimer RA, Salminen SJ, et al. Expert consensus document: The International Scientific Association for

Probiotics and Prebiotics (ISAPP) consensus statement on the definition and scope of prebiotics. *Nat Rev Gastroenterol Hepatol* 2017; **14**: 491–502.

55. Degnan PH, Taga ME, Goodman AL. Vitamin B_{12} as a modulator of gut microbial ecology. *Cell Metab* 2014; **20**: 769–778.

56. Hill C, Guarner F, Reid G, Gibson GR, Merenstein DJ, Pot B, et al. Expert consensus document: The International Scientific Association for Probiotics and Prebiotics consensus statement on the scope and appropriate use of the term probiotic. *Nat Rev Gastroenterol Hepatol* 2014; **11**: 506–514.

57. Chiu W-C, Huang Y-L, Chen Y-L, Peng H-C, Liao W-H, Chuang H-L, et al. Synbiotics reduce ethanol-induced hepatic steatosis and inflammation by improving intestinal permeability and microbiota in rats. *Food Funct* 2015; **6**: 1692–1700.

58. Kurtz CB, Millet YA, Puurunen MK, Perreault M, Charbonneau MR, Isabella VM, et al. An engineered *E. coli* Nissle improves hyperammonemia and survival in mice and shows dose-dependent exposure in healthy humans. *Sci Transl Med* 2019; **11**.

59. Bozkurt HS, Quigley EM, Kara B. *Bifidobacterium animalis* subspecies *lactis* engineered to produce mycosporin-like amino acids in colorectal cancer prevention. *SAGE Open Med* 2019; **7**: 2050312119825784.

60. Foo JL, Ling H, Lee YS, Chang MW. Microbiome engineering: Current applications and its future. *Biotechnol J* 2017; **12**.

61. Jory J. Cobalamin, microbiota and epigenetics. In: Patel V, Preedy V (eds). *Handbook of Nutrition, Diet, and Epigenetics*. 2017. Springer International Publishing, Cham, pp 1–19.

62. Wexler AG, Schofield WB, Degnan PH, Folta-Stogniew E, Barry NA, Goodman AL. Human gut *Bacteroides* capture vitamin B_{12} via cell surface-exposed lipoproteins. *eLife* 2018; **7**: e37138.

63. Kenny C. Mok, Michiko E. Taga. Growth inhibition of *Sporomusa ovata* by incorporation of benzimidazole bases into cobamides. *J Bacteriol* 2013; **195**: 1902–1911.

64. Datsenko KA, Wanner BL. One-step inactivation of chromosomal genes in *Escherichia coli* K-12 using PCR products. *Proc Natl Acad Sci U S A* 2000; **97**: 6640–6645.

65. Caccavo F, Lonergan DJ, Lovley DR, Davis M, Stolz JF, McInerney MJ. *Geobacter sulfurreducens*) sp. nov., a hydrogen- and acetate-oxidizing dissimilatory metal-reducing microorganism. *Appl Environ Microbiol* 1994; **60**: 3752–3759.

CHAPTER III
G. SULFURREDUCENS METHYLATES MERCURY INDEPENDENT OF THE TYPE OF CORRINOID LOWER BASE

Reproduced in part with permission from Jiang N, Soren AB, Cooper SJ, Date SS, Parks JM, Johs A, Yan J, Gilmour CC, and Löffler FE. *G. sulfurreducens* methylates mercury independent of the type of corrinoid lower base. In preparation. All copyright interests will be exclusively transferred to the publisher upon submission.

Abstract

Mercury is a pervasive global contaminant and neurotoxin. Its methylated and dimethylated forms exacerbate the toxicity and can lead to bioaccumulation in aquatic species leading up the food chain. Mercury contamination is especially relevant to Oak Ridge, TN, USA, where upwards of 2.4 million pounds of mercury have been introduced to the environment since 1950. The macroscopic effects of mercury exposure and poisoning are indeed mediated by microscopic reactions. In 2013, the ORNL Mercury Science Focus Area (SFA) team discovered two genes involved in the mercury methylation process, *hgcA* and *hgcB* (1). HgcA is annotated as a corrinoid binding protein and HgcB is an iron-sulfur cluster containing protein, suggesting cofactor availability and specificity may regulate mercury methylation. Genetic studies then followed in the model mercury methylator *Desulfovibrio desulfuricans* strain ND132. Recent studies in reductive dehalogenase enzyme systems have demonstrated the importance of the specific type of corrinoid bound in corrinoid-dependent reactions. Contrary to the reductive dehalogenase enzymes, we show in this study that the corrinoid-dependent mercury methylation reaction may function independently of the type of corrinoid lower base.

Importance

Bacterial mercury methylation plays a major role in the formation of methylmercury from elemental mercury. Identifying factors regulating this methylation process may provide predictive power in assessing environmental methylmercury concentrations and flux. Here, we show that the corrinoid lower base may not play a dominant role in the mercury methylation reaction.

Introduction

Mercury (Hg) is a persistent environmental contaminant originating from natural and anthropogenic sources (2). Methylmercury (MeHg), its organic methylated form, causes increased neurotoxicity and bioaccumulation, particularly in the aquatic food chain (3). As such, it is important to identify and characterize the mercury methylation process on a molecular scale. In this respect, a key 2013 study identified the *hgcAB* genes responsible for mercury methylation in *Desulfovibrio desulfuricans* strain ND132 and *Geobacter sulfurreducens* strain PCA. Subsequent deletion of these genes abolished mercury methylation activity (1).

HgcAB are both cofactor-binding proteins, where HgcA binds a corrinoid cofactor and HgcB binds an iron-sulfur cluster. These annotations, together with homology modeling, suggest mercury methylation may intimately depend on accessibility to specific cofactors. Nature has already revealed several corrinoid-dependent enzyme systems, including methionine synthases, epoxyqueuosine

reductases, isobutyryl-CoA mutases, and the reductive dehalogenases (4). More recent studies have added an additional role for corrinoids as light-dependent gene regulators at the level of gene transcription (5, 6). Indeed, many organisms are auxotrophic for essential cofactors and thus may rely entirely on environmental availability. For example, a study that screened over 11,000 species found that only 37% could produce cobamides although 86% required them as cofactors (7).

Structurally, corrinoids are characterized by a corrin ring connected to a lower base by a ribonucleotide tail (8). Recent studies have implicated the lower base of corrinoid cofactors as potentially regulating enzymatic activity (9, 10). Other studies have revealed how the native methylator *G. sulfurreducens* can produce corrinoids carrying different lower bases, including 5-hydroxybenzimidazole (5-OHBza), 5-methoxybenzimidazole (5-OMeBza) (Chapter 2), and 5,6-dimethylbenzimidazole (DMB) (11). Here, we hypothesize that these different lower base structures can impact the rate and extent of mercury methylation.

Materials and Methods

Chemicals

All chemicals were previously described (Chapter 2).

Cultures

G. sulfurreducens strain PCA (ATCC 51573) was obtained from laboratory stocks. All strains used in this study are described in **Table 5**.

Medium and growth conditions

Geobacter cultures were maintained on basal salts medium at 35°C as previously described (Chapter 2). Batch cultures were grown to mid-exponential phase for mercury analysis. pH was determined using 3 ml of endpoint cultures.

Growth curves

Geobacter growth curves were performed in previously defined anoxic medium (Chapter 2) in an anoxic chamber (Coy Laboratory Products, Inc.) with headspace composition 10% CO_2, 3% H_2, balance N_2. Optical densities (OD) at 600 nm were measured in triplicate cultures using an ULTROSPEC® 10 Cell Density Meter (Biochrom Ltd, Cambridge, UK). Endpoint ODs were taken using 3 ml of culture following mercury methylation assays.

Table 5: Strains used in Chapter 3.

Lab stock #	Species	Genotype	Reference
FEL005	*G. sulfurreducens* strain PCA	Wild type	(22)
FEL048	*G. sulfurreducens* strain PCA	Δ*imcH*::pDImcH2	(Chapter 2)
FEL050	*G. sulfurreducens* strain PCA	Δ*imcH*::pNJ052	(Chapter 2)

Guided cobalamin biosynthesis

Geobacter cultures were amended with exogenous 5,6-dimethylbenzimidazole (DMB) to produce cobalamin through guided cobalamin biosynthesis (11).

Mercury methylation quantification

Methylation assays lasted 71 hours and were amended with 1 nM $^{201}HgCl_2$. Hg and MeHg quantification were performed using enriched stable isotopes as described (12). Each measurement used 10 ml of acidified culture. Mercury was amended using $^{201}HgCl_2$.

Sulfide quantification

For sulfide quantification, 3 ml of culture were transferred into sulfide antioxidant buffer (SAOB) (13) and measured immediately with an ion-specific electrode as described (14).

PCR screens

All strain genotypes were verified by PCR following MeHg analysis. Two PCR-based screens were performed on endpoint cultures to ensure mutant genotype. The first screen used primers NJ487 (5'-ATGATCCCGATTGTGGATGACTCCTTTG-3') and NJ488 (5'-TAGTTCGTCCCTGTGCAGGGCAAC-3') that produced a 1,032-bp amplicon from Glov_3676. This amplicon is only expected from strain FEL050. The second PCR screen used primers NJ489 (5'-CGGGATAGTTCCGCAGGACCCGG-3') and NJ490 (5'-AGCGCCATCGGTGCCGCTCATC-3') that flank the GSU3259

locus to produce a 3,157-bp amplicon exclusively from strain FEL005. It should be noted that applying the latter screen could in principle produce a 10,304-bp amplicon from strain FEL048 or an 11,437-bp amplicon from strain FEL050, but the PCR extension time was limited to 5 min to prevent such large amplicons from forming. All primers used in this study are described in **Table 6** and apply to the chromosome map displayed in **Figure 10**. Expected amplicon sizes are summarized in **Table 7**.

Table 6: Primers used in Chapter 3.

Primers		
#	**Sequence (5'-3')**	**Reference**
NJ487	**ATGATCCCGATTGTGGATGACTCCTTTG**	This study
NJ488	**TAGTTCGTCCCTGTGCAGGGCAAC**	This study
NJ489	**CGGGATAGTTCCGCAGGACCCGG**	(Chapter 2)
NJ490	**AGCGCCATCGGTGCCGCTCATC**	(Chapter 2)

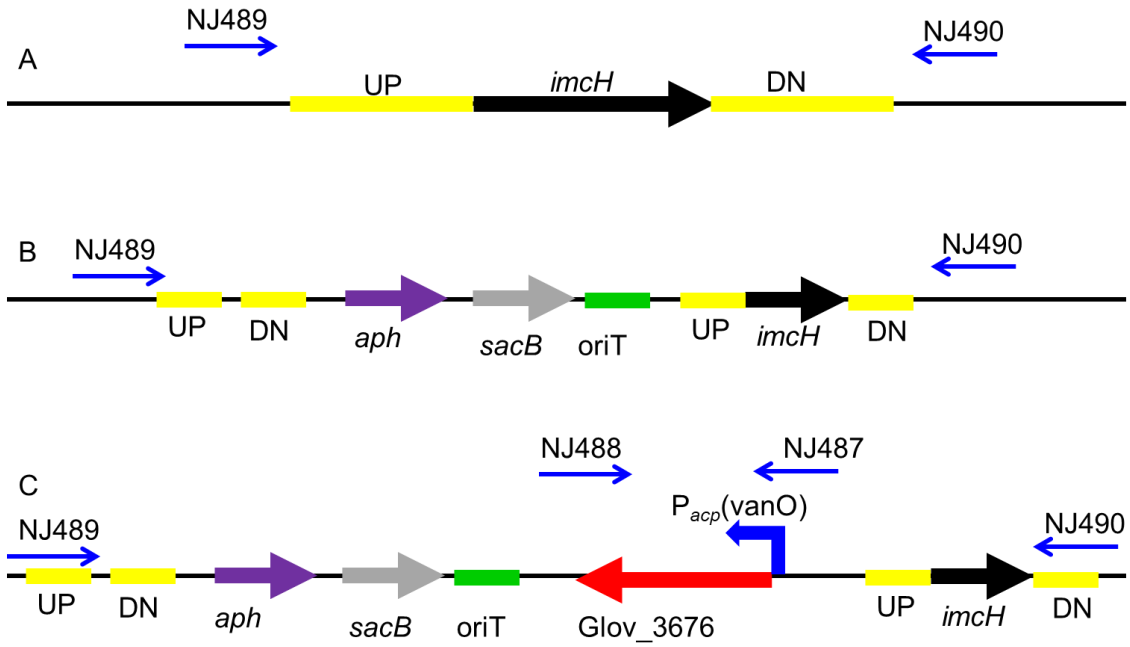


Figure 10: Chromosome map of the *imcH* locus.
Chromosome maps of the *imcH* locus in strains **(a)** FEL005, **(b)** FEL048, and **(c)** FEL050 used in PCR verification.

Table 7: Expected amplicon sizes of the *imcH* locus for PCR verification suicide vector integrations.

	Primers	
Strains	**NJ487-NJ488**	**NJ489-NJ490**
FEL005	N/A	3,157 bp
FEL048	N/A	N/A
FEL050	1,032 bp	N/A

Results

Growth of Geobacter strains producing different lower bases

To ensure no adverse phenotypic effects while producing different corrinoids, we performed growth curves of all three *Geobacter* strains (FEL005, FEL048, and FEL050) with and without vitamin B_{12} supplementation. As shown in **Figure 11AB**, no significant differences in growth were observed. Additionally, as shown in **Figure 12**, pH exhibited a slight downward trend over time from ~7.1 to ~6.6, but remained consistent across cultures. Overall, *Geobacter* cultures producing different corrinoid lower bases did not show any obvious growth phenotypes, suggesting that the production of different corrinoids does not cause any observable effects on growth rate **(Figure 11A)** or maximum OD **(Figure 11B)**. These results may not be surprising since the *Geobacter* wild type is a corrinoid prototroph. Unlike strain FEL005, both strain FEL048 and strain FEL050 decreased in OD after reaching stationary phase, possibly due to cell lysis. Though strain FEL048 and strain FEL050 both have suicide vectors integrated at the GSU3259 locus, chromosomal integration at this locus was not reported to exhibit phenotypic changes (15). Even so, the observation that the mutant strains decreased in OD after reaching stationary phase did not correlate with cobalamin availability in the medium.

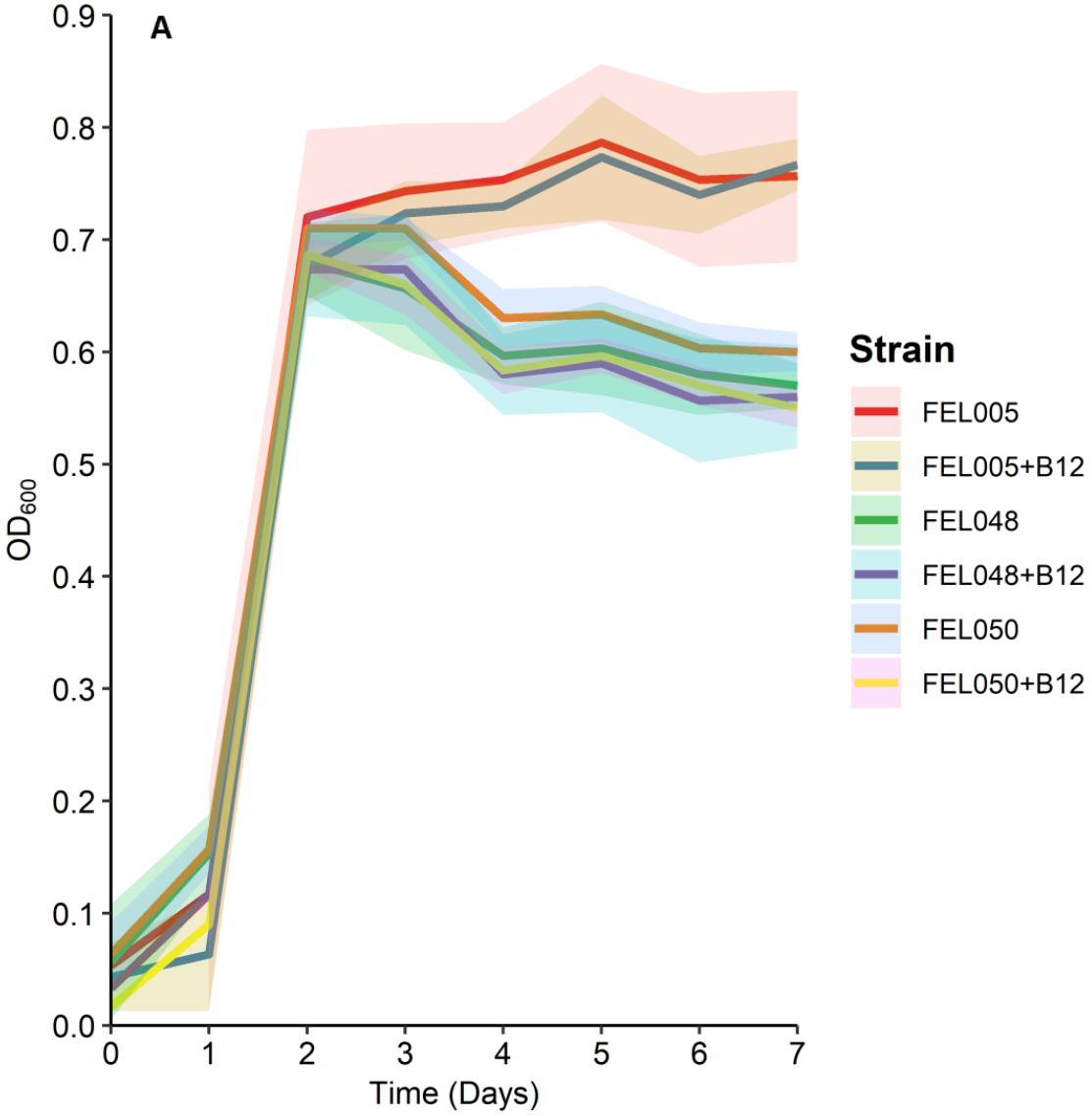


Figure 11: Growth of *Geobacter* cultures producing different corrinoids.
(A) Three strains of *Geobacter* growth curves performed in triplicate with and without the addition of vitamin B_{12}. Ribbons represent standard deviation amongst triplicate cultures. **(B)** Endpoint OD_{600} readings, taken from 3 ml of cultures following mercury methylation analysis. Each bar represents the average of biological duplicates. Error bars denote standard deviation between biological duplicates.

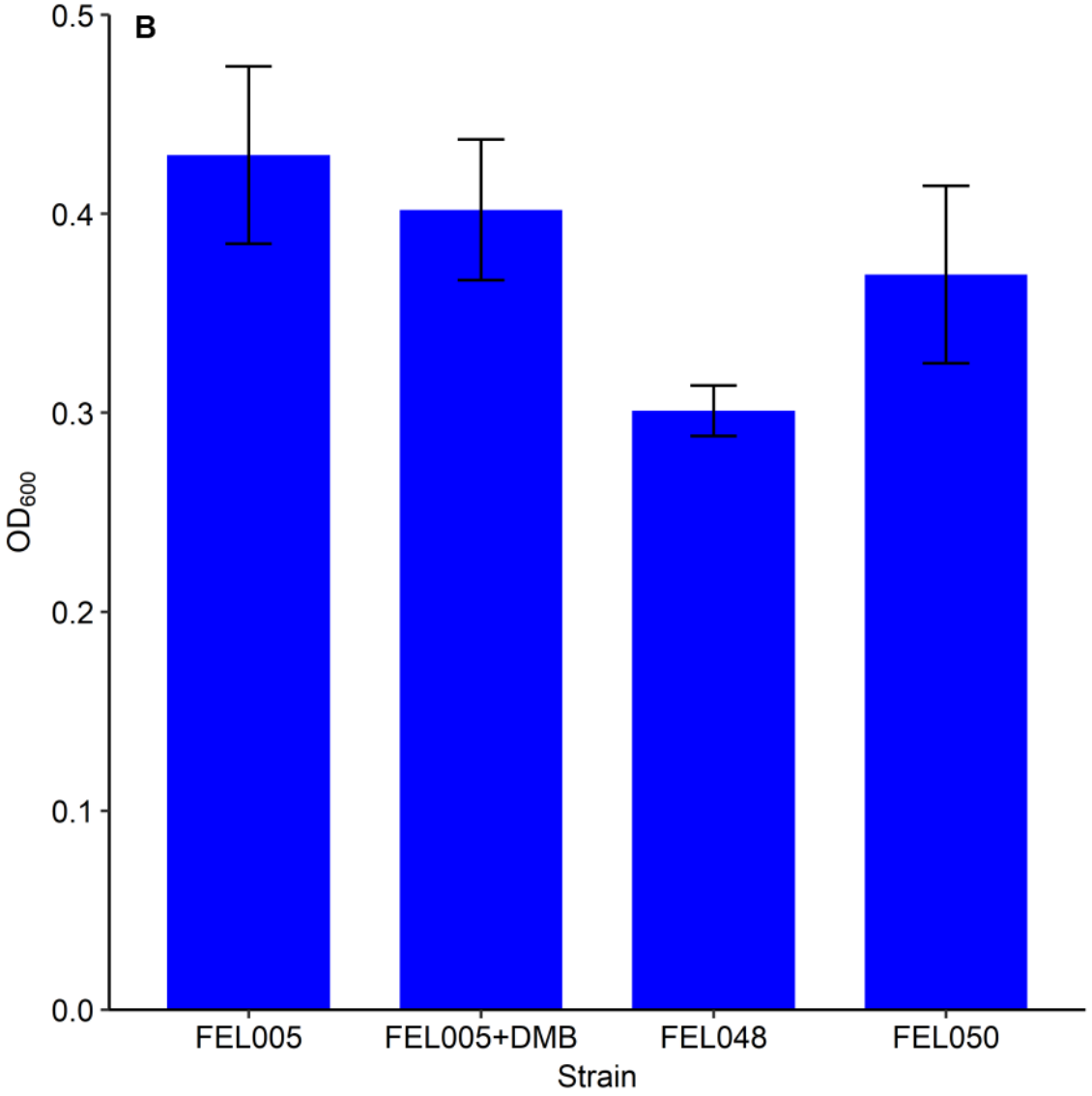


Figure 11: Growth of *Geobacter* cultures producing different corrinoids (continued).

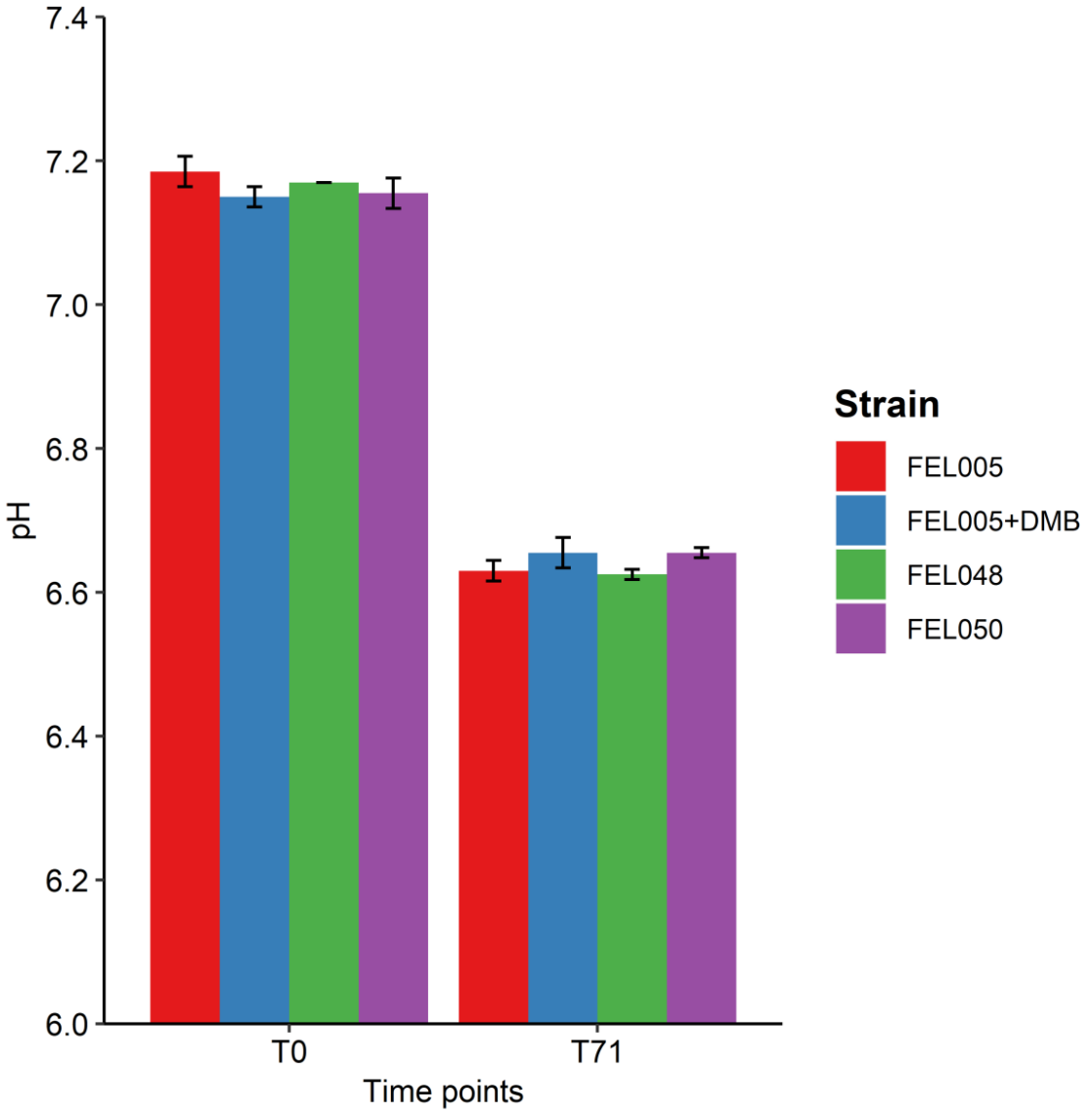


Figure 12: pH of different *Geobacter* strains.
Beginning and endpoint pH values in the medium of all three *Geobacter* strains during mercury methylation analysis. pH was determined using 3 ml of each endpoint culture. Each bar represents the average of biological duplicates. Error bars denote standard deviation between biological duplicates.

Methylmercury analysis

Figure 13 shows endpoint MeHg concentrations for each of the conditions tested normalized to OD. No significant differences in MeHg production were observed in cultures producing corrinoids carrying different lower bases.

Sulfide analysis

Previous studies have established that sulfide can decrease mercury methylation by limiting the bioavailability of mercury (19, 20). Endpoint sulfide concentrations were thus measured to control for mercury bioavailability. As shown in **Figure 14**, overall sulfide concentrations remained relatively steady from inoculation to endpoint measurements, only decreasing slightly from an average of 5.5 μM to 4.3 μM. The limited change in sulfide concentration over the 71-hour experimental period suggests stable Hg bioavailability was maintained.

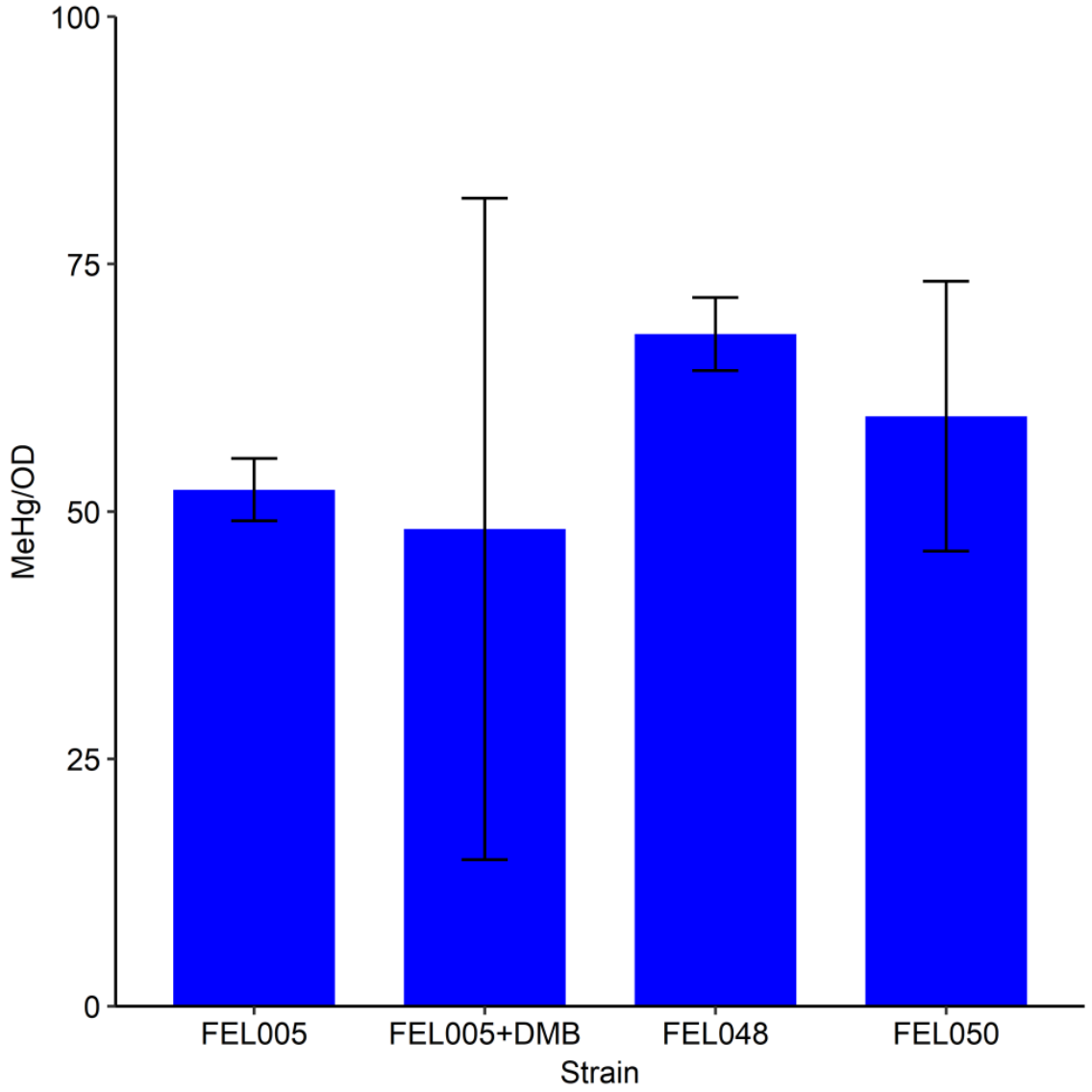


Figure 13: Methylmercury analysis.
Methylmercury quantification normalized to final OD for all three *Geobacter* strains. Each bar represents the average of biological duplicates. Error bars denote standard deviation between biological duplicates.

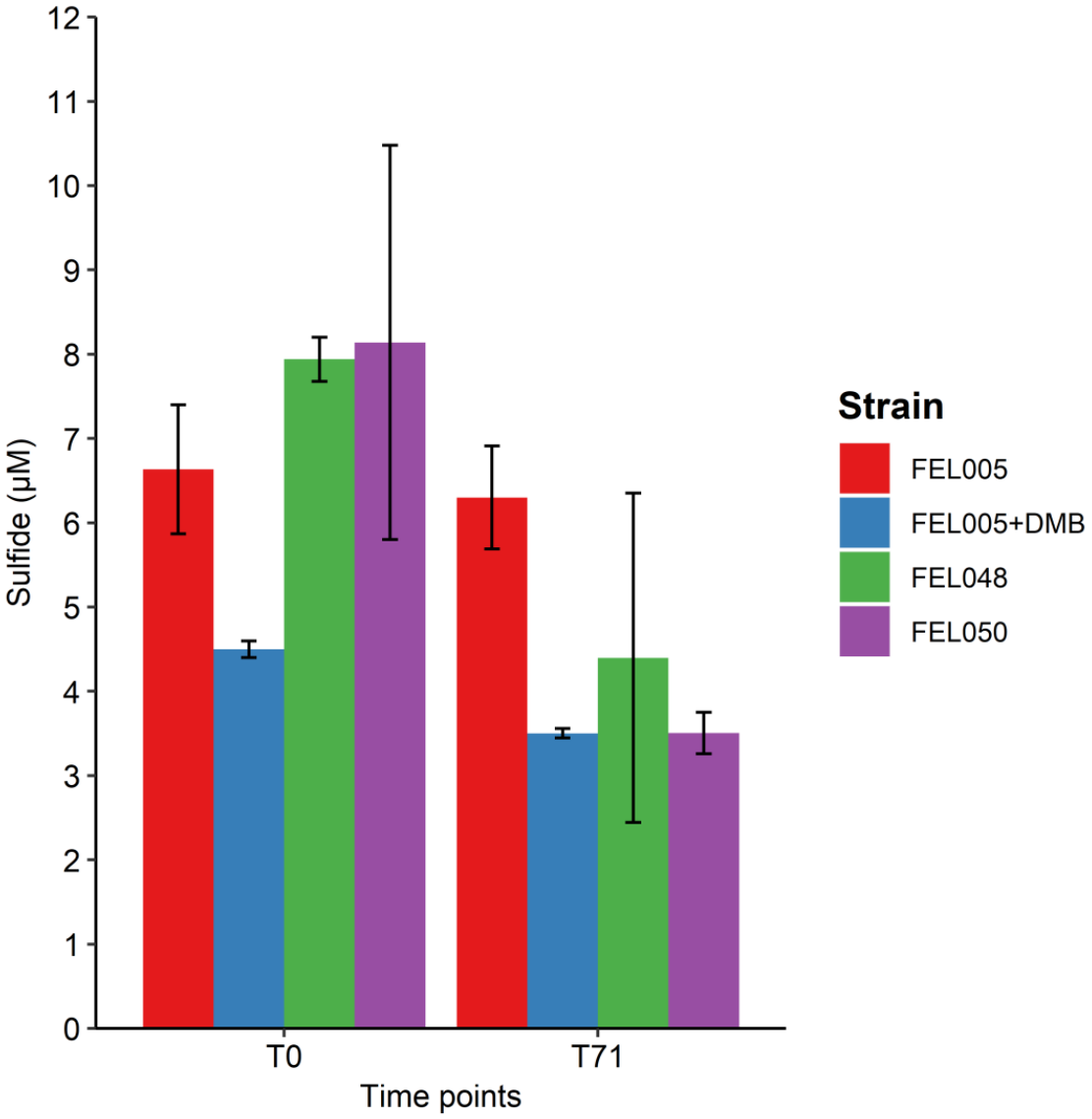


Figure 14: Sulfide content in different *Geobacter* strains.
Beginning and endpoint sulfide concentrations from all 3 *Geobacter* strains following methylmercury analysis. Each bar represents the average of biological duplicates. Error bars denote standard deviation between biological duplicates.

Discussion

Numerous reactions in nature depend on corrinoid cofactors, including mercury methylation. Using these corrinoid cofactors can depend on a number of conditions, including environmental availability, lower base specificity, and horizontal transfer of genes encoding different lower bases (Chapter 2). Still, many species are auxotrophic for essential corrinoid cofactors, and thus rely entirely on salvaging from their environmental neighbors. In some cases, enzyme systems such as the reductive dehalogenases exhibit highly restricted preferences for corrinoids carrying specific lower bases (9). In this study, we show that in the case of mercury methylation, the corrinoid lower base specificity of HgcA may be sufficiently promiscuous, methylating mercury at native rates and extents in the presence of 5-OHBza, 5-OMeBza, or DMB.

The HgcA of ND132 is predicted to bind its corrinoid cofactor in the “base-off” conformation (18), which would indicate no direct coordination with the cobalt. This configuration is consistent with that predicted in the norpseudo-B_{12} cofactor of the membrane-bound PceA of *Sulfurospirillum multivorans* (19) and the vitamin B_{12} cofactor of the soluble $RdhA_{NP}$ from *Nitratireductor pacificus* strain pht-$3B^T$ (20). Although these three corrinoid-dependent enzyme systems preserve the “base-off” conformation, different corrinoid lower bases still produce different results for different enzymes, warranting continued structural investigation into corrinoid structure and binding. Furthermore, another corrinoid-

binding protein haptocorrin, which serves as a cobalamin transport protein, has been shown to bind to the baseless cobinamide molecule (21), suggesting some corrinoid-binding enzymes remain unaffected by the lower base. Future structural and docking studies of HgcAB may reveal further insights into the role of the corrinoid lower base in mercury methylation.

Moreover, there exist over 16 different naturally occurring lower bases in corrinoid cofactors, with many more synthetic ones (10). With this diversity in mind, these results do not exclude the possibility that other lower bases may indeed impose effects on mercury methylation in the case of *G. sulfurreducens*, or in the case of other methylators.

There exist numerous corrinoid-dependent enzymes of significant importance, many of which play key roles in our environment. Further investigation into corrinoid-dependent chemistry may reveal the role(s) of the corrinoid lower base. The apparent independence of mercury methylation with respect to corrinoid lower base structure adds to our current knowledge base of how corrinoid-dependent enzyme systems function. These results further demonstrate our limited understanding of the role of the lower base in corrinoid-dependent reactions, especially when compared to the reductive dehalogenase system (9).

These conclusions emphasize the role of lower base specificity in corrinoid-dependent enzyme systems. Previous studies proposed that the CobT enzyme, which activates lower bases prior to attachment onto the larger cobinamide molecule, may be a significant contributor in determining lower base specificity (10, 21). Some systems have evolved to demand high selectivity (9), while others may have remained more adaptive in function. Functional and evolutionary advantages based on selectivity and availability may exist in either case.

Acknowledgements

We thank AWM for assistance with the methylmercury analysis.

References

1. Parks JM, Johs A, Podar M, Bridou R, Hurt RA, Smith SD, Tomanicek SJ, Qian Y, Brown SD, Brandt CC, Palumbo AV, Smith JC, Wall JD, Elias DA, Liang L. 2013. The genetic basis for bacterial mercury methylation. Science 339:1332–1335.

2. Wu P, Kainz MJ, Bravo AG, Åkerblom S, Sonesten L, Bishop K. 2019. The importance of bioconcentration into the pelagic food web base for methylmercury biomagnification: A meta-analysis. Sci Total Environ 646:357–367.

3. Tollefson L, Cordle F. 1986. Methylmercury in fish: A review of residue levels, fish consumption, and regulatory action in the United States. Environ Health Perspect 68:203–208.

4. Bridwell-Rabb J, Drennan CL. 2017. Vitamin B_{12} in the spotlight again. Curr Opin Chem Biol 37:63–70.

5. Jost M, Fernández-Zapata J, Polanco MC, Ortiz-Guerrero JM, Chen PY-T, Kang G, Padmanabhan S, Elías-Arnanz M, Drennan CL. 2015. Structural basis for gene regulation by a B_{12}-dependent photoreceptor. Nature 526:536–541.

6. Jost M, Simpson JH, Drennan CL. 2015. The transcription factor CarH safeguards use of adenosylcobalamin as a light sensor by altering the photolysis products. Biochemistry (Mosc) 54:3231–3234.

7. Shelton AN, Seth EC, Mok KC, Han AW, Jackson SN, Haft DR, Taga ME. 2018. Uneven distribution of cobamide biosynthesis and dependence in bacteria predicted by comparative genomics. ISME J.

8. Padmanabhan S, Jost M, Drennan CL, Elías-Arnanz M. 2017. A new facet of vitamin B_{12}: Gene regulation by cobalamin-based photoreceptors. Annu Rev Biochem 86:485–514.

9. Yan J, Şimşir B, Farmer AT, Bi M, Yang Y, Campagna SR, Löffler FE. 2015. The corrinoid cofactor of reductive dehalogenases affects dechlorination rates and extents in organohalide-respiring *Dehalococcoides mccartyi*. ISME J 10:1092–1101.

10. Yan J, Bi M, Bourdon AK, Farmer AT, Wang P-H, Molenda O, Quaile AT, Jiang N, Yang Y, Yin Y, Şimşir B, Campagna SR, Edwards EA, Löffler FE. 2017. Purinyl-cobamide is a native prosthetic group of reductive dehalogenases. Nat Chem Biol.

11. Yan J, Im J, Yang Y, Löffler FE. 2013. Guided cobalamin biosynthesis supports *Dehalococcoides mccartyi* reductive dechlorination activity. Philos Trans R Soc B Biol Sci 368:20120320.

12. Graham AM, Bullock AL, Maizel AC, Elias DA, Gilmour CC. 2012. Detailed assessment of the kinetics of Hg-cell association, Hg methylation, and methylmercury degradation in several *Desulfovibrio* species. Appl Environ Microbiol 78:7337–7346.

13. Brouwer H, Murphy TP. 1994. Diffusion method for the determination of acid-volatile sulfides (AVS) in sediment. Environ Toxicol Chem 13:1273–1275.

14. Mitchell CPJ, Gilmour CC. 2008. Methylmercury production in a Chesapeake Bay salt marsh. J Geophys Res Biogeosciences 113.

15. Chan CH, Levar CE, Zacharoff L, Badalamenti JP, Bond DR. 2015. Scarless genome editing and stable inducible expression vectors for *Geobacter sulfurreducens*. Appl Environ Microbiol 81:7178–7186.

16. Gilmour CC, Henry EA. 1991. Mercury methylation in aquatic systems affected by acid deposition. Environ Pollut Barking Essex 1987 71:131–169.

17. Benoit JM, Gilmour CC, Mason RP, Heyes A. 1999. Sulfide controls on mercury speciation and bioavailability to methylating bacteria in sediment pore waters. Environ Sci Technol 33:951–957.

18. Smith SD, Bridou R, Johs A, Parks JM, Elias DA, Hurt RA, Brown SD, Podar M, Wall JD. 2015. Site-directed mutagenesis of HgcA and HgcB reveals amino acid residues important for mercury methylation. Appl Env Microbiol 81:3205–3217.

19. Bommer M, Kunze C, Fesseler J, Schubert T, Diekert G, Dobbek H. 2014. Structural basis for organohalide respiration. Science 346:455–458.

20. Payne KA, Quezada CP, Fisher K, Dunstan MS, Collins FA, Sjuts H, Levy C, Hay S, Rigby SE, Leys D. 2015. Reductive dehalogenase structure suggests a mechanism for B_{12}-dependent dehalogenation. Nature 517:513–516.

21. Furger E, Frei DC, Schibli R, Fischer E, Prota AE. 2013. Structural basis for universal corrinoid recognition by the cobalamin transport protein haptocorrin. J Biol Chem 288:25466–25476.

22. Crofts TS, Seth EC, Hazra AB, Taga ME. 2013. Cobamide structure depends on both lower ligand availability and CobT substrate specificity. Chem Biol 20:1265–1274.

23. Caccavo F, Lonergan DJ, Lovley DR, Davis M, Stolz JF, McInerney MJ. 1994. *Geobacter sulfurreducens*) sp. nov., a hydrogen- and acetate-oxidizing dissimilatory metal-reducing microorganism. Appl Environ Microbiol 60:3752–3759.

CHAPTER IV
UNEXPECTED EFFECTS OF VANILLATE ON MERCURY METHYLATION IN *GEOBACTER SULFURREDUCENS*

Reproduced in part with permission from Jiang N, Date SS, Parks JM, Johs A, and Löffler FE. Unexpected effects of vanillate on mercury methylation in *Geobacter sulfurreducens.* In preparation. All copyright interests will be exclusively transferred to the publisher upon submission.

Abstract

Mercury is an environmental pollutant that is readily accumulated via the aquatic food chain. The degree of toxicity and bioaccumulation increase following methylation, an intracellular reaction mediated by the *hgcAB* genes (1). The two genes encode the proteins HgcA, a corrinoid-dependent membrane protein, and HgcB, a 2[4Fe-4S] ferredoxin. Purification of HgcAB would allow for higher resolution characterization of molecular structure and function. However, attempts to isolate native HgcA and HgcB from the model mercury methylator *Desulfovibrio desulfuricans* ND132 (ND132) were unsuccessful due to extremely low expression levels and limited corrinoid concentrations in this strain. Here we present a strategy to overexpress native HgcA and HgcB in the native mercury methylator *Geobacter sulfurreducens* PCA (PCA). Preliminary studies show that PCA produces large quantities of corrinoid, which is necessary for obtaining fully cofactor-replete HgcA. Here, we implemented a synthetic biology strategy to control the expression of native HgcAB in PCA, using a homologous recombination approach to introduce a vanillate-inducible promoter to control overexpression of HgcAB. Surprisingly, we found vanillate may not only affect *Geobacter* physiology, but also mercury methylation.

Importance

Mercury toxicity increases upon methylation, which bioaccumulates through the aquatic food web. Mercury methylation is catalyzed by two proteins, HgcA and HgcB. Surprisingly, we present findings suggesting the small molecule vanillate impacts mercury methylation.

Introduction

Heavy metal poisoning poses a continuing threat to humans and their surrounding environments. Mercury (Hg) is one such heavy metal, which has been linked to several detrimental health effects, often resulting in chronic effects of the brain and kidneys (2). Methylmercury (MeHg), the monomethylated form of mercury, intensifies the toxicity issue by increasing its bioaccumulation potential through the aquatic food chain. Investigations at the enzymatic and molecular levels are thus necessary and may lead to characterizing and predicting methylmercury formation across different environments.

A pivotal study came in 2013 when Parks *et al.* discovered the *hgcAB* genes responsible for mercury methylation (1). Both HgcAB were predicted to bind cofactors, where HgcA bound a corrinoid and HgcB bound an iron-sulfur cluster. Heterologous studies in the *E. coli* model organism have since not produced functional HgcAB proteins. Further complicating this endeavor is the mysterious corrinoid cofactor produced by the model mercury methylator *Desulfovibrio desulfuricans* ND132 (ND132). Lack of structural and genetic identity of this

cofactor presented challenges in reconstituting enzymatic activity. Additionally, attempts to extract full corrinoids using established protocols (3) from ND132 have yielded insufficient quantity for analysis.

A scarcity of synthetic promoters in the ND132 system posed another limitation. Regulated promoters are particularly important in this case, as HgcA is an integral membrane protein. Overexpression of membrane-bound proteins has been commonly shown to result in inclusion bodies or lead to sick strains (4, 5).

To address these challenges and limitations, we propose shifting HgcAB overexpression experiments into the native mercury methylator *Geobacter sulfurreducens* strain PCA (PCA). A synthetic regulated promoter system (6) has already been developed for PCA. Furthermore, PCA produces ample quantities of a known corrinoid carrying the 5-hydroxybenzimidazole lower base (Chapter 2), which is likely required by the HgcA of strain PCA. Here, we present a strategy to superimpose a vanillate-inducible promoter immediately upstream of the native PCA *hgcAB* operon, and the surprising results of using the small inducer molecule vanillate.

Materials and Methods

Chemicals

Vanillate (≥97.0%) was purchased from Sigma-Aldrich (St. Louis, MO). All other chemicals were described elsewhere (Chapter 2).

Cultures

All *E. coli* and *G. sulfurreducens* strain PCA (ATCC 51573) cultures were obtained from laboratory stocks. All wild type and mutant strains are described in **Table 8**.

Media and growth conditions

E. coli cultures were maintained at 37°C in lysogeny broth (LB) medium (7). All *G. sulfurreducens* cultures were maintained at 35°C in basal salts medium as described (Chapter 2). To minimize the possibility of mercury-cysteine complexes, the L-cysteine HCl concentration was decreased to 0.2 mM in cultures grown for methylmercury analysis.

Plasmid construction

pNJ179

The GSU1440(501)' fragment was PCR-amplified from strain FEL005 using primers NJ971 (5'-CATATGGTGCCGGTCATCTCCACGCAAC-3') and NJ972 (5'-TCAGACAGTTGTGAACGTGAGCTGCCG-3'). The 510-bp amplicon was purified using the DNA Clean & Concentrator (Zymo Research, Irvine, CA) kit, treated with DpnI, purified again, and treated with Quick-Load® Taq 2X Master Mix (New England Biolabs, Ipswich, MA). The final amplicon was cloned using the TOPO™ TA Cloning™ Kit for Subcloning (Thermo Fisher Scientific, Waltham, MA) as per the manufacturer's instructions. The TOPO® reaction was electroporated into strain FEL008 electrocompetent cells **(Table 8)**. The recombinant vector was verified by Sanger sequencing at the University of

Table 8: Strains used in Chapter 4.

Lab stock #	Strain	Species	Genotype	Reference
FEL002	BW25113	*E. coli*	*lacI*$^{+}$*rrnB*$_{T14}$ Δ*lacZ*$_{WJ16}$ *hsdR*514 Δ*araBAD*$_{AH33}$ Δ*rhaBAD*$_{LD78}$ *rph-1* Δ*(araB–D)567* Δ*(rhaD–B)568* Δ*lacZ4787*(::*rrnB-3*) *hsdR514 rph-1*	(21)
FEL003	BW29427	*E. coli*	*thrB1004 pro thi rpsL hsdS lacZ*Δ*M15 RP4-1360* Δ*(araBAD)567* Δ*dapA1341*::[*erm pir*]	K. Datsenko and B.L. Wanner
FEL005	—	*G. sulfurreducens* strain PCA	Wild type	(22)
FEL008	TOP10	*E. coli*	F- *mcrA* Δ(*mrr-hsdRMS-mcrBC*) φ80*lacZ*Δ*M15* Δ*lac*X74 *nupG rec*A1 *ara*D139 Δ(*ara-leu*)7697 *galE15 galK16 rpsL*(Str^{R}) *endA1* λ^{-}	(Thermo Fisher Scientific, Waltham, MA)
FEL018	—	*E. coli*	*lacI*$^{+}$*rrnB*$_{T14}$ Δ*lacZ*$_{WJ16}$ *hsdR*514 Δ*araBAD*$_{AH33}$ Δ*rhaBAD*$_{LD78}$ *rph-1* Δ*(araB–D)567* Δ*(rhaD–B)568* Δ*lacZ4787*(::*rrnB-3*) *hsdR514 rph-1* / pKD46	(21)

Table 8: Strains used in Chapter 4 (continued).

Lab stock #	Strain	Species	Genotype	Reference
FEL263	—	*E. coli*	F- *mcrA* Δ(*mrr-hsdRMS-mcrBC*) φ80*lacZ*Δ*M15* Δ*lac*X74 *nupG rec*A1 *ara*D139 Δ(*ara-leu*)7697 *galE15 galK16 rpsL*(Str^R) *endA1* λ^- / pNJ179	This study
FEL264	—	*E. coli*	F- *mcrA* Δ(*mrr-hsdRMS-mcrBC*) φ80*lacZ*Δ*M15* Δ*lac*X74 *nupG rec*A1 *ara*D139 Δ(*ara-leu*)7697 *galE15 galK16 rpsL*(Str^R) *endA1* λ^- / pNJ180	This study
FEL265	—	*E. coli*	F- *mcrA* Δ(*mrr-hsdRMS-mcrBC*) φ80*lacZ*Δ*M15* Δ*lac*X74 *nupG rec*A1 *ara*D139 Δ(*ara-leu*)7697 *galE15 galK16 rpsL*(Str^R) *endA1* λ^- / pNJ181	This study
FEL266	—	*E. coli*	*lacI*$^+$*rrnB*$_{T14}$ Δ*lacZ*$_{WJ16}$ *hsdR*514 Δ*araBAD*$_{AH33}$ Δ*rhaBAD*$_{LD78}$ *rph-1* Δ*(araB–D)567* Δ*(rhaD–B)568* Δ*lacZ4787*(::*rrnB-3*) *hsdR514 rph-1* / pNJ182	This study

Table 8: Strains used in Chapter 4 (continued).

Lab stock #	Strain	Species	Genotype	Reference
FEL267	—	*E. coli*	*lacI*$^{+}$*rrnB*$_{T14}$ Δ*lacZ*$_{WJ16}$ *hsdR*514 Δ*araBAD*$_{AH33}$ Δ*rhaBAD*$_{LD78}$ *rph-1* Δ*(araB–D)567* Δ*(rhaD–B)568* Δ*lacZ4787*(::*rrnB-3*) *hsdR514 rph-1* / pNJ183	This study
FEL268	—	*E. coli*	*lacI*$^{+}$*rrnB*$_{T14}$ Δ*lacZ*$_{WJ16}$ *hsdR*514 Δ*araBAD*$_{AH33}$ Δ*rhaBAD*$_{LD78}$ *rph-1* Δ*(araB–D)567* Δ*(rhaD–B)568* Δ*lacZ4787*(::*rrnB-3*) *hsdR514 rph-1* / pNJ184	This study
FEL269	—	*E. coli*	*lacI*$^{+}$*rrnB*$_{T14}$ Δ*lacZ*$_{WJ16}$ *hsdR*514 Δ*araBAD*$_{AH33}$ Δ*rhaBAD*$_{LD78}$ *rph-1* Δ*(araB–D)567* Δ*(rhaD–B)568* Δ*lacZ4787*(::*rrnB-3*) *hsdR514 rph-1* / pNJ185	This study
FEL270	—	*E. coli*	*thrB1004 pro thi rpsL hsdS lacZ*Δ*M15 RP4-1360* Δ*(araBAD)567* Δ*dapA1341*::[*erm pir*] / pNJ184	This study

Table 8: Strains used in Chapter 4 (continued).

Lab stock #	Strain	Species	Genotype	Reference
FEL271	—	*E. coli*	*thrB1004 pro thi rpsL hsdS lacZΔM15 RP4-1360 Δ(araBAD)567 ΔdapA1341*::[*erm pir*] / pNJ185	This study
FEL273	—	*G. sulfurreducens* strain PCA	ΔGSU1440::pNJ184	This study
FEL274	—	*G. sulfurreducens* strain PCA	ΔGSU1440::pNJ185	This study

Tennessee Genomics Core using primers NJ015 (M13 F) (5'-GTAAAACGACGGCCAG-3') and NJ016 (M13 R) (5'-CAGGAAACAGCTATGAC-3'). **Table 10** contain all plasmids and primers used in Chapter 4, respectively.

pNJ180

The *vanR*+P_{acp}(vanO) amplicon (998 bp) was PCR-amplified using primers NJ969 (5'-TCAGTCGGCGCGAATGCTCC-3') and NJ970 (5'-catatgATGGCTTGTTCACCTCCGTTTGG-3') from pRK2-Geo2i-lacZa (6). The 998-bp amplicon was purified using the DNA Clean & Concentrator (Zymo Research, Irvine, CA) kit, treated with DpnI, purified again, and treated with Quick-Load® Taq 2X Master Mix (New England Biolabs, Ipswich, MA). The final amplicon was cloned using the TOPO™ TA Cloning™ Kit for Subcloning (Thermo Fisher Scientific, Waltham, MA) as per the manufacturer's instructions. The TOPO® reaction was electroporated into strain FEL008 electrocompetent cells **(Table 8)**. The recombinant vector was verified by Sanger sequencing at the University of Tennessee Genomics Core using primers NJ015 (5'-GTAAAACGACGGCCAG-3') and NJ016 (5'-CAGGAAACAGCTATGAC-3'). Sequencing revealed a single point mutation in the stop codon of the *vanR* gene, which now reads "TAA" as opposed to "TGA." We proceeded with this construct because the point mutation is silent and maintains the original function of a stop codon.

Table 9: Plasmids used in Chapter 4.

Plasmids		
Plasmid	**Description**	**Reference**
pCR™2.1-TOPO™	Empty TOPO® vector backbone	(Thermo Fisher Scientific, Waltham, MA)
pDImcH2	Suicide vector containing *vanR* and P_{acp}(vanO); suitable for conjugation into *G. sulfurreducens*	(6)
pNJ179	TOPO®-cloned GSU1440(501)'	This study
pNJ180	TOPO®-cloned *vanR*+P_{acp}(vanO)	This study
pNJ181	TOPO®-cloned GSU1440(702)'	This study
pNJ182	pNJ180 carrying GSU1440(501')	This study
pNJ183	pNJ180 carrying GSU1440(702')	This study
pNJ184	pDImcH2 carrying *vanR* and the P_{acp}(vanO) promoter driving GSU1440(501')	This study
pNJ185	pDImcH2 carrying *vanR* and the P_{acp}(vanO) promoter driving GSU1440(702')	This study
pRK2-Geo2i-lacZa	Autonomously replicating vector in *G. sulfurreducens* carrying P_{acp}(vanO) promoter	(6)

Table 10: Primers used in Chapter 4.

Primers			
#	Sequence (5'-3')	5'-End	Reference
NJ015	**GTAAAACGACGGCCAG**	N/A	(Thermo Fisher Scientific, Waltham, MA)
NJ016	**CAGGAAACAGCTATGAC**	N/A	(Thermo Fisher Scientific, Waltham, MA)
NJ485	**CAAGCGTTCAATTGGATCCAATCTTG**	N/A	This study
NJ492	**GAGCGCCCAATACGCAAACCGCC**	N/A	This study
NJ493	**TTCCTGCTCCAGACTCCGCAAG**	N/A	This study
NJ513	**CCGCTTCCTTTAGCAGCCCTTG**	N/A	This study
NJ517	**GCGCGTGATGATGGCTCTTC**	N/A	This study
NJ627	**CTCGAAGACCTTGGCGTTACG**	N/A	This study
NJ628	**GAGCCCTTCCTGCTCCAGACTC**	N/A	This study
NJ659	**GTTTGTTTGCCGGATCAAGAGCTAC**	N/A	This study
NJ952	**CCCAGTCACGACGTTGTAAAACGACGGCCAGTGCCAAGCTTCAGTCGGCGCGAATGCTCC**	Homology	This study
NJ954	**GCGGCCGCCAGTGTGATGGATATCTGCAGAATTCGCCCTTTCAGCCGGGAAGCCATGGCAGCAGAAGTG**	Homology	This study
NJ955	**TATGACATGATTACGAATTCGAGCTCGGTACCCGGGGATCTTATCAGACAGTTGTGAACGTGAGCTGCCG**	Homology	This study

Table 10: Primers used in Chapter 4 (continued)

Primers			
#	Sequence (5'-3')	5'-End	Reference
NJ956	**TATGACATGATTACGAATTCGAGCTCGGTACCCGGGGATCTTATCAGCCGGGAAGCCATGGCAGCAGAAGTG**	Homology	This study
NJ957	**AACTACAAGATGAGCTACGATAGTGTCCG**	N/A	This study
NJ969	**TCAGTCGGCGCGAATGCTCC**	N/A	This study
NJ970	**CATATGATGGCTTGTTCACCTCCGTTTGG**	NdeI	This study
NJ971	**CATATGGTGCCGGTCATCTCCACGCAAC**	NdeI	This study
NJ972	**TCAGACAGTTGTGAACGTGAGCTGCCG**	Opal codon	This study
NJ973	**CATATGGTGCCGGTCATCTCCACGCAAC**	NdeI	This study
NJ974	**TCAGCCGGGAAGCCATGGCAGCAGAAGTG**	Opal codon	This study
NJ976	**TCCACTAGTAACGGCCGCCAGTGTGCTGGAATTCGCCCTTTCAGCCGGGAAGCCATGGCAGCAGAAGTG**	Homology	This study
NJ978	**TCCACTAGTAACGGCCGCCAGTGTGCTGGAATTCGCCCTTTCAGCCGGGAAGCCATGGCAGCAGAAGTG**	Homology	This study
NJ983	**CCCGAGCGGATGGAGGATAATC**	N/A	This study

Regions of homology or restriction endonuclease sites are highlighted in green.

pNJ181

The GSU1440(702)' fragment was PCR-amplified from strain FEL005 using primers NJ973 (5’-catatgGTGCCGGTCATCTCCACGCAAC-3') and NJ974 (5’-tcaGCCGGGAAGCCATGGCAGCAGAAGTG-3'). The 711-bp amplicon was purified using the DNA Clean & Concentrator (Zymo Research, Irvine, CA) kit, treated with DpnI, purified again, and treated with Quick-Load® Taq 2X Master Mix (New England Biolabs, Ipswich, MA). The final amplicon was cloned using the TOPO™ TA Cloning™ Kit for Subcloning (Thermo Fisher Scientific, Waltham, MA) as per the manufacturer’s instructions. The TOPO® reaction was electroporated into strain FEL008 electrocompetent cells **(Table 8)**. The recombinant vector was verified by Sanger sequencing at the University of Tennessee Genomics Core using primers NJ015 (5’-GTAAAACGACGGCCAG-3’) and NJ016 (5’-CAGGAAACAGCTATGAC-3’). Sequencing revealed a single point mutation in the synthetic premature stop codon in GSU1440(702)', which now reads “TAA” as opposed to “TGA.” We proceeded with this construct because the point mutation is silent and maintains the original function of a stop codon.

pNJ182

GSU1440(501)' was PCR-amplified from pNJ179 using primers NJ954 (5’-GCGGCCGCCAGTGTGATGGATATCTGCAGAATTCGCCCTTTCAGCCGGGAAGCCATGGCAGCAGAAGTG-3’) and NJ976 (5’-

TCCACTAGTAACGGCCGCCAGTGTGCTGGAATTCGCCCTTTCAGCCGGGAA GCCATGGCAGCAGAAGTG-3'). The 584-bp amplicon was purified using the DNA Clean & Concentrator (Zymo Research, Irvine, CA) kit, treated with DpnI, and purified again. The pNJ180 vector was linearized with NdeI and gel extracted using the Zymoclean Gel DNA Recovery (Zymo Research, Irvine, CA) kit. The PCR amplicon and linearized vector were co-transformed into strain FEL018 electrocompetent cells as described (3). All recombinant vectors were verified by Sanger sequencing at the University of Tennessee Genomics Core using primers NJ015(5'-GTAAAACGACGGCCAG-3'), NJ016 (5'-CAGGAAACAGCTATGAC-3'), NJ493 (5'-TTCCTGCTCCAGACTCCGCAAG-3'), and NJ517 (5'-GCGCGTGATGATGGCTCTTC-3').

pNJ183

GSU1440(702)' was PCR-amplified from pNJ181 using primers NJ954 (5'-GCGGCCGCCAGTGTGATGGATATCTGCAGAATTCGCCCTTTCAGCCGGGAA GCCATGGCAGCAGAAGTG-3') and NJ978 (5'-TCCACTAGTAACGGCCGCCAGTGTGCTGGAATTCGCCCTTTCAGCCGGGAA GCCATGGCAGCAGAAGTG-3').

The 785-bp amplicon was purified using the DNA Clean & Concentrator (Zymo Research, Irvine, CA) kit, treated with DpnI, and purified again. The pNJ180 vector was linearized with NdeI and gel extracted using the Zymoclean Gel DNA

Recovery (Zymo Research, Irvine, CA) kit. The PCR amplicon and linearized vector were co-transformed into strain FEL018 electrocompetent cells as described (3). All recombinant vectors were verified by Sanger sequencing at the University of Tennessee Genomics Core using primers NJ015 (5'-GTAAAACGACGGCCAG-3'), NJ016 (5'-CAGGAAACAGCTATGAC-3'), NJ493 (5'-TTCCTGCTCCAGACTCCGCAAG-3'), NJ517 (5'-GCGCGTGATGATGGCTCTTC-3'), and NJ957 (5'-AACTACAAGATGAGCTACGATAGTGTCCG-3').

pNJ184

The *vanR*+P_{acp}(vanO)+GSU1440(501)' fragment was PCR-amplified from pNJ182 using primers NJ952 (5'-CCCAGTCACGACGTTGTAAAACGACGGCCAGTGCCAAGCTTCAGTCGGCG CGAATGCTCC-3') and NJ955 (5'-TATGACATGATTACGAATTCGAGCTCGGTACCCGGGGATCTTATCAGACAGT TGTGAACGTGAGCTGCCG-3'). The 1579-bp amplicon was purified using the DNA Clean & Concentrator (Zymo Research, Irvine, CA) kit, treated with DpnI, EcoRI, and HindIII, and purified again. The pDImcH2 vector was linearized with EcoRI and HindIII and gel extracted using the Zymoclean Gel DNA Recovery (Zymo Research, Irvine, CA) kit. The resulting vector and insert were ligated overnight using T4 DNA Ligase (New England Biolabs, Ipswich, MA), and transformed into strain FEL002 electrocompetent cells **(Table 8)**. All recombinant

vectors were verified by Sanger sequencing at the University of Tennessee Genomics Core using primers NJ485 (5'-CAAGCGTTCAATTGGATCCAATCTTG-3'), NJ492 (5'-GAGCGCCCAATACGCAAACCGCC-3'), NJ513 (5'-CCGCTTCCTTTAGCAGCCCTTG-3'), NJ627 (5'-CTCGAAGACCTTGGCGTTACG-3'), and NJ628 (5'-GAGCCCTTCCTGCTCCAGACTC-3').

pNJ185

The *vanR*+P_{acp}(vanO)+GSU1440(702)' fragment was PCR-amplified from pNJ183 using primers NJ952 (5'-CCCAGTCACGACGTTGTAAAACGACGGCCAGTGCCAAGCTTCAGTCGGCGCGAATGCTCC-3') and NJ956 (5'-TATGACATGATTACGAATTCGAGCTCGGTACCCGGGGATCTTATCAGCCGGGAAGCCATGGCAGCAGAAGTG-3'). The 1780-bp amplicon was purified using the DNA Clean & Concentrator (Zymo Research, Irvine, CA) kit, treated with DpnI, EcoRI, and HindIII, and purified again. The pDImcH2 vector was linearized with EcoRI and HindIII and gel extracted using the Zymoclean Gel DNA Recovery (Zymo Research, Irvine, CA) kit. The resulting vector and insert were ligated overnight using T4 DNA Ligase (New England Biolabs, Ipswich, MA), and transformed into strain FEL002 electrocompetent cells **(Table 8)**. All recombinant vectors were verified by Sanger sequencing at the University of Tennessee

Genomics Core using primers NJ485 (5'-CAAGCGTTCAATTGGATCCAATCTTG-3'), NJ492 (5'-GAGCGCCCAATACGCAAACCGCC-3'), NJ513 (5'-CCGCTTCCTTTAGCAGCCCTTG-3'), NJ627 (5'-CTCGAAGACCTTGGCGTTACG-3'), and NJ628 (5'-GAGCCCTTCCTGCTCCAGACTC-3').

Strain construction

E. coli strains were transformed via electroporation as described (Chapter 2). *Geobacter* strains were constructed via conjugal mating as described (Chapter 2) using a 1:1 donor:recipient ratio, where all cultures were diluted to an OD_{600} of 0.427. Detailed homologous recombination events are described in **Figure 15**.

PCR verification of mutant strains

Conjugants were verified by PCR screening using primers NJ983 (5'-CCCGAGCGGATGGAGGATAATC-3') and NJ659 (5'-GTTTGTTTGCCGGATCAAGAGCTAC-3'). Diagnostic bands are 1,965 bp for strain FEL273 and 2,166 bp for strain FEL274, with no expected amplicons from the wild type. Chromosome maps for wild type and mutant strains are displayed in **Figure 16**. PCR screens were performed using Quick-Load® Taq 2X Master Mix (New England Biolabs, Ipswich, MA) according to the manufacturer's instructions.

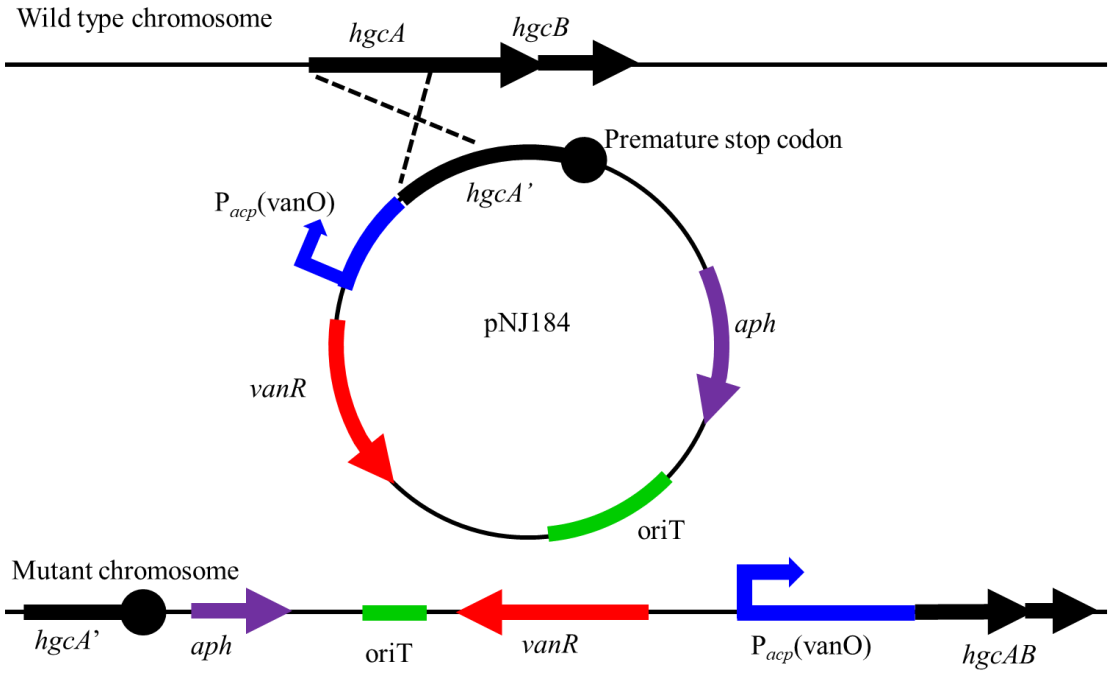


Figure 15: Homologous recombination.
Schematic representing the homologous recombination of pNJ184 (and similarly for pNJ185) following conjugation into strain FEL005. Dotted lines indicate recombination into the *hgcA* locus of the wild type chromosome, resulting in the full-vector integration as shown in the mutant chromosome. *aph*, aminoglycoside phosphotransferase; *hgcA*, encodes membrane-bound protein responsible for mercury methylation; *hgcA'*, encodes the N-terminal 501 bp of the membrane-bound protein responsible for mercury methylation (702 bp in pNJ185); *hgcB*, encodes iron-sulfur cluster binding protein responsible for mercury; oriT, origin of transfer; P_{acp}(vanO), synthetic acyl carrier protein promoter carrying vanillate operator site; premature stop codon, stop codon preventing further translation of HgcA after 501 bp (702 bp in pNJ185); *vanR*, vanillate regulator.

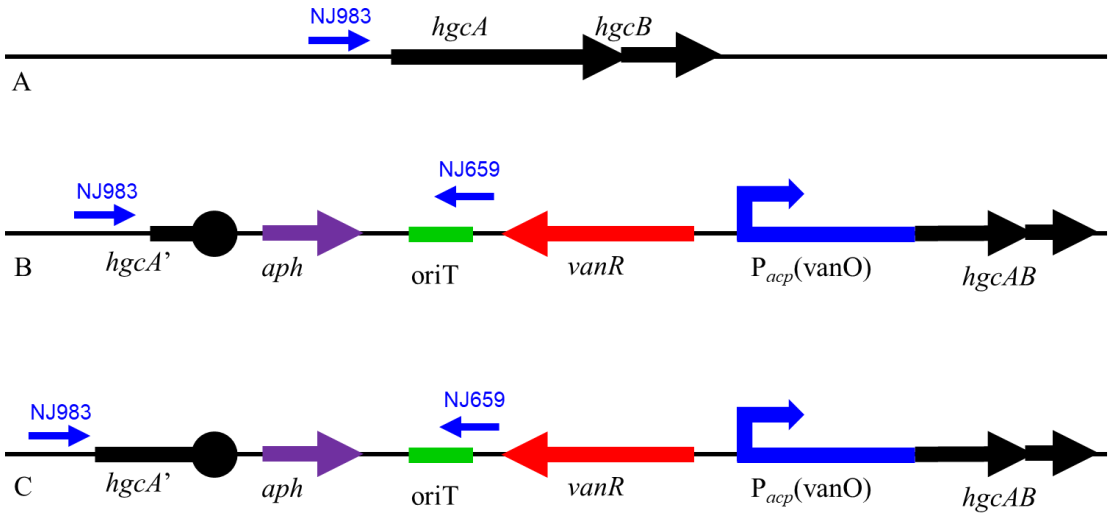


Figure 16: PCR screen.
(a) Chromosome map of wild type GSU1440 locus in *G. sulfurreducens* (FEL005). **(b)** Chromosome map of GSU1440 following integration of pNJ174 in strain FEL273. **(c)** Chromosome map of GSU1440 following integration of pNJ175 in strain FEL274. *aph*, aminoglycoside phosphotransferase; *hgcA*, encodes membrane-bound protein responsible for mercury methylation; *hgcA'*, encodes the N-terminal 501 bp of the membrane-bound protein responsible for mercury methylation (702 bp in pNJ185); *hgcB*, encodes iron-sulfur cluster binding protein responsible for mercury; oriT, origin of transfer; P_{acp}(vanO), synthetic acyl carrier protein promoter carrying vanillate operator site; *vanR*, vanillate regulator; NJ primers are described in **Table 10**.

Growth curves

Growth curves were performed on a Multiskan™ FC Microplate Photometer (Thermo Fisher Scientific, Waltham, MA), under anoxic conditions with head space consisting of N_2, H_2 (3%), and CO_2 (10%). Strains FEL005, FEL273, and FEL274 **(Table 8)** were grown in basal salts medium as described (Chapter 2) and induced across 8 concentrations of vanillate (0 µM, 3 µM, 10 µM, 30 µM, 100 µM, 300 µM, 1,000 µM, and 3,000 µM) in triplicate. OD_{620} values were read every 2 hours for 200-µl reaction volumes while maintaining an internal temperature of 35°C with background shaking.

MeHg washed cell assays

Cultures for MeHg analysis were grown to early exponential phase (OD_{600} 0.06-0.18) in basal salts medium as described (Chapter 2). Cells were then pelleted at 7.5Kxg for 10 min. at 4°C under anoxic conditions. Cells were then washed 3 times using phosphate-buffered saline (PBS) at pH 7.0 as described (8). Cells were then normalized by OD to 10^8 cells/ml and supplemented with 1 mM acetate and fumarate. Incubation was carried out at room temperature in dark conditions. Methylation reactions were stopped after 24 hours and stored in 0.2% H_2SO_4 at -20°C prior to analysis.

Statistical analysis

Welch's t-test was performed on data from strain FEL005 MeHg washed cell assays (n = 2) using a 95% confidence interval in R. The t statistic (*t*), degrees of

freedom (*df*), and p-value (*p*) were calculated when comparing 0 μM to 30 μM (*t* = 12.008, *df* = 1.5599, *p* = 0.01597), 30 μM to 100 μM (*t* = -8.0484, *df* = 1.9302, *p* = 0.01672), and 0 μM to 100 μM (*t* = 5.5846, *df* = 1.7484, *p* = 0.04092).

Results

Growth curves

Growth curves for all 3 strains (FEL005, FEL273, and FEL274) were carried out in the presence of varying concentrations of vanillate to determine the optimal vanillate induction concentration. As shown in **Figure 17-Figure 19,** the 100 μM and 300 μM vanillate cultures seemed to track well with the 0 μM vanillate cultures. Surprisingly, dramatic growth effects were observed upon the addition of varying concentrations of vanillate, particularly in the 3 μM, 10 μM, 30 μM, 1,000 μM, and 3,000 μM cultures. All cultures except for the 3,000 μM vanillate cultures entered exponential phase just before the 24-hour time point (~22 hours). The 3,000 μM vanillate cultures entered exponential phase closer to the 48-hour mark. These observations held true across all 3 strains, suggesting that the physiological response to vanillate was independent of genetic manipulations.

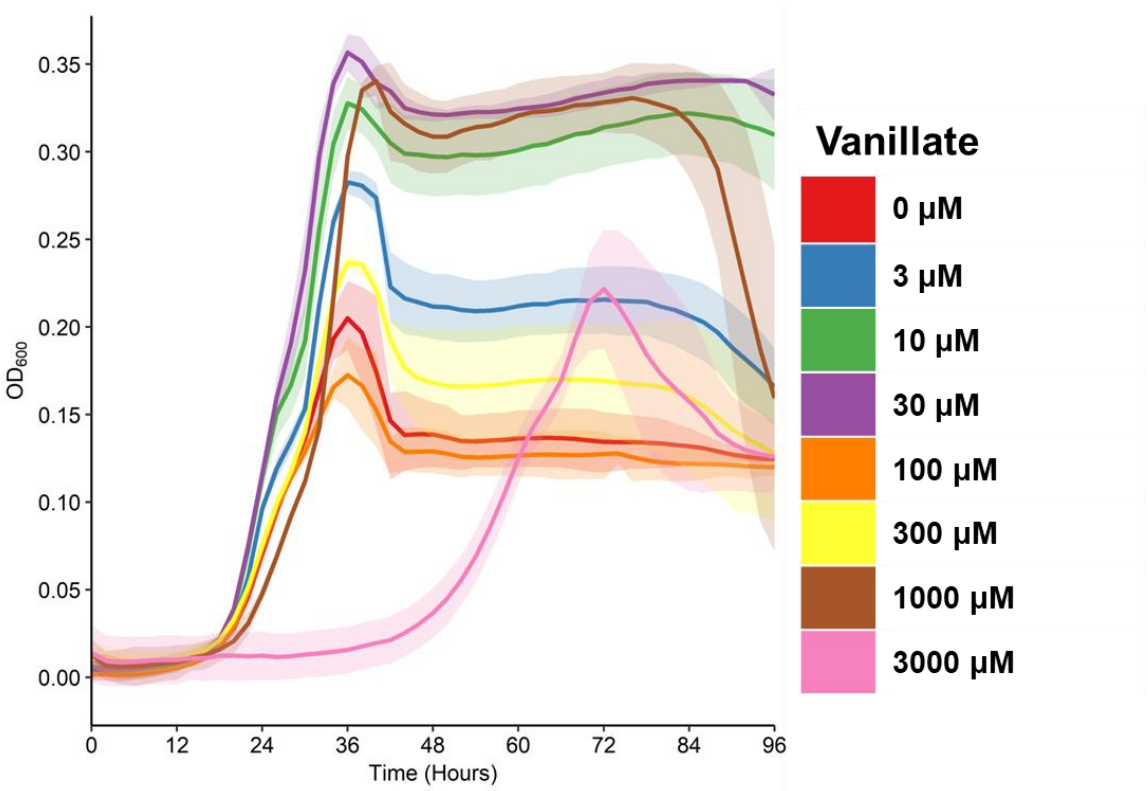


Figure 17: Growth curve of wild type on varying concentrations of vanillate. Growth of strain FEL005 tracked at OD_{620} over 96 hours in 2-hour intervals. Each curve is an average of biological triplicates. Ribbons represent standard deviation amongst 3 replicates.

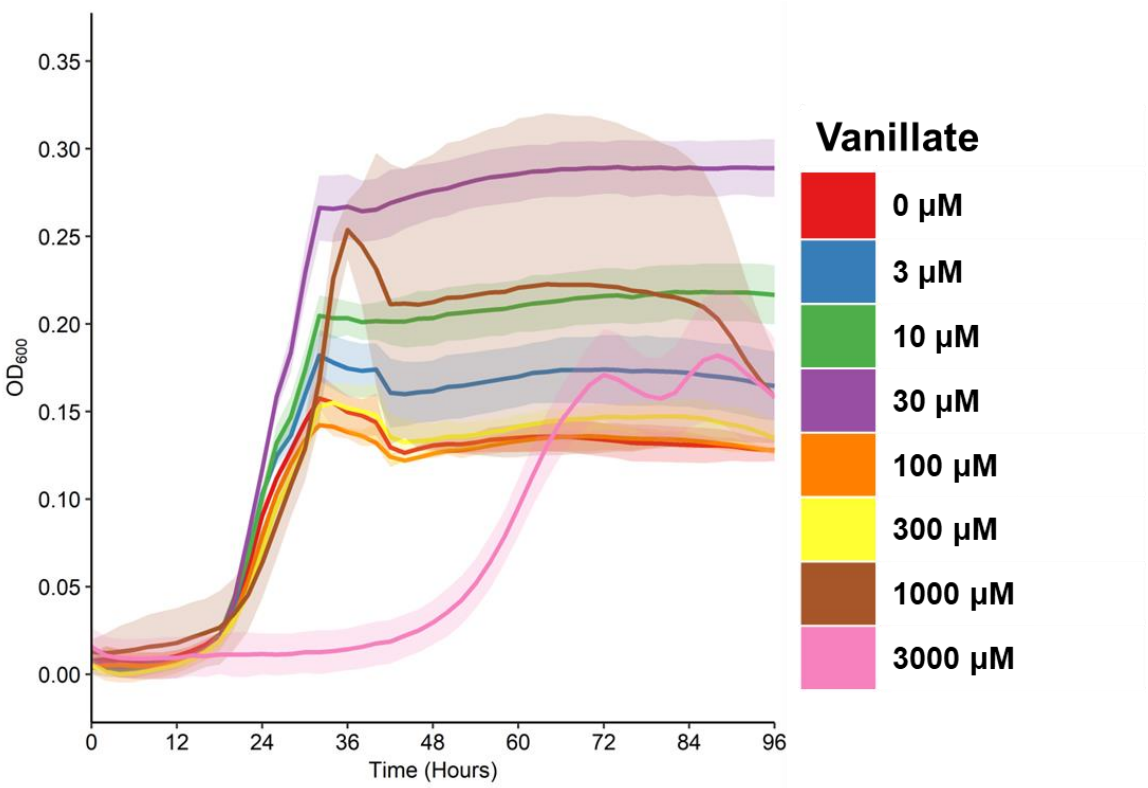


Figure 18: Growth curve of strain FEL273 on varying concentrations of vanillate. Growth of strain FEL273 tracked at OD_{620} over 96 hours in 2-hour intervals. Each curve is an average of biological triplicates. Ribbons represent standard deviation amongst 3 replicates.

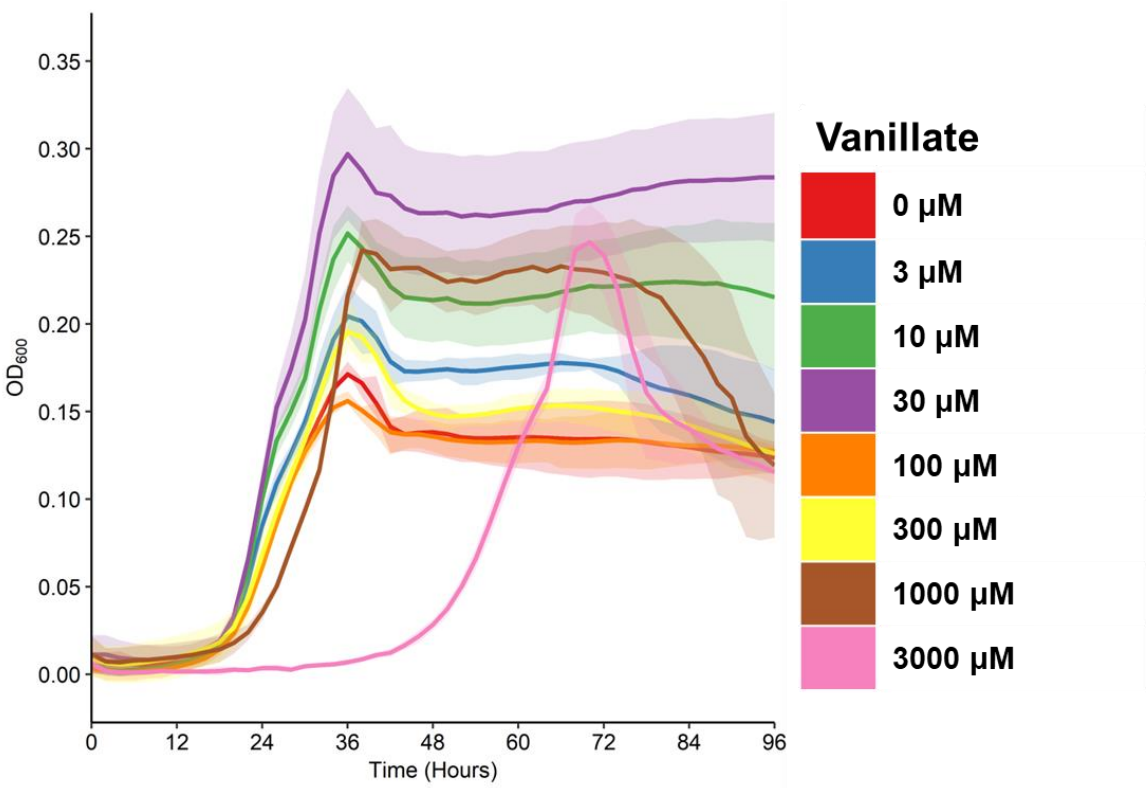


Figure 19: Growth curve of strain FEL274 on varying concentrations of vanillate. Growth of strain FEL274 tracked at OD_{620} over 96 hours in 2-hour intervals. Each curve is an average of biological triplicates. Ribbons represent standard deviation amongst 3 replicates.

Maximum optical density

Despite differences observed during growth curves in the presence of vanillate, the 30 μM vanillate cultures actually reached the highest OD for all 3 strains, as shown in **Figure 20**. Strain FEL005 generally surpassed the two mutant strains in biomass production regardless of vanillate induction.

Time to reach maximum optical density

The time to reach maximum OD was analyzed to further investigate the physiological effects of vanillate. As seen in **Figure 21**, most culture conditions reached maximum OD close to the 34-hour mark. Possible outliers to this trend were strains FEL005 and FEL273 with 10 μM vanillate, FEL273 with 30 μM and 1,000 μM vanillate, and all strains with 3,000 μM vanillate, all of which took considerably longer to reach their respective maximum OD.

Mercury methylation following lag phase induction

Based on the growth curves discussed above, three vanillate induction concentrations were chosen to proceed with MeHg analysis. In addition to 0 μM vanillate, 30 μM vanillate resulted in the most growth, while the 100 μM vanillate induction resulted in similar growth patterns compared with the 0 μM cultures. All 3 strains were amended with 0 μM, 30 μM, and 100 μM vanillate upon inoculation and were allowed to grow to mid-exponential phase (OD_{600} ~0.14) as described in **Figure 22**. Surprisingly, as seen in **Figure 23**, mercury methylation appeared to be dependent on vanillate induction; these differences were statistically

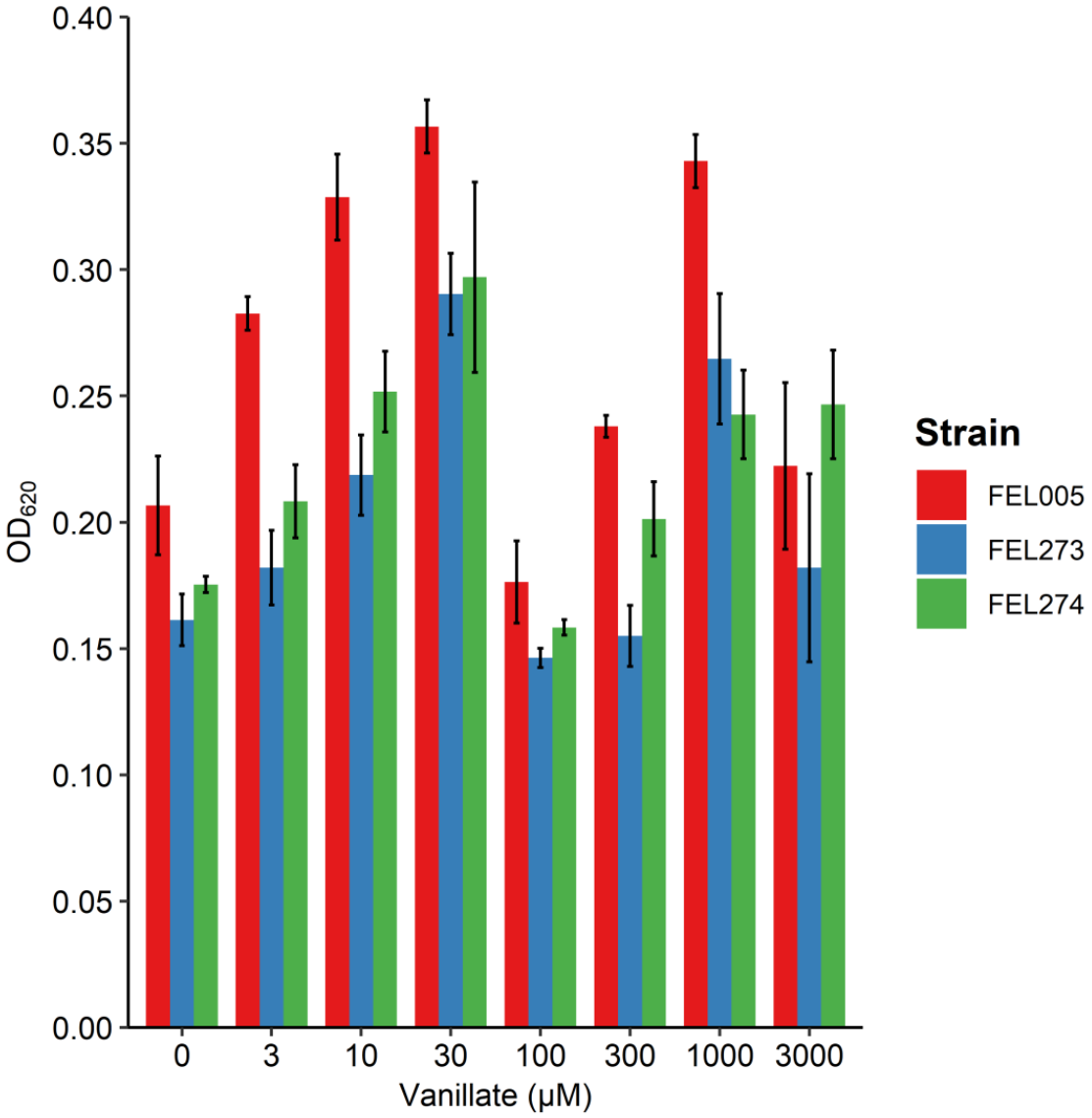


Figure 20: Maximum optical density.
Maximum $OD6_{20}$ reached by each culture. Each bar is the average of biological triplicates. Error bars represent standard deviation amongst 3 cultures.

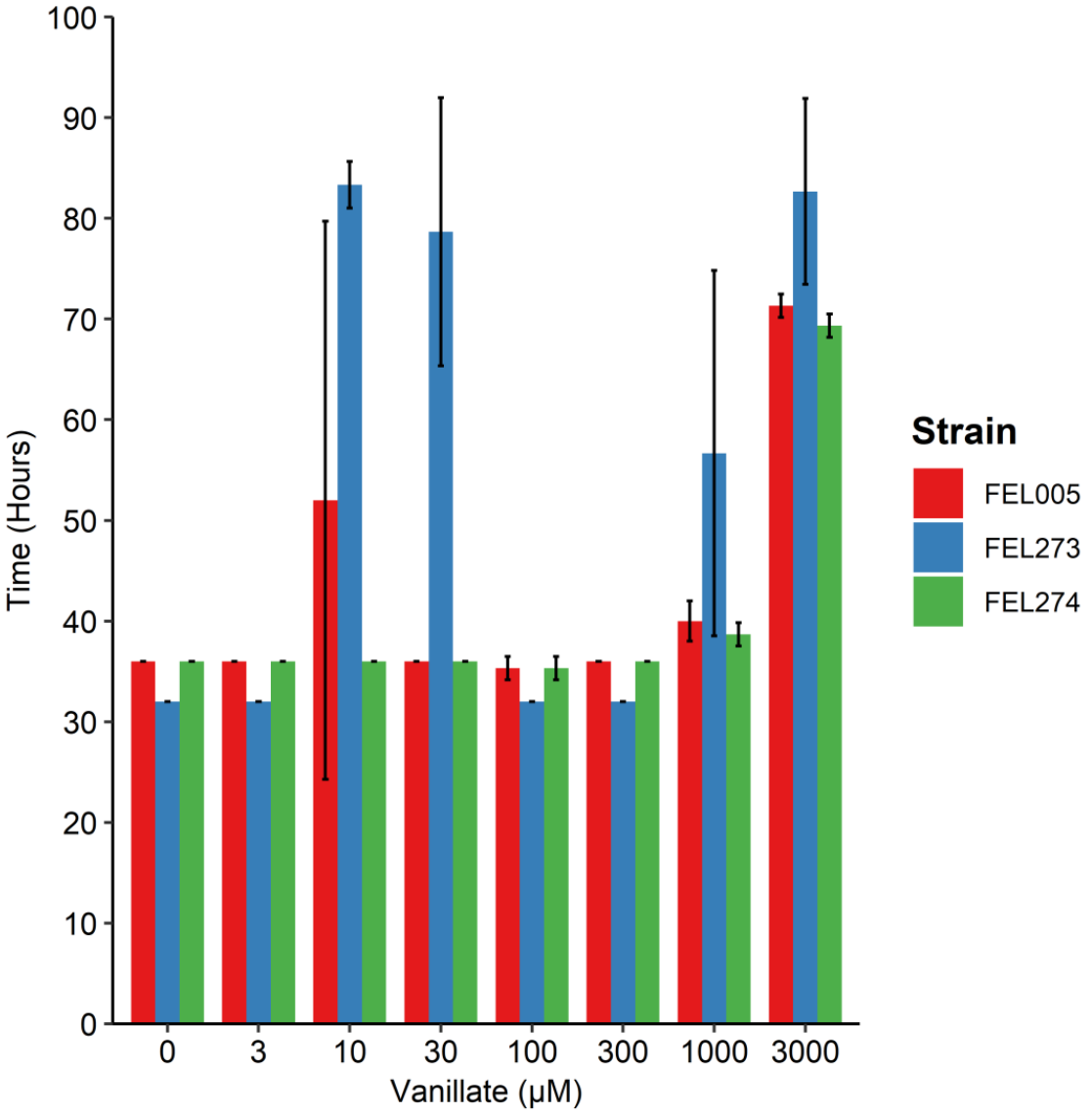


Figure 21: Time to reach maximum optical density.
Time taken to reach maximum OD_{620} by each culture. Each bar is the average of biological triplicates. Error bars represent standard deviation amongst 3 cultures.

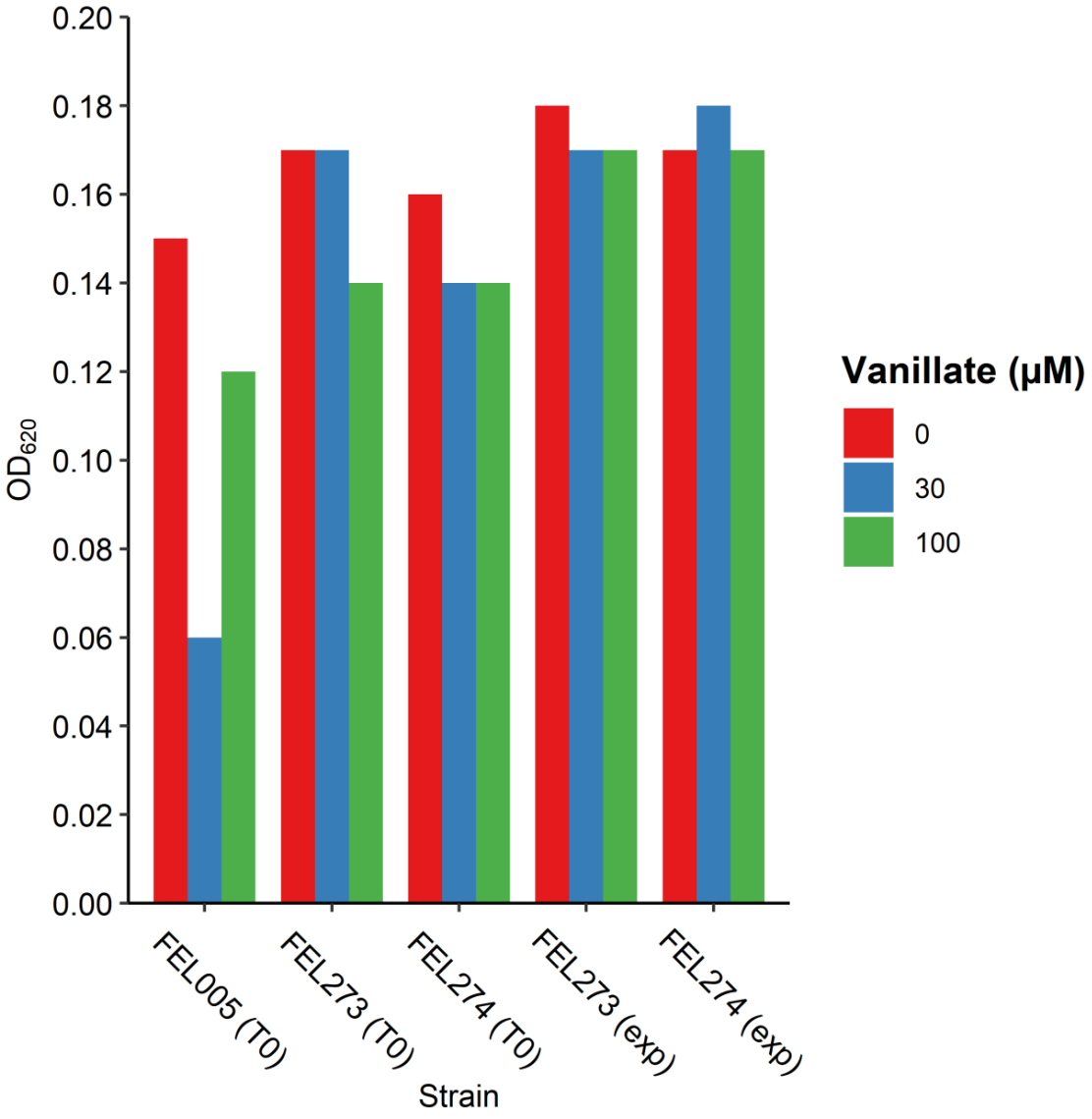


Figure 22: Optical density at harvesting.
OD_{620} when cultures were harvested or induced. Cultures induced at T0 were harvested at the OD values shown. Cultures induced in mid-exponential phase were induced at the OD values shown. T0, induced at time 0; exp, induced in mid-exponential phase.

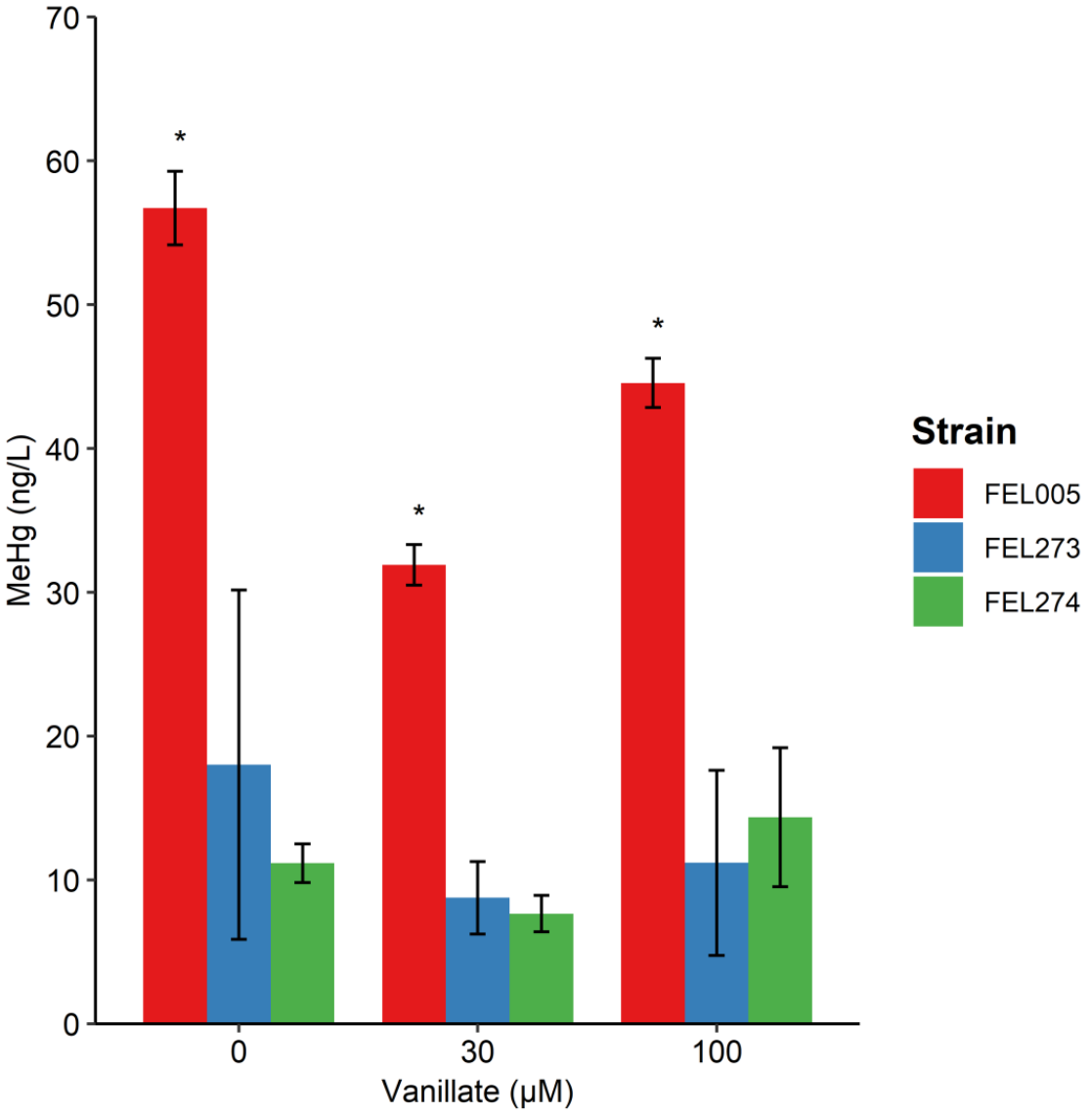


Figure 23: Endpoint methylmercury concentrations following lag-phase induction.
MeHg concentrations following 24-hour incubation at room temperature. Each bar represents the average of biological duplicates. Error bars represent standard deviation between two replicates. Strain FEL005 was statistically significant ($p < 0.05$) with respect to each level of induction.

significant ($p < 0.05$) in the wild type strain. Strains FEL273 and FEL274 only exhibited background levels of methylmercury production, even following induction, suggesting either a faulty promoter or HgcAB expression may not be the rate-limiting step in mercury methylation.

Mercury methylation following exponential phase induction

As seen above, vanillate induction appears to alter mercury methylation. The same strains were then induced after reaching mid-exponential phase (OD_{600} ~0.17) to decouple growth from methylation induction. Following vanillate amendment at mid-exponential phase, cultures were incubated at 15°C for 12 hours. As seen in **Figure 24**, both strains FEL273 and FEL274 produced basal levels of methylmercury following induction at mid-exponential phase.

Discussion

The *hgcAB* genes encode the enzymes that are responsible for methylating mercury (1). HgcA in particular binds a corrinoid cofactor, which is unidentified and produced in low quantities in the native methylator ND132. Furthermore, no regulated promoters existed for the ND132 host system. To overcome these limitations, we attempted to apply PCA as a model organism for HgcAB overexpression. We observed surprising results while using the vanillate inducible promoter system (6), as discussed below.

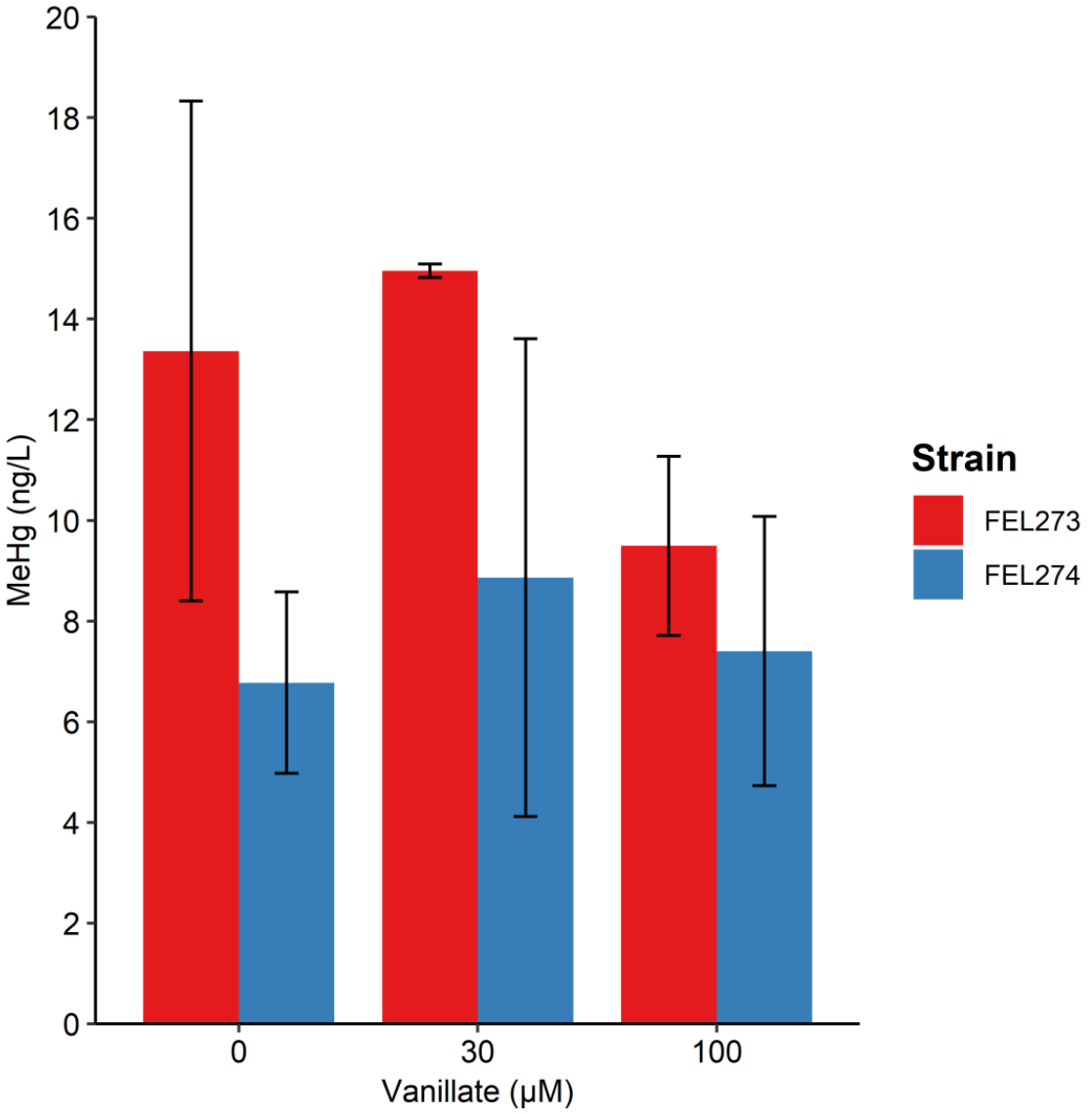


Figure 24: Endpoint methylmercury concentrations following exponential-phase induction.
MeHg concentrations following 24-hour incubation at room temperature. Each bar represents the average of biological duplicates. Error bars represent standard deviation between two replicates.

Attempts to overexpress HgcAB in *G. sulfurreducens* revealed surprising physiological effects on *Geobacter* growth and mercury methylation. **Figure 23** shows that even the wild type *G. sulfurreducens* responded to the addition of vanillate, resulting in differential growth rates and maximum cell density. The micromolar concentrations of vanillate used in this study are unlikely to lead to increased biomass formation, as growth on vanillate as a sole carbon and energy source requires millimolar levels (9, 10). Furthermore, no precipitation or turbidity was observed when dissolving vanillate in the growth medium, which would have otherwise impacted optical density readings. Interestingly, we observed no direct correlation between vanillate concentration and growth rate, suggesting a non-linear relationship.

Similar to what was observed in the growth curves, mercury methylation appeared to be influenced by vanillate addition. Interestingly, neither growth nor mercury methylation appeared to correlate linearly with vanillate concentration.

The successful creation of strain FEL273 shows that homologous recombination of single-copy suicide vectors functions sufficiently with 501 bp of homology, whereas most other studies have used approximately twice the length of homology (6). Successful chromosomal integration via half the typical homology length may not be surprising, given the constitutively expressed *Geobacter recA*

(11). Future studies may apply this finding for faster and cheaper plasmid construction.

Though mutant strains were induced with varying concentrations of vanillate at multiple growth phases, no obvious effects on mercury methylation were observed. What little methylmercury was observed resulted in approximately 11 ng/L on average, which is within background levels of previous studies (1). This result may suggest that HgcAB may not be the rate-limiting step, or the promoter was non-functional. The P_{acp}(vanO) synthetic promoter is one of the few regulated promoters in *Geobacter*, with the exception of the IPTG-inducible *taclac* promoter (6, 12). Future studies may use the *taclac* promoter to decouple growth from methylation induction by inducing after reaching exponential phase to mitigate the apparent growth effects of vanillate. Additionally, the lack of methylation in strains FEL273 and FEL274 without induction suggests the initial N-terminal 167 and 234 residues of HgcAB are insufficient to confer methylation activity, despite being driven by the native promoter.

We may have inadvertently identified unknown growth effects of vanillate even in wild type *Geobacter*. This result opens the door to further physiological aspects of mercury methylation, as its native function is still under debate.

Vanillate is one of several organics derived from phenylalanine and tyrosine, often found in lignin degradation (13, 14). Genes involved in this process may thus carry implications in cellulose degradation (15, 16). In addition to biofuels, it is also worth mentioning that a closely related molecule vanillin is of commercial importance in the food industry (13).

Initial exploration on the Kyoto Encyclopedia of Genes and Genomes (KEGG) (15–17) revealed that *G. sulfurreducens* only possesses 2 enzymes involved in aminobenzoate metabolism: acylphosphatase (GSU0889) and flavin prenyltransferase (GSU0440). Closer examination into aminobenzoate metabolism revealed nodes where vanillate specifically enters central metabolism, via either vanillate demethylase or vanillate monooxygenase, neither of which are encoded on the *G. sulfurreducens* genome according to KEGG metabolic pathway maps. These enzymes have been shown to transfer the methyl group from vanillate and subsequently feed it into the Wood-Ljungdahl pathway (18).

The *vanAB* genes (locus tags NCgl2300-NCgl2301 in *C. glutamicum*) encode two subunits of vanillate demethylase (oxygenase and reductase, respectively), whose demethylated product can feed into central metabolism (14). Protein BLASTs of these candidates against the PCA proteome did not reveal any paralogs ($E < 1.0$).

Further investigation into vanillate metabolism revealed a 3-component vanillate O-demethylase system duplicated in *Moorella thermoacetica* as Moth_0385-Moth_0387 and Moth_1316-Moth_1318 (*mtvABC*, respectively) (15, 21, 22). Protein BLAST searches **(Table 11)** against these loci revealed two hits in PCA, GSU2921 and GSU3400. Further genome analysis did not positively identify *mtvB* paralogs, suggesting it may be nonexistent in *G. sulfurreducens* or cryptic in nature. Though their annotations **(Table 12)** may not suggest participation in vanillate metabolism, their low e-value and high percent coverage suggest these enzymes may be able to act upon vanillate. A feasible hypothesis may be that methylation reactions may be stimulated in the presence of the methyl donor vanillate via GSU2921 and GSU3400, whose corrinoid dependence may deplete the corrinoid pool, thus leading to decreased levels of other corrinoid-dependent activities, such as mercury methylation.

Vanillate may not serve as a suitable inducer molecule in all systems, specifically in those harboring the LigM demethylase (23). LigM removes the methyl group from vanillate, producing protocatechuate, and transfers the methyl group to tetrahydrofolate to produce 5-methyltetrahydrofolate. The resulting 5-methyltetrahydrofolate serves as an enzymatic cofactor and methyl donor, as may be the case in HgcA (1). We compared the LigM (Accession number 5TL4_A) of *Sphingomonas paucimobilis* (23) via protein BLAST to the PCA proteome and found an ortholog aminomethyltransferase GcvT (locus tag

Table 11: Protein BLAST results.

BLASTP Results								
	Length			Length		BLASTP		
M. thermoacetica	**bp**	**AA**	**PCA Hit**	**bp**	**AA**	**E-value**	**%Coverage**	**%ID**
Moth_0385	795	265	GSU2921	2412	804	6E-42	92	35
Moth_0386	1167	389	GSU3400	3069	1023	4.9	6	33
Moth_0387	621	207	GSU2921	2412	804	1E-37	93	38
Moth_1316	621	207	GSU2921	2412	804	4E-37	93	37
Moth_1317	1170	390	N/A	N/A	N/A	N/A	N/A	N/A
Moth_1318	795	265	GSU2921	2412	804	4E-42	92	35

Closest protein BLAST hits from vanillate demethylase genes in *M. thermoacetica* against the PCA proteome.

Table 12: Locus tag annotations.

Locus Tag Annotations

Locus	Annotation
GSU2921	Methionine synthase (B_{12}-dependent)
GSU3400	Heavy metal efflux pump, CzcA family
Moth_0385	5-Methyltetrahydrofolate--homocysteine S-methyltransferase
Moth_0386	Hypothetical protein
Moth_0387	5-Methyltetrahydrofolate--homocysteine S-methyltransferase
Moth_1316	5-Methyltetrahydrofolate--homocysteine S-methyltransferase
Moth_1317	Hypothetical protein
Moth_1318	5-Methyltetrahydrofolate--homocysteine S-methyltransferase

Annotations are derived from IMG Product Names.

WP_010941043) (E-value 1e-5, 59% coverage, 21.75% identity). This aminomethyltransferase may allow vanillate to feed into central metabolism, which would decrease induction concentration over time.

This study unexpectedly discovered that vanillate modulates *Geobacter* growth, likely independent of its use as a carbon source. More specifically, the experiments showed that vanillate can decrease mercury methylation rates *in vivo*. These results call into consideration how other aminobenzoates in the environment may be impacting microbial physiology, or perhaps decreasing mercury methylation rates *in situ*. One hypothesis is that vanillate triggers methyl transfer reactions that in turn deplete the corrinoid pool, which if held true, introduces methyl donor availability as a mechanism regulating mercury methylation.

Acknowledgements

We thank Xiangping Yin of the ORNL Environmental Sciences Division for support with methylmercury analyses.

References

1. Parks JM, Johs A, Podar M, Bridou R, Hurt RA, Smith SD, Tomanicek SJ, Qian Y, Brown SD, Brandt CC, Palumbo AV, Smith JC, Wall JD, Elias DA, Liang L. 2013. The genetic basis for bacterial mercury methylation. Science 339:1332–1335.

2. Rana MN, Tangpong J, Rahman MM. 2018. Toxicodynamics of lead, cadmium, mercury and arsenic- induced kidney toxicity and treatment strategy: A mini review. Toxicol Rep 5:704–713.

3. Yan J, Bi M, Bourdon AK, Farmer AT, Wang P-H, Molenda O, Quaile AT, Jiang N, Yang Y, Yin Y, Şimşir B, Campagna SR, Edwards EA, Löffler FE. 2017. Purinyl-cobamide is a native prosthetic group of reductive dehalogenases. Nat Chem Biol.

4. Banères J-L, Popot J-L, Mouillac B. 2011. New advances in production and functional folding of G-protein-coupled receptors. Trends Biotechnol 29:314–322.

5. Yamaguchi H, Miyazaki M. 2014. Refolding techniques for recovering biologically active recombinant proteins from inclusion bodies. Biomolecules 4:235–251.

6. Chan CH, Levar CE, Zacharoff L, Badalamenti JP, Bond DR. 2015. Scarless genome editing and stable inducible expression vectors for *Geobacter sulfurreducens*. Appl Environ Microbiol 81:7178–7186.

7. Bertani G. 1951. Studies on lysogenesis. I. The mode of phage liberation by lysogenic *Escherichia coli*. J Bacteriol 62:293–300.

8. Lin H, Lu X, Liang L, Gu B. 2015. Cysteine inhibits mercury methylation by *Geobacter sulfurreducens* PCA mutant Δ*omcBESTZ*. Environ Sci Technol Lett 2:144–148.

9. Morawski B, Segura A, Ornston LN. 2000. Substrate range and genetic analysis of *Acinetobacter* vanillate demethylase. J Bacteriol 182:1383–1389.

10. Chen H-P, Chow M, Liu C-C, Lau A, Liu J, Eltis LD. 2012. Vanillin catabolism in *Rhodococcus jostii* RHA1. Appl Env Microbiol 78:586–588.

11. Giloteaux L, Holmes DE, Williams KH, Wrighton KC, Wilkins MJ, Montgomery AP, Smith JA, Orellana R, Thompson CA, Roper TJ, Long PE, Lovley DR. 2013. Characterization and transcription of arsenic respiration and resistance genes during in situ uranium bioremediation. ISME J 7:370–383.

12. Dehio M, Knorre A, Lanz C, Dehio C. 1998. Construction of versatile high-level expression vectors for *Bartonella henselae* and the use of green fluorescent protein as a new expression marker. Gene 215:223–229.

13. Datta S, S. Annapure U, J. Timson D. 2016. Characterization of Cd36_03230p, a putative vanillin dehydrogenase from *Candida dubliniensis*. RSC Adv 6:99774–99780.

14. Merkens H, Beckers G, Wirtz A, Burkovski A. 2005. Vanillate metabolism in *Corynebacterium glutamicum*. Curr Microbiol 51:59–65.

15. Ragsdale SW. 2008. Catalysis of methyl group transfers involving tetrahydrofolate and B_{12}. Vitam Horm 79:293–324.

16. Abe T, Masai E, Miyauchi K, Katayama Y, Fukuda M. 2005. A tetrahydrofolate-dependent O-demethylase, LigM, is crucial for catabolism of vanillate and syringate in *Sphingomonas paucimobilis* SYK-6. J Bacteriol 187:2030–2037.

17. Kanehisa M, Goto S. 2000. KEGG: Kyoto Encyclopedia of Genes and Genomes. Nucleic Acids Res 28:27–30.

18. Kanehisa M, Furumichi M, Tanabe M, Sato Y, Morishima K. 2017. KEGG: new perspectives on genomes, pathways, diseases and drugs. Nucleic Acids Res 45:D353–D361.

19. Kanehisa M, Sato Y, Furumichi M, Morishima K, Tanabe M. 2019. New approach for understanding genome variations in KEGG. Nucleic Acids Res 47:D590–D595.

20. Izquierdo JA, Goodwin L, Davenport KW, Teshima H, Bruce D, Detter C, Tapia R, Han S, Land M, Hauser L, Jeffries CD, Han J, Pitluck S, Nolan M, Chen A, Huntemann M, Mavromatis K, Mikhailova N, Liolios K, Woyke T, Lynd LR. 2012. Complete Genome Sequence of *Clostridium clariflavum* DSM 19732. Stand Genomic Sci 6:104–115.

21. Pierce E, Xie G, Barabote RD, Saunders E, Han CS, Detter JC, Richardson P, Brettin TS, Das A, Ljungdahl LG, Ragsdale SW. 2008. The complete genome sequence of *Moorella thermoacetica* (f. *Clostridium thermoaceticum*). Environ Microbiol 10:2550–2573.

22. Naidu D, Ragsdale SW. 2001. Characterization of a three-component vanillate O-demethylase from *Moorella thermoacetica*. J Bacteriol 183:3276–3281.

23. Kohler AC, Mills MJL, Adams PD, Simmons BA, Sale KL. 2017. Structure of aryl O-demethylase offers molecular insight into a catalytic tyrosine-dependent mechanism. Proc Natl Acad Sci 114:E3205–E3214.

24. Datsenko KA, Wanner BL. 2000. One-step inactivation of chromosomal genes in *Escherichia coli* K-12 using PCR products. Proc Natl Acad Sci U S A 97:6640–6645.

25. Caccavo F, Lonergan DJ, Lovley DR, Davis M, Stolz JF, McInerney MJ. 1994. *Geobacter sulfurreducens*) sp. nov., a hydrogen- and acetate-oxidizing dissimilatory metal-reducing microorganism. Appl Environ Microbiol 60:3752–3759.

CHAPTER V
CONCLUSION

Summary

As discussed in Chapter 1, the structure and availability of corrinoids govern a variety of biological reactions in our environment. In Chapter 2, we identify a new gene involved in the synthesis of the 5-methoxybenzimidazole lower base. Though the structure of the lower bases modulates activity of reductive dehalogenases, the same does not hold true in mercury methylation, as described in Chapter 3. In Chapter 4, we surprisingly discover the small molecule vanillate may have an effect an unexpected effect on mercury methylation.

VITA

Nannan initially developed an interest in global sustainability at the undergraduate level while working with Clifford F. Weil at Purdue University. In pursuing this interest, he was awarded a Howard Hughes Medical Institute (HHMI) internship to work in the laboratory of Louis A. Sherman with mentor Vilas B. Shukla to investigate polyhydroxyalkanoate (PHA) biosynthesis in the photosynthetic cyanobacteria. During this time, Nannan realized the power of harnessing microbes to produce compounds such as PHAs, which can be processed into biodegradable plastics. Following his B.S. in Biological Sciences, Nannan pursued his M.S. in Microbiology at the University of Illinois at Urbana-Champaign. Here, he worked under the direction of William W. Metcalf to study gene regulation in the strictly anaerobic, methanogenic archaea, which produce the clean and renewable energy source methane. With an interest in bioenergy, Nannan then took a post-masters metabolic engineering position at the Oak Ridge National Laboratory. Here, he applied molecular genetics to develop microbial strains as candidates for consolidated bioprocessing (CBP) in the BioEnergy Science Center (BESC).